CAPITAL UNIVERSITY OF SCIENCE AND TECHNOLOGY, ISLAMABAD

Linear Parameter Varying Control of Quadcopter with Varying Payload

by

Azmat Saeed

A dissertation submitted in partial fulfillment for the degree of Doctor of Philosophy

in the

Faculty of Engineering
Department of Electrical Engineering

2024

Linear Parameter Varying Control of Quadcopter with Varying Payload

By

Azmat Saeed

(DEE161003)

Dr. Muwahida Liaquat, Senior Research Scientist

Finnish Geospatial Research Institute, Espoo, Uusimaa, Finland

(Foreign Evaluator 1)

Dr. Yingyun Sun, Professor

North China Electric Power University, Beijing, China

(Foreign Evaluator 2)

Dr. Fazal Ur Rehman

(Research Supervisor)

Dr. Noor Muhammad Khan

(Head, Department of Electrical Engineering)

Dr. Imtiaz Ahmad Taj

(Dean, Faculty of Engineering)

DEPARTMENT OF ELECTRICAL ENGINEERING

CAPITAL UNIVERSITY OF SCIENCE AND TECHNOLOGY

ISLAMABAD

2024

Copyright © 2024 by Azmat Saeed

All rights reserved. No part of this dissertation may be reproduced, distributed, or transmitted in any form or by any means, including photocopying, recording, or other electronic or mechanical methods, by any information storage and retrieval system without the prior written permission of the author.

I would like to dedicate this dissertation to my loving parents, wife, and respected teachers.

CAPITAL UNIVERSITY OF SCIENCE & TECHNOLOGY
ISLAMABAD

Expressway, Kahuta Road, Zone-V, Islamabad
Phone:+92-51-111-555-666 Fax: +92-51-4486705
Email: info@cust.edu.pk Website: https://www.cust.edu.pk

CERTIFICATE OF APPROVAL

This is to certify that the research work presented in the dissertation, entitled "**Linear Parameter Varying Control of Quadcopter with Varying Payload**" was conducted under the supervision of **Dr. Fazal ur Rehman**. No part of this dissertation has been submitted anywhere else for any other degree. This dissertation is submitted to the **Department of Electrical Engineering, Capital University of Science and Technology** in partial fulfillment of the requirements for the degree of Doctor in Philosophy in the field of **Electrical Engineering.** The open defence of the dissertation was conducted on **December 29, 2023**.

Student Name : Azmat Saeed (DEE161003)

The Examination Committee unanimously agrees to award PhD degree in the mentioned field.

Examination Committee :

(a) External Examiner 1: Dr. Iftikhar Ahmed Rana
Associate Professor
SEECS, NUST, Islamabad

(b) External Examiner 2: Dr. Azhar ul Haq
Associate Professor
CEME, NUST, Islamabad

(c) Internal Examiner : Dr. Noor Muhammad Khan
Professor
CUST, Islamabad

Supervisor Name : Dr. Fazal ur Rehman
Professor
CUST, Islamabad

Name of HoD : Dr. Noor Muhammad Khan
Professor
CUST, Islamabad

Name of Dean : Dr. Imtiaz Ahmad Taj
Professor
CUST, Islamabad

AUTHOR'S DECLARATION

I, **Azmat Saeed** (Registration No. **DEE161003**), hereby state that my dissertation titled, "**Linear Parameter Varying Control of Quadcopter with Varying Payload**" is my own work and has not been submitted previously by me for taking any degree from Capital University of Science and Technology, Islamabad or anywhere else in the country/ world.

At any time, if my statement is found to be incorrect even after my graduation, the University has the right to withdraw my PhD Degree.

(Azmat Saeed)

Dated: 29 December, 2023

Registration No : DEE161003

PLAGIARISM UNDERTAKING

I solemnly declare that research work presented in the dissertation titled "**Linear Parameter Varying Control of Quadcopter with Varying Payload**" is solely my research work with no significant contribution from any other person. Small contribution/ help wherever taken has been duly acknowledged and that complete dissertation has been written by me.

I understand the zero-tolerance policy of the HEC and Capital University of Science and Technology towards plagiarism. Therefore, I as an author of the above titled dissertation declare that no portion of my dissertation has been plagiarized and any material used as reference is properly referred/ cited.

I undertake that if I am found guilty of any formal plagiarism in the above titled dissertation even after award of PhD Degree, the University reserves the right to withdraw/ revoke my PhD degree and that HEC and the University have the right to publish my name on the HEC/ University Website on which names of students are placed who submitted plagiarized dissertation.

(**Azmat Saeed**)

Dated: 29 December, 2023

Registration No : DEE161003

List of Publications

It is certified that following publication(s) have been made out of the research work that has been carried out for this dissertation:-

1. **Saeed, Azmat**, Aamer I. Bhatti, and Fahad M. Malik. "LMIs-Based LPV Control of Quadrotor with Time-Varying Payload," Applied Sciences 13, no. 11 (2023): 6553.

2. **Saeed, Azmat**, Aamer I. Bhatti, and Fahad M. Malik. "2-DOF H_∞ Output Feedback Control of Quadrotor Subject to Parametric Uncertainties and Time Delay," In 2022 International Conference on Recent Advances in Electrical Engineering & Computer Sciences (RAEE & CS), pp. 1-5. IEEE, 2022.

(Azmat Saeed)
Registration No: DEE161003

Acknowledgement

All Praises to ALLAH Almighty, the Most Gracious and the Most Merciful.

First of all, I want to express my gratitude to Almighty Allah, who blessed me with both physical strength and intellectual abilities. With the patience and determination bestowed upon me by Allah, I managed to overcome the difficult circumstances and successfully complete my dissertation.

I am profoundly grateful to my supervisor, Dr. Fazal ur Rehman, whose invaluable and unwavering support, as well as technical guidance, have consistently been sources of inspiration throughout my post-graduation studies.

I express my gratitude to Dr. Aamer Iqbal Bhatti, Dr. Fahad Mumtaz Malik, Dr. Imtiaz Taj, and Dr. Noor Muhammad Khan for their exceptional guidance, steadfast support, and inspiring teaching throughout my PhD coursework.

Furthermore, I would like to thank the CASPR Dynamics team. My colleagues: Mr. Abrar Hashmi, Mr. Usman, Mr. Farhan, Mr. Zohaib Latif, Mr. Hafiz Muhammad Yasir Naeem, Mr. Faheem Manzoor, Mr. Faheem Gulzar , Mr. Ahmed Mehmood, and Ms. Sidra, for their guidance and encouragement.

Above all, I am highly grateful to my father, who taught me patience, devotion, and commitment with affection. I am thankful to my wife and our kids, Muhammad Aarish and Muhammad Azan, for understanding and accompanying me in difficult times. I am also indebted to my mother, brothers, and sisters, who have always provided me with motivation and relentless support to pursue higher studies.

(Azmat Saeed)

Abstract

Applications of a quadcopter with payload, particularly for chemical spraying, have increased in recent times. In a sprayer drone, mass will not be fixed and will vary over time. The variation in payload mass will alter the moments of inertia (MOI). Moreover, large tilt angles are required for fast reference tracking and wind disturbance rejection. These variations in plant parameters (i.e., mass and inertia) and large tilt angles can degrade the control scheme's performance and stability. This dissertation proposes a linear matrix inequalities (LMIs)-based linear parameter varying (LPV) control scheme for a quadrotor subject to varying mass, varying inertia, large tilt angles, and wind disturbances. The control strategy is designed by solving LMIs derived from quadratic H_∞ performance and D-stability. The robust stability and quadratic H_∞ performance are assessed by LMIs. The effectiveness of the presented methodology is validated through comprehensive numerical simulations. Its performance is systematically contrasted with both the linear time-invariant (LTI) H_∞ control design with pole placement constraints and sliding mode control (SMC) across diverse scenarios. This comparative evaluation encompasses various cases, providing a robust analysis of the proposed methodology's capabilities. The obtained results demonstrate that the LPV control scheme outperforms in tracking precision under dynamic conditions, including varying parameters, wind disturbances, and noise, while avoiding actuator saturation. In contrast to the H_∞ design technique, the proposed LPV scheme enhances key performance metrics such as rise time (t_r), settling time (t_s), root mean squared error (RMSE), and root mean squared (RMS) of the control signal by up to 28%, 26%, 91%, and 92%, respectively. Moreover, smooth transitions are observed in the tilt angles and control signals with the LPV scheme, contrary to the H_∞ control design incorporating constraints on pole placement, which exhibits significant oscillations. When compared to the SMC design technique, the LPV scheme demonstrates improvements of up to 26% in t_r, 55% in t_s, and 42% in RMSE, respectively.

Contents

List of Figures

List of Tables

Abbreviations

ANFTSMC	Adaptive Nonlinear Fast Terminal Sliding Mode Control
ASMC	Adaptive Sliding Mode Control
DOF	Degrees of Freedom
H_∞	H-infinity
ISMC	Integral Sliding Mode Control
LMI	Linear Matrix Inequality
LPV	Linear Parameter Varying
LQR	Linear Quadration Regualtor
LTI	Linear Time Invariant
MSE	Mean Squared Error
PID	Proportinal-Integral-Derivative
RBSMC	Robust Backstepping Sliding Mode Control
RMS	Root Mean Square
RMSE	Root Mean Squared Error
RP	Robust Performance
RS	Robust Stability
SMC	Sliding Mode Control
UAV	Quadrotor Unmaned Aerial Vehical
VTOL	Vertical Takeoff and Landing

Symbols

g	Acceleration due to gravity
$\ddot{x}$	Acceleration in x-direction in the inertial frame
$\ddot{y}$	Acceleration in y-direction in the inertial frame
$\ddot{z}$	Acceleration in z-direction in the inertial frame
$\ddot{\phi}$	Angular acceleration about x-axis in inertial frame
$\ddot{\theta}$	Angular acceleration about y-axis in inertial frame
$\ddot{\psi}$	Angular acceleration about z-axis in inertial frame
I_x	Inertia about the x-axis
I_y	Inertia about the y-axis
I_z	Inertia about the z-axis
l	Length of an arm
m	Mass of quadrotor with varying payload
$\overline{m}$	Mass of quadrotor with full payload
$\underline{m}$	Mass of quadrotor with empty payload
θ	Pitch angle
$\dot{\theta}$	Pitch rate
Q_v	Pitch rate about y-axis in the body frame
τ_θ	Pitching moment
ϕ	Roll angle
$\dot{\phi}$	Roll rate
P_v	Roll rate about x-axis in the body frame
τ_ϕ	Rolling moment
J_r	Rotor inertia

k_s	Sideward drag factor
T	Thrust
K_f	Thrust coefficient
k_u	Upward drag factor
U	Velocity in x-direction in the body frame
$\dot{x}$	Velocity in x-direction in the inertial frame
V	Velocity in y-direction in the body frame
$\dot{y}$	Velocity in y-direction in the inertial frame
W	Velocity in z-direction in the body frame
$\dot{z}$	Velocity in z-direction in the inertial frame
Fwx	Wind force in x-direction
Fwy	Wind force in y-direction
Fwz	Wind force in z-direction
x	x-position
ψ	Yaw angle
$\dot{\psi}$	Yaw rate
R_v	Yaw rate about z-axis in the body frame
τ_ψ	Yawing moment
y	y-position
z	z-position

Chapter 1

Introduction

This chapter provides the preliminary knowledge necessary to understand the rest of the dissertation.

1.1 Background

Quadcopters, commonly referred to as quadrotors, belong to the category of unmanned aerial vehicles (UAVs) and have evolved from the broader domain of rotorcraft and multi-rotor systems. Rotorcraft, a diverse class of aircraft, relies on spinning rotor blades for lift instead of conventional fixed wings. This category of aircraft includes vehicles capable of vertical takeoff and landing (VTOL) due to the rotary wings or rotor blades. The most well-known multi-rotor rotorcrafts are quadcopters which are equipped with four rotors. The concept of quadcopters dates back to the early 20th century, when various inventors and engineers experimented with multi-rotor designs. Early research on quadcopters focused on stability and control challenges. As computational power, sensors, and battery technology improved, researchers and engineers made strides in quadcopter autonomous control, navigation, and stabilization algorithms. The field gained momentum in the late 20th century and continued to progress rapidly into the 21st century [1].

1.1.1 Quadcopter Configuration

Quadcopters are rotary-wing aircraft with four vertically oriented propellers arranged in a square or cross configuration. Quadcopters utilize four rotors, each providing lift and propulsion. The rotors spin in opposite pairs (clockwise and counterclockwise) to maintain stability and balance. Quadcopter is a four-rotor, under-actuated system as depicted in Figure 1.1. The thrust forces produced by rotors are represented by $T_i(i = 1, 2, 3, 4)$. The adjacent rotors spin in opposite directions. Two rotors (1 & 3) rotate clockwise, while rotors (2 & 4) spin anti-clockwise [2, 3].

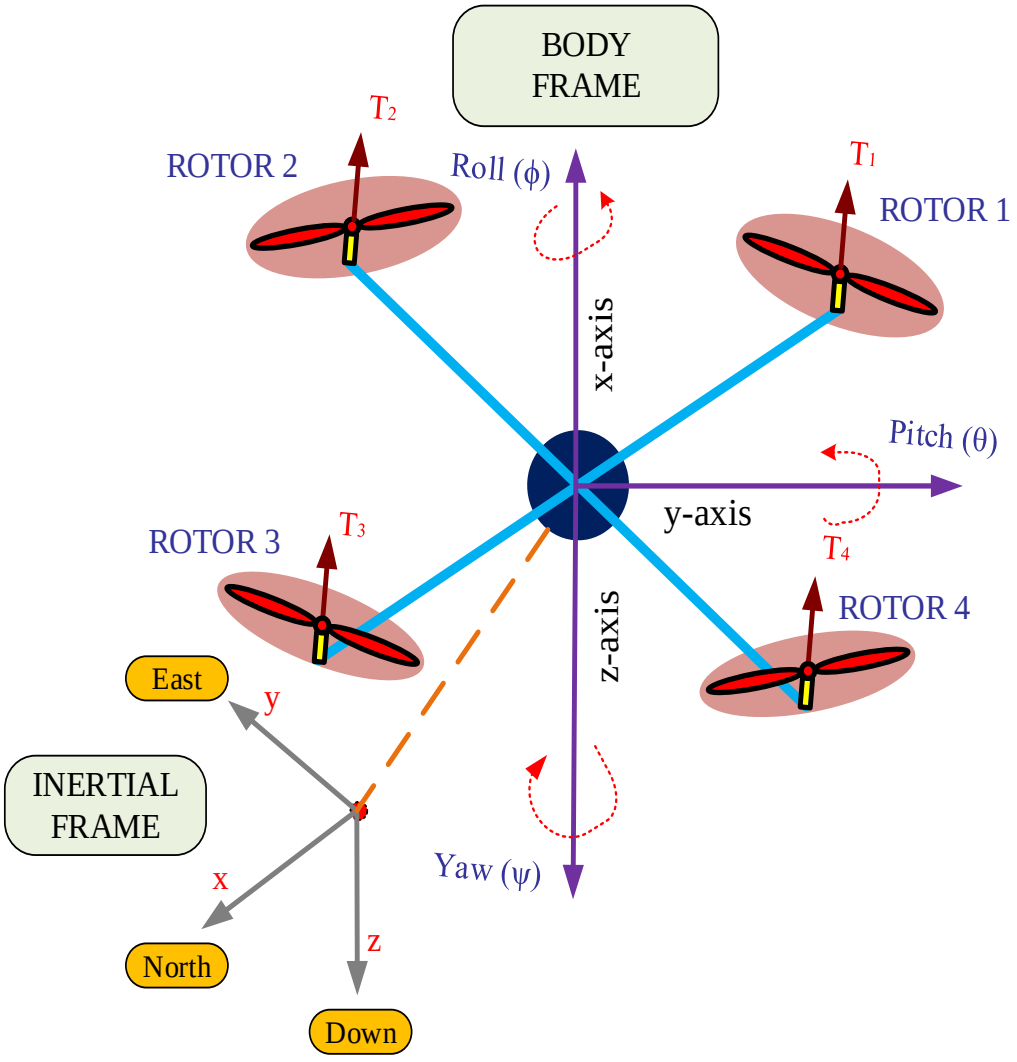

FIGURE 1.1: The configuration of quadcopter

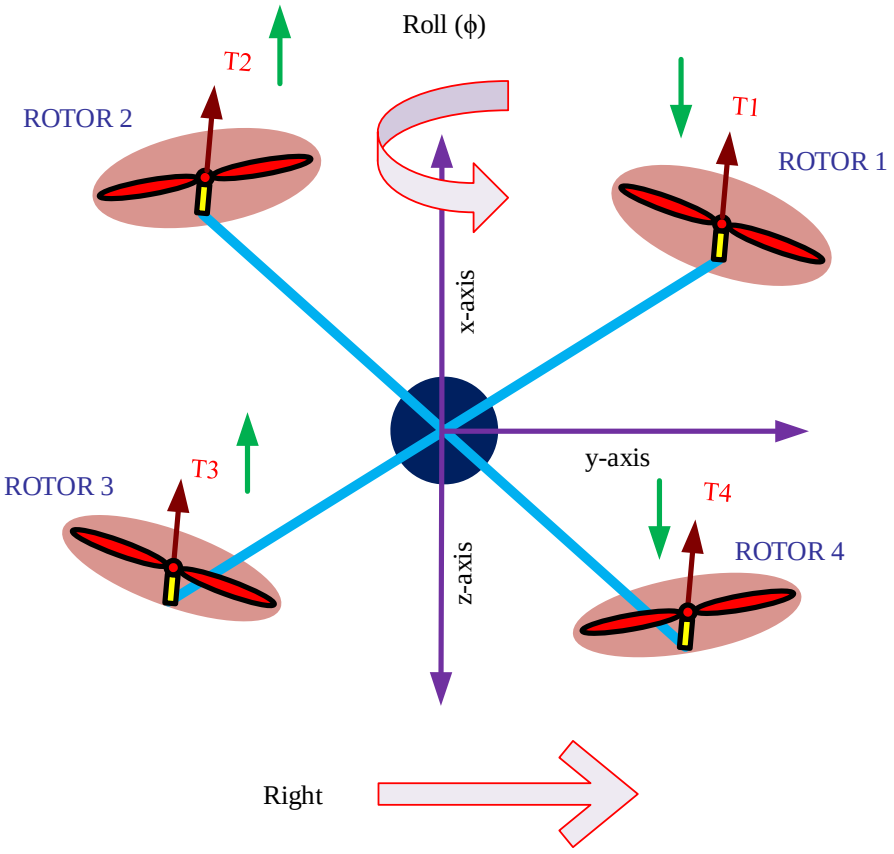

FIGURE 1.2: Roll maneuver of quadcopter

Quadcopters are capable of performing various maneuvers. Some common maneuvers that a quadcopter can perform are:

1. **Roll maneuver:**

   The roll maneuver refers to tilting the quadcopter along its longitudinal axis, causing it to roll to one side while maintaining a constant altitude. This maneuver is achieved by changing the speeds of the rotors on opposite sides. The quadcopter has four rotors, Rotors 1 & 3 are diagonal from each other, and rotors 2 & 4 are diagonal from one other. To perform the roll maneuver, increase the speed of rotors 2 & 3 and decrease the speed of rotors 1 & 4 simultaneously. The roll maneuver of the quadcopter is shown in Figure 1.2.

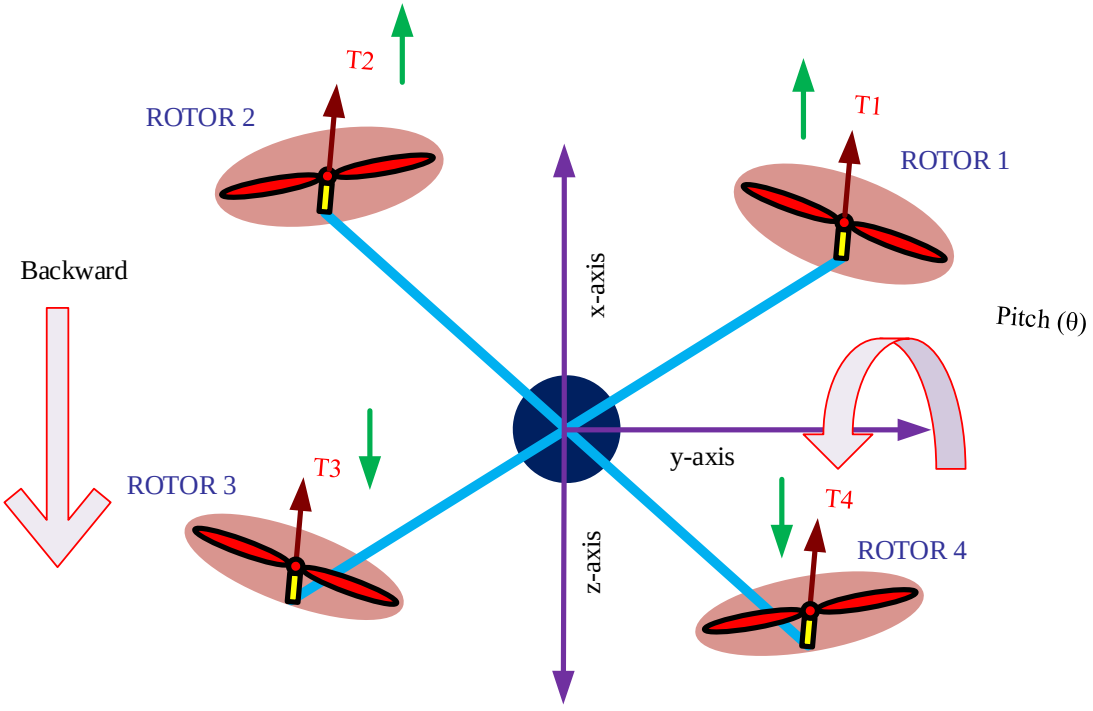

FIGURE 1.3: Pitch maneuver of quadcopter

2. **Pitch maneuver:**

   Pitch maneuver refers to the tilting of the quadcopter forward or backward about its lateral axis. This maneuver is achieved by changing the speeds of the front and rear rotors. Forward pitch is achieved by increasing speed of rotors 1 & 2 while simultaneously decreasing the speed of rotors 3 & 4. Backward pitch is achieved by decreasing the speed of rotors 1 & 2 while increasing speed of rotor 3 & 4 simultaneously. Forward pitch means the quadcopter will tilt forward, and backward pitch means the quadcopter will tilt backward. Pitch maneuver is shown in Figure 1.3.

3. **Yaw Maneuver:**

   The yaw maneuver is the rotation of a quadcopter clockwise or anticlockwise around its vertical axis. This maneuver is achieved by changing the speeds of the rotors on the same side in opposite directions. Yaw rotation is achieved by increasing the speed of rotors 1 & 3 and decreasing the speed of rotors

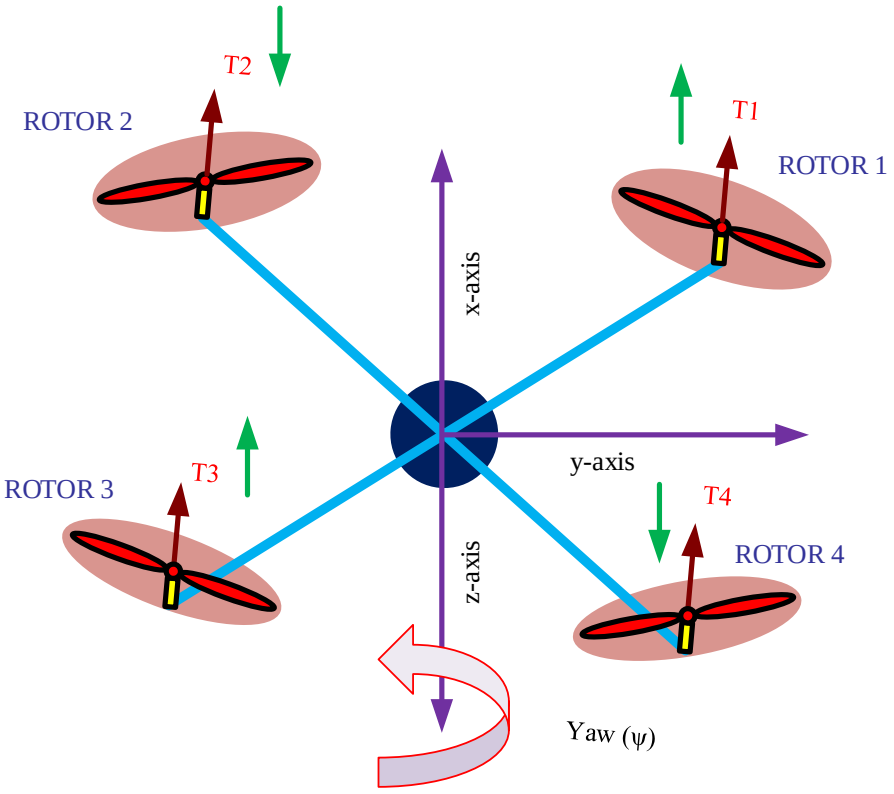

FIGURE 1.4: Yaw maneuver of quadcopter

2 and 4, making sure that total thrust remains constant. By increasing the speeds of the front-right rotor and rear-left rotor while decreasing the speed of the other two rotors, the quadcopter will rotate clockwise. By increasing the speeds of the front-left rotor and rear-right rotor while decreasing the speed of the other two rotors , the quadcopter will rotate anticlockwise. Yaw rotation is shown in Figure 1.4.

4. **Vertical Takeoff and Landing (VTOL):**
   VTOL is a flight capability in which a quadcopter lifts off from the ground vertically and also lands vertically without the need for a runway or additional landing equipment. Quadcopters also achieve VTOL by controlling the speed of their rotors. How it works is as follows:

   (a) **Takeoff:**

   During takeoff, all four rotors of the quadcopter spin at the same speed,

providing an upward force that lifts the vehicle off the ground in the presence of a gravitational force acting downward. The vehicle remains steady during takeoff because the thrust created by each rotor is balanced.

(b) **Howering:**

Hovering in a quadcopter refers to the state in which the vehicle maintains a stable position at a fixed height in the air. During hovering, the quadcopter balances upward thrust and gravitational force. Hovering is accomplished by altering the speeds of the four rotors to achieve a balance between the upward thrust and the gravitational force that pulls the vehicle downward.

(c) **Landing:**

During landing, the speeds of all four quadcopter rotors are gradually reduced, reducing the upward force created by each rotor. The quadcopter lowers vertically downward in a controlled manner as the lift declines. When the quadcopter gets close to the ground, the rotors come to a halt, allowing the vehicle to land gently.

The vertical takeoff of the quadcopter is shown in Figure 1.5.

1.1.2 Flight Control

Quadcopter flight control is achieved using a combination of mechanical design, control algorithms, and onboard sensors such as accelerometers, gyroscopes, magnetometers, and, in certain cases, extra sensors such as barometers and cameras. The flight controller adjusts the speed of individual rotors, which provide the torques and forces required for manoeuvring. Flight control in quadcopters is composed of three major components:

1. **Stabilization:**

   Quadcopters are inherently unstable due to their design, although they can

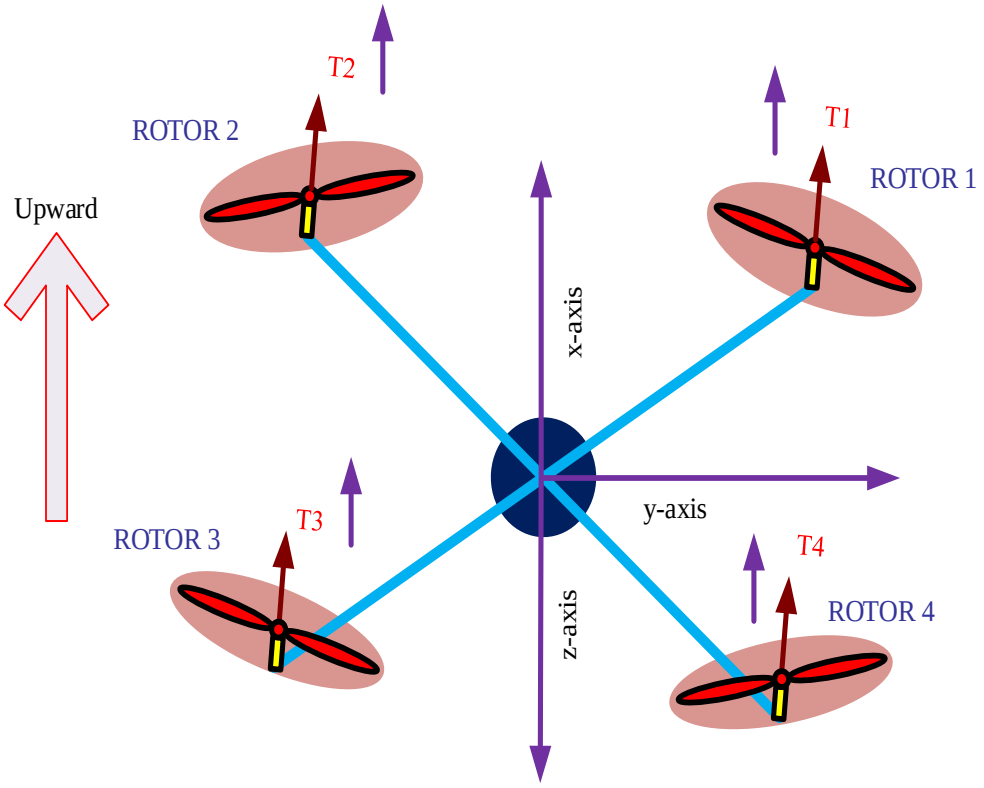

FIGURE 1.5: Vertical takeoff and landing of quadcopter

attain stability by altering rotor speeds in real-time. Onboard sensors such as gyroscopes and accelerometers continuously monitor the orientation and rate of change of the quadcopter. Based on this data, the flight controller changes the rotor speeds to maintain a steady hover and prevent drift.

2. **Attitude Control:**

   The capacity of the quadcopter to change its orientation (roll, pitch, and yaw) is referred to as attitude control. The flight controller regulates the rotor speeds to do this. For example: To roll, the flight controller advances two rotors on one side while slowing the other two. To pitch, the flight controller increases the front rotors while decreasing the rear rotors, or vice versa. To yaw, the flight controller adjusts the rotor speeds in opposite directions, increasing one set while decreasing the other.

3. **Position Control:**

   Position control means maintaining a desired position or performing precise manoeuvres in space. This is accomplished via GPS (Global Positioning System) and other sensors such as barometers and vision systems. The flight controller modifies the rotor speeds based on GPS data and other sensor inputs to move the quadcopter to a specific point or follow a predefined flight route.

1.1.3 Key Features

Quadcopters have several distinctive features that contribute to their popularity and versatility:

- **Maneuverability:**

  Quadcopters have excellent manoeuvrability due to their ability to independently control the thrust of each rotor. They can hover, do acrobatic manoeuvres, and instantly change direction.

- **Vertical Takeoff and Landing (VTOL):**

  Quadcopters can take off and land vertically, eliminating the need for runways. This ability allows them to operate in limited spaces and access locations that other aircraft may not be able to reach.

- **Payload Capacity:**

  Quadcopters can carry a variety of payloads, such as cameras, sensors, liquid tanks, or other equipment, depending on their size and design. Because of their adaptability, they are suited for a wide range of applications such as aerial photography, surveillance, mapping, delivery, and research.

- **Ease of Operation:**

  Quadcopters are relatively easier to control and operate as compared to fixed-wing aircraft. The advancements in control design algorithms enable automated flight and precise navigation of quadcopters in 3D space.

FIGURE 1.6: Agriculture sprayer drone [7]

1.1.4 Application

Quadcopters have a wide range of applications, including payload transportation, aerial photography, cinematography, surveillance, agriculture, research, search and rescue, and others. Continuous research and development is improving quadcopter capabilities, with advances in control algorithms, sensor integration, power systems, and materials all contributing to expanding the capabilities and performance of the quadcopters [4–6]. Some of the well-known quadcopters used in different applications are depicted in Figures 1.6, 1.7, and 1.8 [7–9].

Sprayer Drone:

As seen in Figure 1.6, sprayer drones can be employed on a variety of farms and in various locations. Sprayer drones can be used in a wide variety of areas and farms. They are used for the spraying of chemicals to kill insects and pests and enhance crop quality in urban areas. They can spray fertilisers, pesticides, and herbicides on crops efficiently and accurately, reducing the need for manual labour

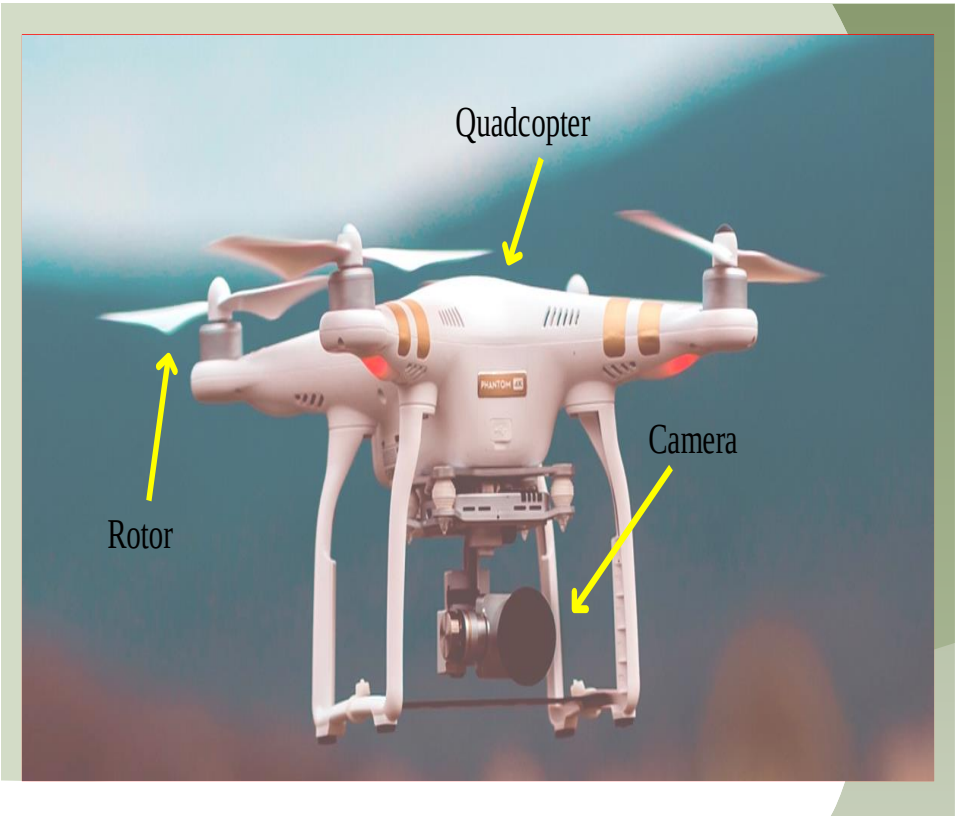

FIGURE 1.7: Camera drone [8]

FIGURE 1.8: Toy drone [9]

and minimising human exposure to chemicals to avoid the health problems that humans face when spraying manually, making the spraying job easier and faster than manual work, saving manpower, and lowering costs. They are used in forestry to spray fire retardants or water from the air during firefighting operations. With the recent COVID-19 outbreak, sprayer drones have gained appeal for disinfection purposes. They can spray disinfectants in public areas, hospitals, schools, and other populated places, reducing the danger of viral transmission.

Camera Drone:

Camera drones have a wide range of applications across various industries and fields. The camera drone is depicted in Figure 1.7. Camera drones are extensively used for aerial photography and videography. They have provided filmmakers and photographers with unprecedented opportunities to capture stunning aerial shots, adding a new level of dynamism, angles, viewpoints, and visual appeal to their work. They are used in various industries, such as construction, urban planning, and land surveying, to create accurate aerial maps, 3D models, and site surveys. Furthermore, camera drones have found utility in sectors such as agriculture, where they aid in crop monitoring, disease detection, and precision agriculture.

Toy Drone:

Toy drones have various applications, the most common of which are entertainment and hobbies. Figure 1.8 shows the toy drone. They may be flown indoors or outdoors and frequently include features like stunts, flips, and obstacle avoidance. Toy drones are increasingly being utilized in educational settings to teach concepts related to science, technology, engineering, and mathematics. They can help students learn about aerodynamics, electronics, coding, and problem-solving while gaining hands-on experience. Controlling the movement of the drone in various locations improves the user's ability to navigate and adapt to changing scenarios. Toy drones offer a platform for creative experimentation. Users can modify and customize drones, attach small objects, or create unique flying experiences. Toy drones can be used as a learning tool for individuals who want to develop the skills needed to operate larger and more professional drones. They offer a safe and

inexpensive way to practise basic flight manoeuvres and acquire confidence before progressing to more advanced drone models.

1.2 Motivation

Agriculture, as the backbone of our civilization. In today's rapidly evolving agricultural landscape, there is more demand for creative, effective, and sustainable farming strategies. Traditional methods of crop spraying often lead to inefficiencies, such as overuse of chemicals, imprecise targeting, and wastage of resources. With the global population steadily increasing, there is an urgent need to enhance agricultural productivity while minimizing environmental impact. To address this, optimizing agricultural practices for efficiency and sustainability is crucial. In recent years, drone technology, particularly quadcopters, has emerged as a transformative tool in precision agriculture. Sprayer drones, equipped with advanced control systems, offer a promising solution to these challenges.

1.3 Research Contributions

The major contribution of the research presented in this thesis is significant in two key areas:

1. **Dynamic Modeling of Quadcopter:**
   Dynamic model of quadcopter with varying payload and wind disturbance, is essential for thorough analysis and control design. This thesis, explores the nonlinear model of quadcopter with varying payload and wind disturbance. A novel LPV model is developed based on the nonlinear 6-DOF model of a quadcopter, incorporating variations in mass, inertia, large tilt angles, and the influence of wind disturbance. The varying parameters of the quadcopter are determined using SOLIDWORKS. The second-order Taylor series is utilized to approximate the tilt angles. The resulting LPV model

captures the system's behavior across the entire range of parameter variations. To underscore the validity and accuracy of the LPV model developed for the quadcopter, a model validation process is undertaken. This validation involved a comparison between the response of the LPV model and the original nonlinear model with varying payload.

2. **Control Design:**
   In control system engineering, designing an effective controller is paramount. In this thesis, Two control strategies are developed for the position control of quadcopter with variable payload:

   - **LMIs-based LPV Control:**
     A novel LMIs-based LPV control scheme is formulated to address position control problem of quadcopter with varying parameters, large tilt angles, and external disturbances. This approach employs Linear Matrix Inequalities (LMIs) to guarantee stability and accurate positioning under challenging operational conditions.

   - **LMIs-based $\mathcal{H}_\infty$ Control:**
     Multi-objective linear controller is designed based on LMIs of "$\mathcal{H}_\infty$ performance" and "Pole Placement in LMI Regions" for the position control of quadcopter.

Furthermore, this thesis encompasses a comparative analysis involving the $\mathcal{H}_\infty$ controller, the SMC controller, and the LMIs-based LPV control scheme. This comparative study provides valuable insights into the effectiveness and adaptability of these control approaches.

These contributions have led to the following journal publication:

Saeed, Azmat, Aamer I. Bhatti, and Fahad M. Malik. "LMIs-Based LPV Control of Quadrotor with Time-Varying Payload," Applied Sciences 13, no. 11 (2023): 6553.

1.4 Overview of the Thesis

In this chapter general problem background and motivation of this dissertation is discussed. The subsequent sections of the thesis are organized as follows:

Chapter 1: In chapter 1, Background, motivation and objective behind this research is discussed in details. Quadcopter configuration and how the quadcopter performs different types of motion are discussed. Moreover, some of the applications of the quadcopters are also presented. The literature survey explains the past efforts of the researchers to control the quadcopter.

Chapter 2: Chapter 2 is devoted to the literature review related to the quadcopter control problem. Literature survey contains different types of control strategies proposed by the researcher for quadcopter efficient control. Moreover, the gap analysis is also presented.

Chapter 3: Chapter 3 discusses mathematical modeling of quadcopter with varying payload. It provides the background details needed for better understanding the quadcopter from a dynamical system viewpoint. The varying parameters found for quadcopter using solidworks are also discussed. The model equatins found using curve fitting techniques are also presented. The LPV modeling and linear modeling of the quadcopter is also explored. Moreover, the comparision between nonlinear model, LPV model and linear model is also presented.

Chapter 4: In chapter 4, control algorithms and their formulation for quadcopter dynamics are discussed in detail. LPV control design technique based on LMIs to control the quadcopter's position is discussed. Multi-objective linear controller designed for the quadcopter linear model to control the position of quadcopter is also presented.

Chapter 5: In chapter 5, simulation results are discussed and compared for different scenarios. The LPV control strategy, linear control technique, and SMC control algorithm are applied to the nonlinear model. Various scenarios are taken into consideration to assess the performance of the designed controllers.

Chapter 6: Chapter 6, concludes the dissertation through outlining the main contributions and list of directions that can be accomplished in the future research. Chapter-wise Layout of this thesis is shown in Figure 1.9.

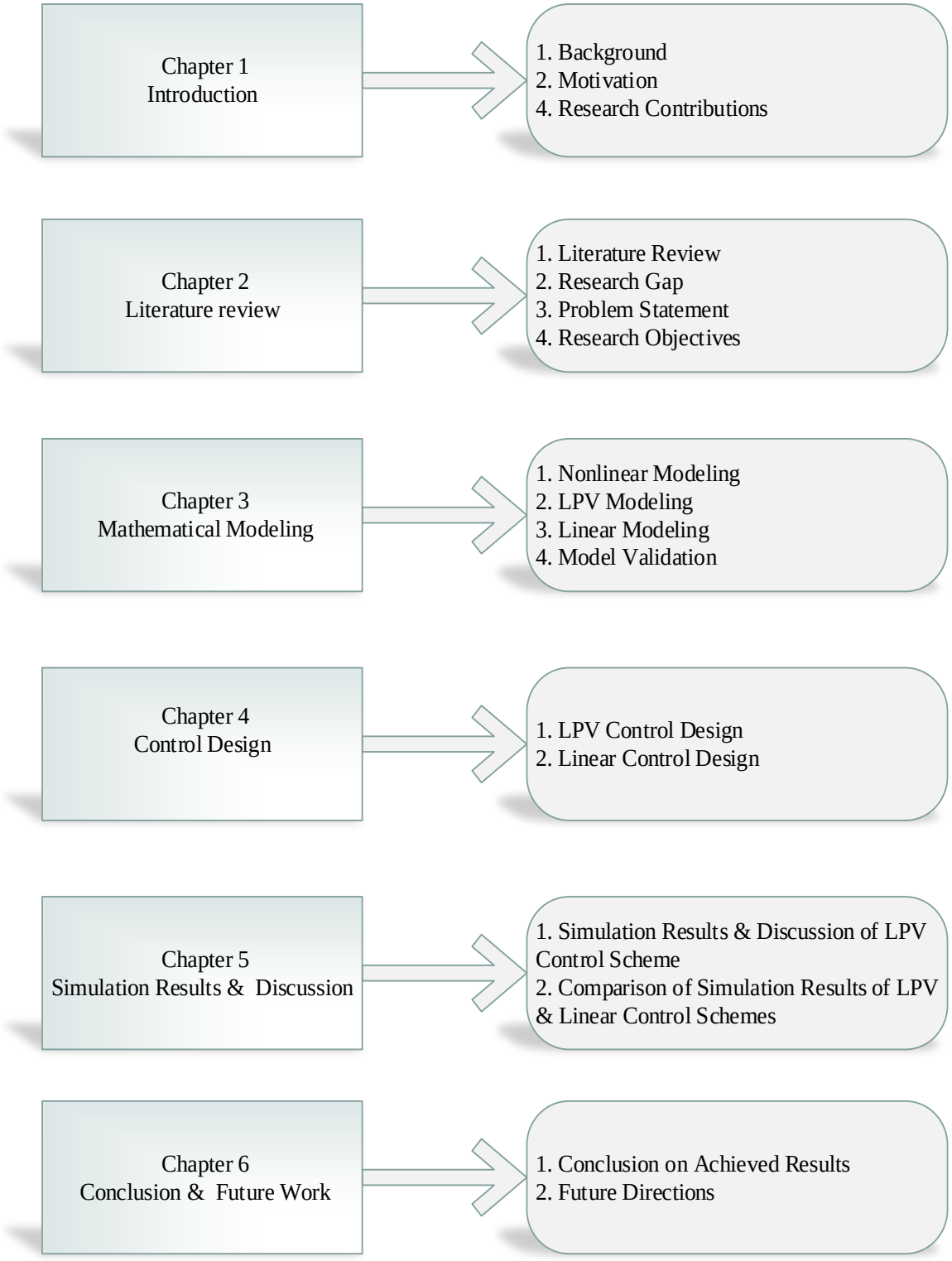

FIGURE 1.9: Thesis layout

Chapter 2

Literature Review, Gap Analysis, and Problem Statement

Quadcopters are used nowadays for a wide range of applications such as aerial photography, surveillance and security, search and rescue operations, precision agriculture, environmental monitoring, package delivery, and entertainment [10, 11]. Among these, the sprayer drone, also known as an agricultural drone, is a significant one that offers several advantages in agricultural and farming practices [12, 13]. Some of the key advantages of using sprayer drones are:

1. **Precision and Efficiency:**
   Sprayer drones provide precise and targeted applications of pesticides, fertilizers, and other agricultural chemicals. They can be programmed to follow specific flight paths, ensuring accurate coverage and minimizing waste. This precision leads to improved efficiency and reduced chemical usage, saving both time and resources.

2. **Increased Safety:**
   Sprayer drones eliminate the need for farmers to handle and apply chemicals manually, reducing their exposure to potentially harmful substances. This aspect improves worker safety and reduces the risk of accidents or health issues associated with chemical handling.

3. **Accessibility and Adaptability:**

   Drones can reach areas that are difficult to access with traditional machinery or manual labour. They can fly over uneven terrain, hilly regions, or densely planted fields without damaging crops. This accessibility allows for the efficient treatment of large areas that might otherwise be challenging or time-consuming to reach.

4. **Time and Labour Savings:**

   Sprayer drones can cover larger areas in a shorter period of time compared to manual or ground-based spraying methods. With their ability to carry substantial payloads, they can complete tasks quickly, reducing the time and labour required for agricultural operations.

5. **Environmental Benefits:**

   Precision spraying by drones helps to reduce the overall amount of chemicals used in agricultural practises. By applying pesticides and fertilizers only where needed, sprayer drones minimize runoff, limit soil contamination, and reduce the impact on nearby water bodies. This targeted approach promotes environmentally friendly and sustainable farming practices.

6. **Data Collection and Analysis:**

   Many sprayer drones come equipped with advanced sensors and imaging technologies, such as thermal cameras and multi-spectral sensors. These sensors enable the collection of valuable data about crop health, plant stress, soil moisture levels, and more. The data can be used to monitor and analyze crop conditions, identify potential issues, and make informed decisions to optimize crop management.

7. **Cost Savings:**

   Although the initial investment in sprayer drone technology can be significant, the long-term cost savings can be substantial. With increased efficiency, reduced chemical usage, and minimized labour requirements, farmers can potentially save money in terms of chemical costs, labour expenses, and overall operational costs.

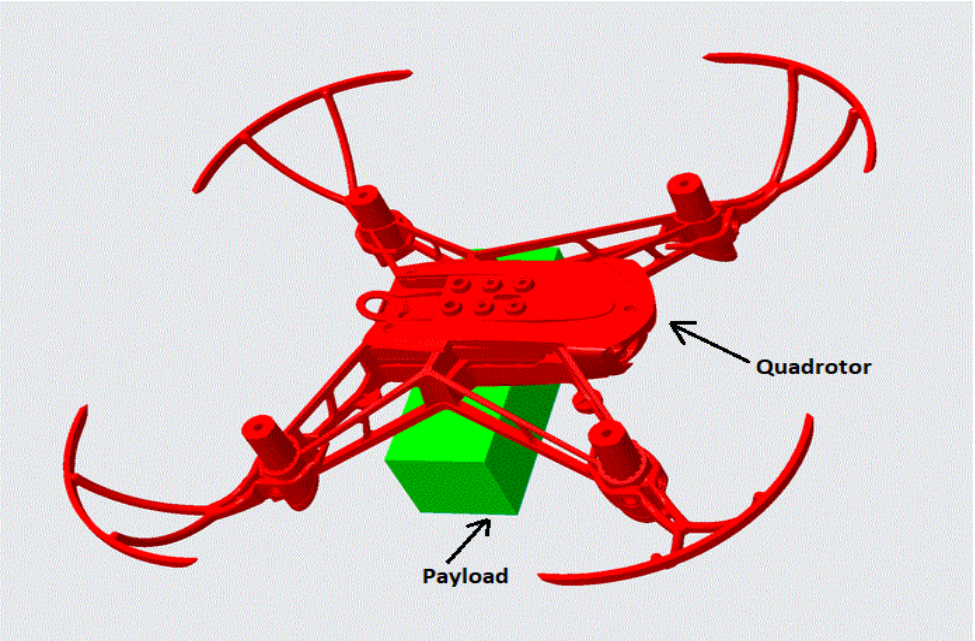

FIGURE 2.1: The 3D CAD model of quadcopter with payload

In a sprayer drone, the quadcopter's mass will not be fixed and will vary over time. The variation in mass with time will alter the moment of inertia. Such variations in the quadcopter's parameters over time, in addition to the standard features of system dynamics, such as nonlinearities, under-actuation, noise, external disturbances, actuator constraints, etc., make the control system design a challenging problem. The quadcopter with payload (liquid tank) is depicted in Figure 2.1.

2.1 Previous Control Design Techniques

Various control strategies have been developed for quadcopters to achieve stability and effective tracking. To tackle the quadcopter's tracking control issue, linear control approaches such as proportional–integral–derivative (PID) [14–18] and linear-quadratic-regulator (LQR) [19–23] are proposed. These schemes required an accurate linear model of the system for obtaining the desired tracking performance. Robust linear control scheme based on H_∞-norm optimization is presented for quadcopter [24–27]. H_∞ control is an effective control design methodology that offers robustness to model uncertainties and disturbances. The above-mentioned

control algorithms are based on local linearization, and the performance of a linear time-invariant (LTI) control scheme deteriorates with deviation from the operating point and can even lead to instability.

To overcome the impediments caused by local linearization, Linear parameter varying (LPV) control approaches have been proposed for the quadcopter. LPV controllers are well-suited for systems with time-varying parameters, nonlinearity, and varying operating conditions. They can achieve better closed-loop performance and robustness, making them advantageous in scenarios where linear controllers may fall short. In [28], LPV control scheme is suggested for a quadcopter to handle the large perturbation from the nominal condition. Tilt angles are limited to $\pm\ \pi/8$ rad (i.e., $\pm$ 22.5°). In [29], the LPV controller is proposed for high-speed maneuvering of quadcopter that requires large tilt angles. Tilt angles are accounted for up to $\pm\ \pi/3$ rad (i.e., $\pm$ 60°). In [30], a switched LPV control approach is recommended in order to handle huge attitude angles and external disturbances. The region for roll angle ϕ is considered to $\pm\ \pi/3$ rad and for pitch angle θ, the region is limited to $\pm\ \pi/8$ rad.

The commonly used nonlinear time-invariant (NLTI) control schemes like feedback linearization and backstepping have been proposed for quadcopter to achieve desired trajectory tracking in [31–34]. These control schemes depend on accurate model of the system for obtaining the performance of the closed loop system. In [35], the authors suggested robust sliding mode controller (SMC) for altitude control of quadcopter. To reduce chattering, they replaced the sign function with a saturation function. This work was extended in [36] by using integral sliding mode controller (ISMC) for quadcopter altitude control. To handle model uncertainties and external disturbances, robust backstepping sliding mode controller (RBSMC) is presented for attitude/position control of quadcopter in [37]. Adaptive sliding mode controller (ASMC) is proposed for quadcopter trajectory tracking under parametric uncertainties, unknown disturbances and actuators constraints in [38]. Quadcopters with variable mass and inertia have not been taken into consideration in the control strategies outlined above.

The design of the control system for a quadcopter with variable payload has also been investigated in the literature. In [39], LMI-based static output feedback LPV controller is suggested for Attitude/Altitude control of quadcopter to handle rotors velocity variation and step change in mass. Rotors velocity and mass are assumed to be measurable. Longitudinal and latitudinal translational motions are ignored, and the small angle assumption (i.e., $cos\phi cos\theta \approx 1$) is employed to design the control scheme. Moreover, the mass flow rate is ignored, and the control scheme is conservative due to coupling in the scheduling parameters. In [40], Hybrid LPV control scheme is suggested for the reference tracking of quadcopter with variable mass and variable inertia. A combination of integral backstepping control and proportional-derivative controls are designed to control the quadcopter's position and altitude. PD controllers are designed using the small angle assumption (i.e., $sin\phi \approx \phi$, $sin\theta \approx \theta$, $cos\phi \approx 1$, and $cos\theta \approx 1$). Variation in mass is not considered during the control algorithm design. LPV H_∞ controller is recommended to control the quadcopter rotational dynamics subject to time-varying inertia and variation in the rotors speed. Mass and rotors speed are considered measurable. The variations in MOI are recalculated in real-time from the changes in the mass. The mass flow rate is not taken into account and the scheduling parameters selected in the proposed scheme do not vary independently, which leads to conservative control. Robust LPV H_∞ controller is proposed for Altitude/Attitude stabilization of quadcopter to handle mass, inertia, and rotor velocity variations [41]. The proposed controller is designed using the LMI framework. The small angle approximation is considered to design the LPV scheme for the 4-DOF model of the quadcopter. Moreover, position control and the mass flow rate are not taken into consideration, and the coupling in the scheduling parameters leads to conservative control. A switched LPV control technique is suggested for the 3-DOF model of a quadcopter subject to large attitude angles, variable inertia, and outside disturbances [42]. Position control dynamics are not considered. In [43], the author recommended a self-tuning PID control scheme for the reference tracking of quadcopter. Mass and wind disturbance estimators based on a neural network with online learning are suggested to cope with the system's mass variation and wind

disturbances. Variations in MOI due to variable mass and mass flow rate are not taken into consideration. Adaptive sliding mode control (SMC) based on backstepping is advised to reduce the effect of variable load and wind disturbances [44]. Only the changing mass is estimated using the adaptive estimation controller. A fractional SMC is designed to cope with external disturbances and variations in inertia. Actuator limitations and mass flow rate are not considered, and chattering issues will exist due to the use of the signum function in the control law. Adaptive non-singular fast terminal SMC is proposed in [45]. External disturbances and mass are estimated online. To address the chattering issue, the saturation function is used in place of the signum function in the control law. Changes in MOI, mass flow rate, and actuator limitation are not taken into consideration. In [46], an adaptive SMC control algorithm is suggested for the quadcopter's altitude tracking in the presence of time-varying payload and ground effect. Position control, MOI variations with mass, and mass flow rate are ignored. Table 2.1 showcases the tabulated literature survey on control methodologies for quadcopters.

TABLE 2.1: Literature review of quadcopter.

Techniques	**Features**	**Varying Payload**	**Issues**
PID[14–18]	It's easy to design and implement.	✗	It's based on local linearization and accurate model is required for the closed loop performance.
LQR[19–23]	It's an optimal control scheme that is easy to design, implement, and computationally efficient.	✗	Its effectiveness heavily relies on the system model accuracy. It's based on local linearization.

Continued on next page

Continued from previous page

Techniques	**Features**	**Varying Payload**	**Issues**
H_∞ [24–27]	It's an optimal robust control scheme that offers a powerful framework for uncertain systems. It's easy to implement.	✗	It's based on local linearization.
LPV [28, 29]	It can handle large perturbations from the nominal condition.	✗	The variation in mass and inertia is not taken into account.
LPV [30]	Switched LPV approach is designed to handle huge attitude angles and external disturbances.	✗	Varying mass and inertia are not considered.
BSC [31–34]	It can handle complex nonlinearities and uses Lyapunov stability analysis to guarantee the system stability.	✗	Its closed loop performance depends on the model accuracy. Variation in the mass and inertia are not considered.
SMC [35]	It's a robust control scheme that can handle uncertainties and disturbances.	✗	Varying mass and inertia are not taken into account.
ISMC [36]	It's an extension of SMC that reduces chattering and improve robustness and steady-state accuracy.	✗	Mass and inertia variations have not been accounted for.

Continued on next page

Continued from previous page

Techniques	**Features**	**Varying Payload**	**Issues**
RBSMC [37]	RBSMC control technique is designed for position control of quadcopter to handle uncertainties and disturbances.	✗	Variation in the mass and inertia are ignored.
ASMC [38]	It's proposed for quadcopter trajectory tracking under parametric uncertainties, unknown disturbances, and actuators constraints.	✗	Varying mass and variation in inertia with mass have not been taken into consideration.
LPV [39]	LPV controller is suggested for Attitude/Altitude control of quadcopter to handle rotors velocity variation and step change in mass.	✓	Longitudinal and latitudinal motions, and variation in inertia are ignored. The small angle assumption is employed and the control scheme is conservative due to coupling in the scheduling parameters.

Continued on next page

Continued from previous page

Techniques	**Features**	**Varying Payload**	**Issues**
LPV [40]	LPV H_∞ controller is recommended to control the quadcopter rotational dynamics subject to time-varying inertia and variation in the rotors speed.	✓	PD scheme is designed using small angle assumption. Mass variation is ignored during position control design. Dependency in scheduling parameters leads to conservatism.
LPV [41]	Robust LPV H_∞ controller is proposed for Altitude/Attitude stabilization of quadcopter to handle mass, inertia, and rotors velocity variations.	✓	Small angle approximation is considered and position control is not taken into consideration. The coupling in the scheduling parameters leads to conservative control.
LPV [42]	A switched LPV technique is suggested for the 3-DOF model of a quadcopter subject to large attitude angles, variable inertia, and outside disturbances.	✗	Position control dynamics and varying mass are not considered.

Continued on next page

Continued from previous page

Techniques	**Features**	**Varying Payload**	**Issues**
PID [43]	Self-tuning PID scheme is proposed for the reference tracking. Mass and wind disturbance estimators are suggested to cope with the system's mass variation and wind disturbance.	✓	Variation in inertia due to mass and mass flow rate are not taken into consideration.
ASMC [44]	It's advised to reduce the effect of variable load and wind disturbances. Only the changing mass is estimated using the adaptive estimation controller.	✓	Actuator limitations and mass flow rate are not considered, and chattering issues will exist due to the use of signum function in the control law.
ANFTSMC [45]	External disturbances and mass are estimated online. To address the chattering issue, the saturation function is used in place of the signum function.	✓	Changes in inertia with mass, mass flow rate, and actuator limitation are not taken into consideration.
ASMC [46]	It's suggested for the quadcopter's altitude tracking in the presence of varying payload and ground effect.	✓	Quadcopter position control, inertia variation with mass, and mass flow rate are ignored.

2.2 Research Gap

In sprayer drones, mass varies with a certain flow rate. The change in payload mass causes a variation in the moment of inertia (MOI). In addition, large tilt angles are required for high-speed trajectory tracking and external disturbance rejection. These variations in plant parameters (i.e., mass and inertia) and large tilt angles can degrade the performance and stability of the control scheme. In the LPV control algorithms described in the literature, time-varying mass and large tilt angles have not been considered simultaneously, whereas, in the nonlinear adaptive control schemes suggested for a quadcopter to handle time-varying mass, the controller gains will take time to adapt to the new values. In addition, the computation and execution of gains are online, which will increase the computational burden compared to the LPV approaches, where the gains are computed offline but executed online.

2.3 Problem Statement

As outlined in the research gap, the problem of position tracking of quadcopter in the presence of varying mass, varying inertia, wind disturbances, and actuator constraint has not been addressed in the literature.

2.4 Research Objectives

The research objectives are outlined as follows:

1. Derive the nonlinear model of a quadcopter with varying payload and wind disturbances.
2. Determine the varying parameters of a quadcopter using SOLIDWORKS and obtain model equations for these parameters through the curve fitting tool.

3. Develop a Linear Parameter-Varying (LPV) model of a quadcopter with varying payload and large tilt angles.

4. Validate the LPV model by comparing its response with the complete nonlinear model with varying payload.

5. Design an LPV control algorithm for quadcopter capable of accurately maintaining a desired position in the presence of variable payload, noise, and wind disturbances without actuator saturation.

6. Validate the proposed LPV technique using numerical simulations and compare the results with the H_∞ controller.

2.5 Chapter Summary

After the discussion on thesis objectives, proposed strategy, and research contribution in Chapter 1, in this chapter, a thorough review of past efforts for quadcopter control is discussed. The literature review is presented in Section 2.1 of this chapter. A literature survey helps to create a gap analysis. The gap analysis presented in Section 2.2 was achieved by the extensive literature review, which assisted in identifying the areas of concern in the previous studies. Finally, the chapter is concluded with a problem statement based on the research gap. In the next chapter, mathematical modeling of quadcopter with variable payload is discussed.

Chapter 3

Mathematical Modeling of Quadcopter

This chapter focuses on constructing a mathematical model for a quadcopter that accounts for varying payload. It provides essential background information necessary for comprehending the quadcopter with different payload configurations from a dynamic systems perspective. The chapter outlines a 6-degree-of-freedom (6-DOF) nonlinear model for the quadcopter with variable payload, detailing changes in system mass, moments of inertia, and equations governing these varying parameters. The nonlinear model is transformed into a 6-DOF linear parameter varying (LPV) model, essential for LPV control design, and a linear model, crucial for designing the linear controller. Additionally, the chapter concludes with the simulation of these mathematical models using MATLAB/SIMULINK software to validate their accuracy, with the nonlinear model serving as the benchmark for validation purposes.

3.1 Reference Frames

To derive the dynamic model of quadcopter, the first step is to define the coordinate frames. Two frames have to be defined [47],

1. Inertial frame ($\mathcal{F}^i$): defined also as World reference frame.

2. Body frame ($\mathcal{F}^b$): centered at the center of gravity of the quadcoptor.

The ($\mathcal{F}^i$) is inertial coordinate system that is fixed to the earth. The ($\mathcal{F}^b$) is the body coordinate system that is fixed to the quadcopter's body. We use the NED (North-East-Down) convention for the inertial coordinate system, with the x-or roll axis along the front of the quadcopter, the y-or pitch axis to the right, and the z-or yaw axis down. These frames are important as on board sensors like accelerometers and gyroscopes measure information with respect to the body frame, and sensors like GPS and pressure sensors measure information with respect to the inertial frame.

3.1.1 Rotation Matrices

To transform the coordinates, i.e., from body frame to inertial frame, transformation matrices are used [48–50]. By considering right-hand oriented coordinate system, the three different rotations can be described by:

- R(x,ϕ) represent rotation about x-axis.
- R(y,θ) represent rotation about y-axis.
- R(z,ψ) represent rotation about z-axis.

The rotation matrix from the body frame to the inertial frame is given by:

$$R_b^i = R(x,\phi).R(y,\theta).R(z,\psi) \tag{3.1}$$

This leads to:

$$R_b^i = \begin{bmatrix} 1 & 0 & 0 \\ 0 & c(\phi) & -s(\phi) \\ 0 & s(\phi) & c(\phi) \end{bmatrix} \begin{bmatrix} c(\theta) & 0 & s(\theta) \\ 0 & 1 & 0 \\ -s(\theta) & 0 & c(\theta) \end{bmatrix} \begin{bmatrix} c(\psi) & -s(\psi) & 0 \\ s(\psi) & c(\psi) & 0 \\ 0 & 0 & 1 \end{bmatrix} \tag{3.2}$$

This results in:

$$R_b^i = \begin{bmatrix} c(\psi)c(\theta) & s(\phi)c(\psi)s(\theta) - s(\psi)c(\phi) & s(\theta)c(\phi)c(\psi) + s(\psi)s(\phi) \\ s(\psi)c(\theta) & s(\theta)s(\psi)s(\phi) + c(\psi)c(\phi) & c(\phi)s(\psi)s(\theta) - c(\psi)s(\phi) \\ -s(\theta) & c(\theta)s(\phi) & c(\theta)c(\phi) \end{bmatrix} \tag{3.3}$$

Similarly, the complete rotation matrix from the inertial frame to the body frame is given by:

$$\mathcal{R}_i^b = (R_b^i)^T \tag{3.4}$$

Hence, we can write:

$$\mathcal{R}_i^b = \begin{bmatrix} c(\psi)c(\theta) & s(\psi)c(\theta) & -s(\theta) \\ s(\phi)c(\psi)s(\theta) - s(\psi)c(\phi) & s(\theta)s(\psi)s(\phi) + c(\psi)c(\phi) & c(\theta)s(\phi) \\ s(\theta)c(\phi)c(\psi) + s(\psi)s(\phi) & c(\phi)s(\psi)s(\theta) - c(\psi)s(\phi) & c(\theta)c(\phi) \end{bmatrix} \tag{3.5}$$

where:

$$s(\theta) = sin(\theta) \text{ and } c(\theta) = cos(\theta).$$

3.1.2 Angular Rates

The angular transformation matrix from $(\dot{\phi}, \dot{\theta}, \dot{\psi})$ to body angular rates (P_v, Q_v, R_v) is given by [51, 52]:

$$\begin{bmatrix} P_v \\ Q_v \\ R_v \end{bmatrix} = R_r \begin{bmatrix} \dot{\phi} \\ \dot{\theta} \\ \dot{\psi} \end{bmatrix} \tag{3.6}$$

where:

$$R_r = \begin{bmatrix} 1 & 0 & -s(\theta) \\ 0 & c(\theta) & s(\phi)c(\theta) \\ 0 & -s(\phi) & c(\phi)c(\theta) \end{bmatrix} \tag{3.7}$$

3.1.3 Quadcopter Kinematics Equations

The state variables x, y, and z are in inertial frame quantities, whereas the velocities U, V, and W are in body frame quantities. Therefore, the relationship between the derivatives of position $(\dot{x}, \dot{y}, \dot{z})$ (i.e., velocities in the inertial frame) and velocities in the body frame is given by

$$\begin{bmatrix} \dot{x} \\ \dot{y} \\ \dot{z} \end{bmatrix} = R_b^i \begin{bmatrix} U \\ V \\ W \end{bmatrix} \tag{3.8}$$

We can write:

$$\begin{bmatrix} U \\ V \\ W \end{bmatrix} = (R_b^i)^{-1} \begin{bmatrix} \dot{x} \\ \dot{y} \\ \dot{z} \end{bmatrix} = (R_b^i)^T \begin{bmatrix} \dot{x} \\ \dot{y} \\ \dot{z} \end{bmatrix} \tag{3.9}$$

This result in:

$$\begin{cases} U &= c(\psi)c(\theta)\dot{x} + s(\psi)c(\theta)\dot{y} - s(\theta)\dot{z} \\ V &= (s(\phi)c(\psi)s(\theta) - s(\psi)c(\phi))\dot{x} + (s(\theta)s(\psi)s(\phi) + c(\psi)c(\phi))\dot{y} + c(\theta)s(\phi)\dot{z} \\ W &= (s(\theta)c(\phi)c(\psi) + s(\psi)s(\phi))\dot{x} + (c(\phi)s(\psi)s(\theta) - c(\psi)s(\phi))\dot{y} + c(\theta)c(\phi)\dot{z} \end{cases} \tag{3.10}$$

3.2 Quadcopter Dynamic Modeling

Quadcopter with variable payload can be mathematically modeled using the Newton and Euler equations. The quadcopter's translational dynamics with varying

mass is given by [53, 54]

$$\sum F = \frac{d}{dt}(P) = m\frac{d}{dt}(v) + v\frac{d}{dt}(m) \tag{3.11}$$

where $\sum F$ stands for the resultant force acting on the quadcopter in the inertial frame, P represents the linear momentum, m denotes the quadcopter's mass with variable payload, and $v = [\dot{x} \quad \dot{y} \quad \dot{z}]^T$ indicates the quadcopter's transnational velocity in the inertial frame.

The resultant force $\sum F$ is given by:

$$\sum F = mge_z - R_b^i T - W_f \tag{3.12}$$

Equation (3.12), leads to

$$\sum F = mg \begin{bmatrix} 0 \\ 0 \\ 1 \end{bmatrix} - R_b^i \begin{bmatrix} 0 \\ 0 \\ T \end{bmatrix} - \begin{bmatrix} W_{fx} \\ W_{fy} \\ W_{fz} \end{bmatrix} \tag{3.13}$$

where,

$$T = \sum_{i=1}^{4} T_i = T_1 + T_2 + T_3 + T_4 \tag{3.14}$$

T represents the thrust force exerted by the rotors, whereas W_{fx}, W_{fy}, and W_{fz} represent the wind forces in the x, y, and z directions, respectively. The wind forces can be expressed as [55]

$$\begin{bmatrix} W_{fx} \\ W_{fy} \\ W_{fz} \end{bmatrix} = \begin{bmatrix} k_s|\dot{x} - \dot{x}_w|(\dot{x} - \dot{x}_w) \\ k_s|\dot{y} - \dot{y}_w|(\dot{y} - \dot{y}_w) \\ k_u|\dot{z} - \dot{z}_w|(\dot{z} - \dot{z}_w) \end{bmatrix} \tag{3.15}$$

$\begin{bmatrix} \dot{x} & \dot{y} & \dot{z} \end{bmatrix}^T$ and $\begin{bmatrix} \dot{x}_w & \dot{y}_w & \dot{z}_w \end{bmatrix}^T$ show the translational and wind velocity, and the parameters k_s and k_u indicate the drag factors on the lower-upper faces and sides of the quadcopter, respectively.

Equation (3.13) can be written as:

$$\begin{cases} \sum F_x &= -(sin(\theta)cos(\phi)cos(\psi) + sin(\psi)sin(\phi))T - W_{fx} \\ \sum F_y &= -(cos(\phi)sin(\psi)sin(\theta) - cos(\psi)sin(\phi))T - W_{fy} \\ \sum Fz &= mg - (cos(\theta)cos(\phi))T - W_{fz} \end{cases} \tag{3.16}$$

Using equations (3.16) and (3.11), we can write:

$$\begin{cases} m\ddot{x} &= -\left(sin\theta cos\phi cos\psi + sin\psi sin\phi\right)T - \dot{m}\dot{x} - W_{fx} \\ m\ddot{y} &= -\left(cos\phi sin\psi sin\theta - cos\psi sin\phi\right)T - \dot{m}\dot{y} - W_{fy} \\ m\ddot{z} &= -cos\theta cos\phi T + mg - \dot{m}\dot{z} - W_{fz} \end{cases} \tag{3.17}$$

Furthermore, referring to [53, 54], the quadcopter's rotational dynamics with varying inertia in the inertial frame is given by

$$\sum M = \frac{d}{dt}(\mathcal{H}) = J\frac{d}{dt}(\mathcal{W}) + \mathcal{W}\frac{d}{dt}(J) + \mathcal{W} \times \ J\mathcal{W} \tag{3.18}$$

where $\sum M$ indicates the net moment, $\mathcal{H}$ represents the angular momentum, J denotes the inertia tensor, and $\mathcal{W} = [\dot{\phi} \ \ \dot{\theta} \ \ \dot{\psi}]^T$ shows the angular speed.

$$\mathcal{W} \times \ \mathcal{H} = \hat{i}(\dot{\theta}\mathcal{H}_z - \dot{\psi}\mathcal{H}_y) + \hat{j}(\dot{\phi}\mathcal{H}_x - \dot{\psi}\mathcal{H}_z) + \hat{k}(\dot{\phi}\mathcal{H}_y - \dot{\theta}\mathcal{H}_x) \tag{3.19}$$

The inertia tensor J is given by [56]:

$$J = \begin{bmatrix} I_x & 0 & 0 \\ 0 & I_y & 0 \\ 0 & 0 & I_z \end{bmatrix} \tag{3.20}$$

The net moment $\sum M$ can be written as:

$$\sum M = \begin{bmatrix} \sum M_\phi \\ \sum M_\theta \\ \sum M_\psi \end{bmatrix} = \begin{bmatrix} \tau_\phi + J_r\Omega_r\dot{\theta} \\ \tau_\theta - J_r\Omega_r\dot{\phi} \\ \tau_\psi \end{bmatrix} \tag{3.21}$$

By using equations (3.18), (3.19), and (3.20), we can write:

$$\begin{cases} \tau_\phi = I_x\ddot{\phi} - (I_y - I_z)\dot{\theta}\dot{\psi} + \dot{I}_x\dot{\phi} - J_r\Omega_r\dot{\theta} \\ \tau_\theta = I_y\ddot{\theta} - (I_z - I_x)\dot{\psi}\dot{\phi} + \dot{I}_y\dot{\theta} + J_r\Omega_r\dot{\phi} \\ \tau_\psi = I_z\ddot{\psi} - (I_x - I_y)\dot{\phi}\dot{\theta} + \dot{I}_z\dot{\psi} \end{cases} \tag{3.22}$$

where τ_ϕ, τ_θ, and τ_ψ represent the rolling, pitching, and yawning moments, respectively. $J_r\Omega_r\dot{\theta}$ and $J_r\Omega_r\dot{\phi}$ represent the rotor gyroscopic effect. J_r represents the rotor inertia, $\Omega_r = \Omega_1 + \Omega_3 - \Omega_2 - \Omega_4$, while $\Omega_i\,(i = 1, 2, 3, 4)$ indicates the speed of rotors.

Equation (3.22) can be written as:

$$\begin{cases} I_x\ddot{\phi} = (I_y - I_z)\dot{\theta}\dot{\psi} - \dot{I}_x\dot{\phi} + J_r\Omega_r\dot{\theta} + \tau_\phi \\ I_y\ddot{\theta} = (I_z - I_x)\dot{\psi}\dot{\phi} - \dot{I}_y\dot{\theta} - J_r\Omega_r\dot{\phi} + \tau_\theta \\ I_z\ddot{\psi} = (I_x - I_y)\dot{\phi}\dot{\theta} - \dot{I}_z\dot{\psi} + \tau_\psi \end{cases} \tag{3.23}$$

Control signals are defined for moments and thrust force, which are as follows,

$$\begin{bmatrix} \tau_\phi \\ \tau_\theta \\ \tau_\psi \\ T \end{bmatrix} = \begin{bmatrix} U_1 \\ U_2 \\ U_3 \\ U_4 \end{bmatrix} \tag{3.24}$$

The relationship between control signals and motor commands is as follows: [57, 58]

$$\begin{bmatrix} \cap_1 \\ \cap_2 \\ \cap_3 \\ \cap_4 \end{bmatrix} = \begin{bmatrix} \frac{1}{2\sqrt{2}lK_f} & \frac{1}{2\sqrt{2}lK_f} & -\frac{1}{4K_m} & \frac{1}{4K_f} \\ -\frac{1}{2\sqrt{2}lK_f} & \frac{1}{2\sqrt{2}lK_f} & \frac{1}{4K_m} & \frac{1}{4K_f} \\ -\frac{1}{2\sqrt{2}lK_f} & -\frac{1}{2\sqrt{2}lK_f} & -\frac{1}{4K_m} & \frac{1}{4K_f} \\ \frac{1}{2\sqrt{2}lK_f} & -\frac{1}{2\sqrt{2}lK_f} & \frac{1}{4K_m} & \frac{1}{4K_f} \end{bmatrix} \begin{bmatrix} U_1 \\ U_2 \\ U_3 \\ U_4 \end{bmatrix} \tag{3.25}$$

where $\cap_i\,(i = 1, 2, 3, 4)$ represent the squared speed references of the motor (i.e., $\cap_i = \Omega_i^2$).

By combining (3.17) and (3.23), the complete nonlinear 6-DOF model of quadcopter can be written as:

$$\begin{cases} I_x\ddot{\phi} = U_1 + (I_y - I_z)\dot{\theta}\dot{\psi} - \dot{I}_x\dot{\phi} + J_r\Omega_r\dot{\theta} \\ I_y\ddot{\theta} = U_2 + (I_z - I_x)\dot{\psi}\dot{\phi} - \dot{I}_y\dot{\theta} - J_r\Omega_r\dot{\phi} \\ I_z\ddot{\psi} = U_3 + (I_x - I_y)\dot{\phi}\dot{\theta} - \dot{I}_z\dot{\psi} \\ m\ddot{x} = -\left(sin\theta cos\phi cos\psi + sin\psi sin\phi\right)U_4 - \dot{m}\dot{x} - W_{fx} \\ m\ddot{y} = -\left(cos\phi sin\psi sin\theta - cos\psi sin\phi\right)U_4 - \dot{m}\dot{y} - W_{fy} \\ m\ddot{z} = -cos\theta cos\phi U_4 - \dot{m}\dot{z} + mg - W_{fz} \end{cases} \tag{3.26}$$

Description of symbols used in quadcopter modeling, and quadcopter's parameters with full payload are shown in Table. 3.1 and Table. 3.2, respectively.

TABLE 3.1: Quadcopter parameters with full payload.

Symbol	**Value**	**Unit**
$\overline{m}$	1.0497×10^{-1}	kg
$\overline{I_x}$	1.1568×10^{-4}	kgm^2
$\overline{I_y}$	1.1378×10^{-4}	kgm^2
$\overline{I_z}$	1.2595×10^{-4}	kgm^2
l	$6.24e-02 \times 10^{-2}$	m
J_r	1.4338×10^{-4}	kgm^2
k_s	2.8×10^{-2}	kg/m
k_u	5.4×10^{-2}	kg/m
K_f	6.5330×10^{-4}	$N/(rad^2/sec^2)$
K_m	1.5769×10^{-6}	$Nm/(rad^2/sec^2)$
g	9.81	m/sec^2

TABLE 3.2: Description of symbols used in quadcopter modeling.

Symbol	**Unit**	**Description**
m	kg	Mass of quadcopter with varying paylaod
I_x	kgm^2	Inertia about the x-axis
I_y	kgm^2	Inertia about the y-axis
I_z	kgm^2	Inertia about the z-axis
l	m	Length of an arm
J_r	kgm^2	Rotor inertia
k_u	kg/m	Upward Drag factors
k_s	kg/m	Sideward drag factor
K_f	$N/(rad^2/sec^2)$	Thrust coefficient
K_m	$Nm/(rad^2/sec^2)$	Thrust coefficient
g	m/sec^2	Acceleration due to gravity
T	N	Thrust
τ_ϕ	Nm	Rolling moment
τ_θ	Nm	Pitching moment
τ_ψ	Nm	Yawing moment
ϕ	rad	Roll angle
θ	rad	Pitch angle
ψ	rad	Yaw angle
x	m	x-position
y	m	y-position
z	m	z-position
U	m/sec	Velocity in x-direction in the body frame
V	m/sec	Velocity in y-direction in the body frame
W	m/sec	Velocity in z-direction in the body frame

3.2.1 Variation in the System's Mass and Moments of Inertia Parameters

To develop the model equations for varying mass and varying inertia, we have used SOLIDWORKS. The 3D-CAD (3-dimensional computer-aided design) model of the quadcopter with payload developed in SOLIDWORKS is shown in Figure 2.1. The selected full payload mass is 0.042 kg , with an empty mass of 0.01 kg. It has a capacity of 0.032 $liters$ of water. The choice of payload mass was determined based on the quadcopter's total thrust. When the payload is full, the thrust can reach up to 80% of its maximum value. The mass and MOI values are noted at different levels of the water in the liquid tank. The values recorded are listed in Table. 3.3. The curve fitting toolbox available in MATLAB is used to find the model equations for mass and MOI. The variation in the values of the system's mass and MOI is shown in Figures 3.1 and 3.2.

The root mean squared error (RMSE) is used to assess the goodness of fit. It is calculated by taking the square root of the average of the squared differences between the predicted values and the actual values. Mathematically, it can be expressed as follows:

$$RMSE = \sqrt{\frac{1}{n}\sum_{i=1}^{n}(y_i - \hat{y}_i)^2} \tag{3.27}$$

where n represents the number of observations in the dataset, y_i represents the actual (observed) value of the ith data point, and $\hat{y}_i$ represents the predicted value of the ith data point.

A parameter ℓ has been introduced which is given as:

$$\ell = \frac{\overline{h} - h}{\overline{h}} \tag{3.28}$$

where h represents the level of the water in the tank and $\overline{h}$ indicates the water level when the payload is filled to capacity.

TABLE 3.3: Mass and inertia values at different water levels.

S.No	**Water Level (m)**	**Mass** (kg)	I_x (kgm^2)	I_y (kgm^2)	I_z (kgm^2)
1	1.71×10^{-2}	1.0497×10^{-1}	1.1568×10^{-4}	1.1378×10^{-4}	1.2595×10^{-4}
2	1.52×10^{-2}	1.0141×10^{-1}	1.1311×10^{-4}	1.1254×10^{-4}	1.2396×10^{-4}
3	1.33×10^{-2}	9.7844×10^{-2}	1.1022×10^{-4}	1.1099×10^{-4}	1.2196×10^{-4}
4	1.14×10^{-2}	9.4281×10^{-2}	1.0697×10^{-4}	1.0906×10^{-4}	1.1994×10^{-4}
5	9.47×10^{-3}	9.0756×10^{-2}	1.0331×10^{-4}	1.067×10^{-4}	1.1794×10^{-4}
6	7.57×10^{-3}	8.7194×10^{-2}	9.910×10^{-5}	1.0380×10^{-4}	1.1590×10^{-4}
7	5.68×10^{-3}	8.3650×10^{-2}	9.431×10^{-5}	1.0028×10^{-4}	1.1386×10^{-4}
8	3.78×10^{-3}	8.0088×10^{-2}	8.876×10^{-5}	9.601×10^{-5}	1.1179×10^{-4}
9	1.86×10^{-3}	7.6488×10^{-2}	8.230×10^{-5}	9.080×10^{-5}	1.0967×10^{-4}
10	0	7.3002×10^{-2}	7.506×10^{-5}	8.477×10^{-5}	1.0760×10^{-4}

The equations of the mass and MOI obtained using curve fitting are:

$$\begin{cases} m = a_1\ell + a_2 \\ I_x = b_1m^2 + b_2m + b_3 \\ I_y = c_1m^2 + c_2m + c_3 \\ I_z = d_1m + d_2 \end{cases} \tag{3.29}$$

The derivatives are:

$$\begin{cases} \dot{m} = a_1\dot{\ell} \\ \dot{I}_x = 2b_1m\dot{m} + b_2\dot{m} \\ \dot{I}_y = 2c_1m\dot{m} + c_2\dot{m} \\ \dot{I}_z = d_1\dot{m} \end{cases} \tag{3.30}$$

The values of parameters in equation (3.29) are given in Table. 3.4.

TABLE 3.4: Parameter values.

Parameter	**Value**	**Unit**
a_1	-3.1967×10^{-2}	kg
a_2	1.0501×10^{-1}	kg
b_1	-2.3181×10^{-2}	$kg^{-1}m^2$
b_2	5.3709×10^{-3}	m^2
b_3	-1.9308×10^{-4}	kgm^2
c_1	-2.3731×10^{-2}	$kg^{-1}m^2$
c_2	5.1061×10^{-3}	m^2
c_3	-1.6102×10^{-4}	kgm^2
d_1	5.7349×10^{-4}	m^2
d_2	6.5828×10^{-5}	kgm^2

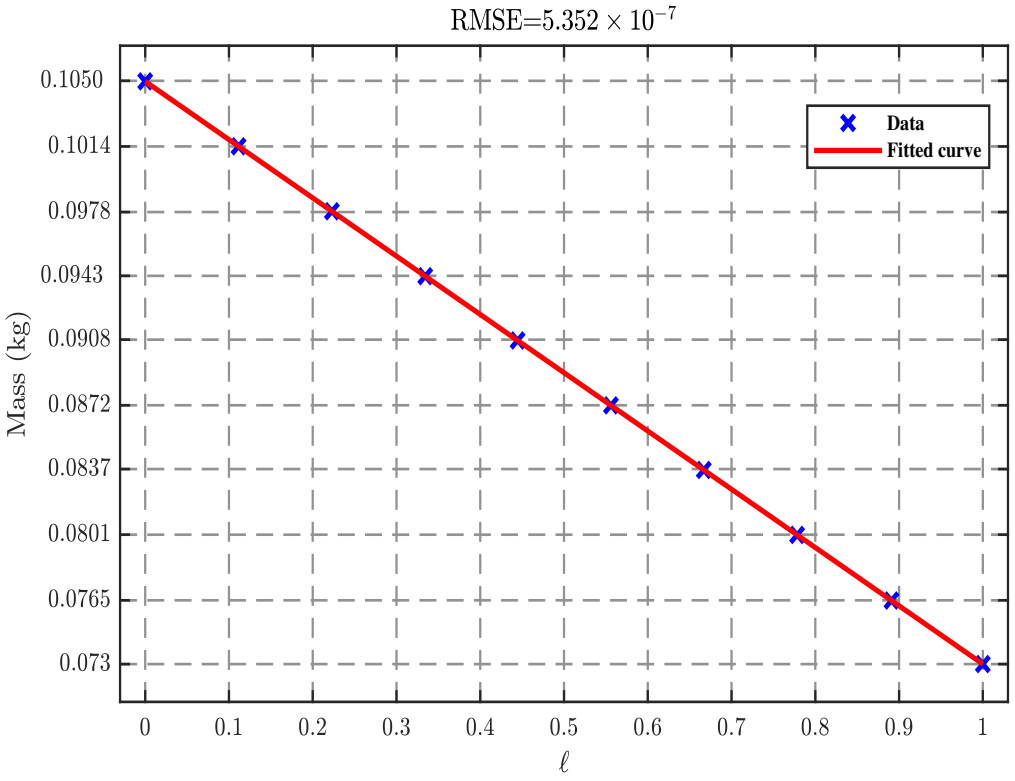

FIGURE 3.1: Variation in mass with parameter ℓ

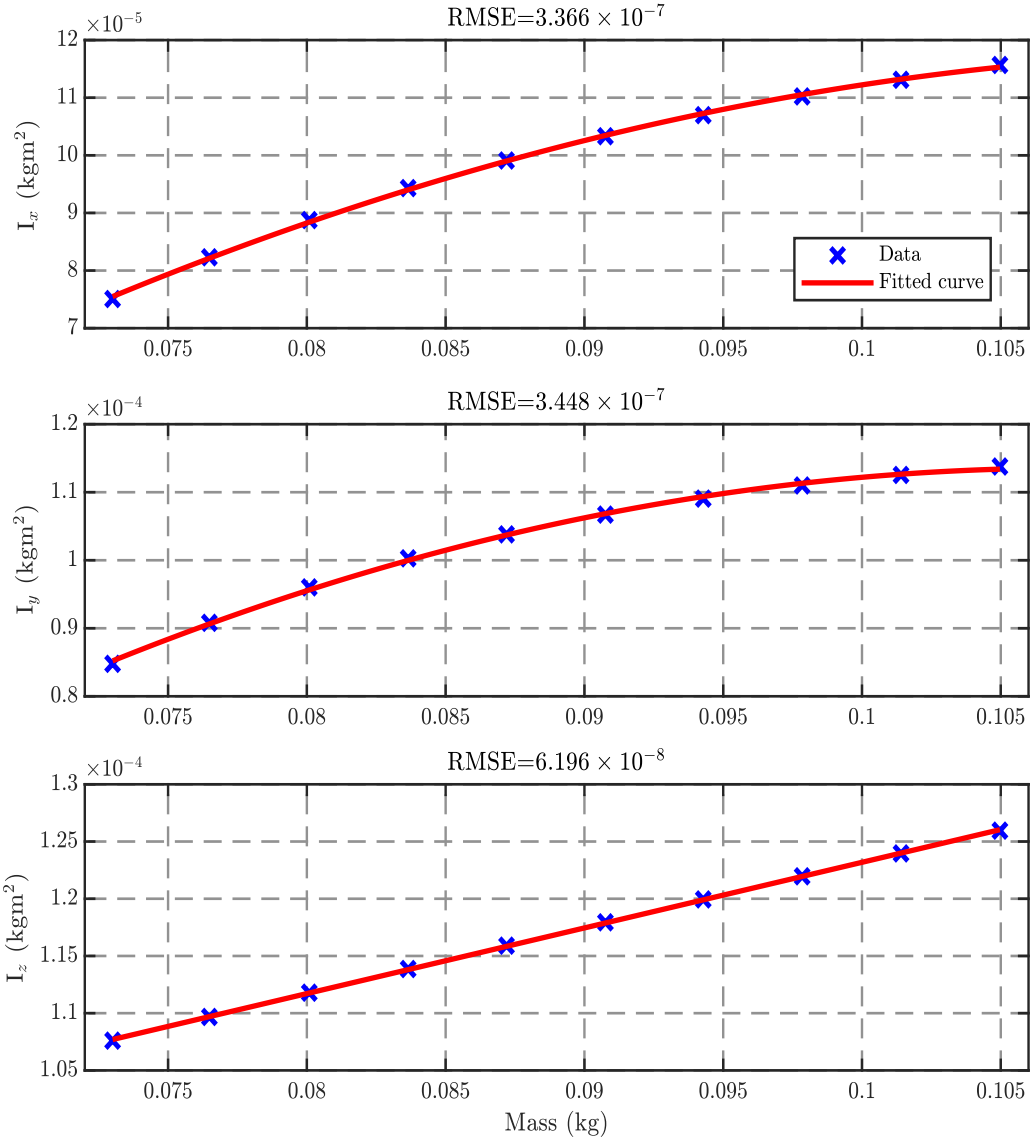

FIGURE 3.2: Variation in MOI with mass

3.3 LPV Model

The LPV model can be described by a set of differential equations that relate the system's state, inputs, outputs, and parameters. These equations are typically expressed in the form of:

$$\begin{cases} dx(t)/dt &= f(x(t), u(t), \rho(t)) \\ y(t) &= g(x(t), u(t), \rho(t)) \end{cases} \tag{3.31}$$

Here, $f(.)$ represents the system dynamics that describe how the state evolves over time, and g(.) represents the output equation that relates the state, inputs, and parameters to the system outputs. The state vector, denoted as $x(t)$, represents the internal state of the system at time t. The input vector, denoted as $u(t)$, represents the inputs or control signals applied to the LPV system. The parameter vector, denoted as $\rho(t)$, represents the time-varying parameters or scheduling variables that influence the system dynamics. These parameters vary with time or with the operating conditions and can affect the system's behaviour, such as its stability, performance, or response characteristics.

The affine LPV model can be described by the following set of state-space equations [59]:

$$G: \begin{cases} E(\rho(t))\dfrac{dx(t)}{dt} &= A(\rho(t))x(t) + B(\rho(t))u(t) \\ y(t) &= C(\rho(t))x(t) + D(\rho(t))u(t) \end{cases} \tag{3.32}$$

Here, $E(\rho(t))$, $A(\rho(t))$, $B(\rho(t))$, $C(\rho(t))$, and $D(\rho(t))$ represent parameter-dependent matrices that capture the linear dynamics of the system. These matrices can vary as a function of the parameters $\rho(t)$.

where,

$x \epsilon R^n$ is model state vector.

$\rho \epsilon R^s$ is time varying vector.

$u \epsilon R^m$ is model input vector.

$y \epsilon R^p$ is model output vector.

Input, system, and output matrices can be written as:

$$E(\rho(t)) = E_0 + \sum_{i=1}^{i=N} \rho_i(t) E_i \tag{3.33}$$

$$A(\rho(t)) = A_0 + \sum_{i=1}^{i=N} \rho_i(t) A_i \tag{3.34}$$

$$B(\rho(t)) = B_0 + \sum_{i=1}^{i=N} \rho_i(t) B_i \tag{3.35}$$

$$C(\rho(t)) = C_0 + \sum_{i=1}^{i=N} \rho_i(t) C_i \tag{3.36}$$

$$D(\rho(t)) = D_0 + \sum_{i=1}^{i=N} \rho_i(t) D_i \tag{3.37}$$

3.3.1 LPV Modeling of Quadcopter

The LPV modeling approach provides a flexible and powerful framework to represent complex dynamic systems. The LPV model for a dynamic system is not unique, as it allows for various representations that capture the system's behaviour under different operating conditions. Multiple LPV models can exist for a plant, each approximating the system's dynamics from distinct perspectives. The construction of an LPV model involves selecting appropriate time-varying parameters that best describe the system's behaviour across its operating range. These parameters act as adjustable coefficients that vary with changing operating conditions. The time-varying parameters chosen in the LPV model determine the complexity and effectiveness of the control system.

To develop the affine LPV model of quadcopter with varying payload, the following assumptions are taken into account [29, 42].

- The sine and cosine of tilt angles are approximated by the second-order Taylor's expansion which is given as:

$$\begin{cases} sin(\phi) \approx \phi - \phi^3/6 \\ cos(\phi) \approx 1 - \phi^2/2 \\ sin(\theta) \approx \theta - \theta^3/6 \\ cos(\theta) \approx 1 - \theta^2/2 \end{cases} \tag{3.38}$$

- The input $U_4 \approx mg + u_4$ and yaw angle $\psi \approx 0$ are considered to make the dependency between system states $\left(i.e., \begin{bmatrix} x & y \end{bmatrix}^T \; on \; \begin{bmatrix} \phi & \theta \end{bmatrix}^T \right)$ explicitly.

Using the above assumptions, and considering the small rotor gyro effect, the simplified 6-DOF nonlinear model is obtained for the nonlinear model of quadcopter with varying payload given in equation (3.26), which is as follows,

$$\begin{cases} I_x\ddot{\phi} = U_1 - \dot{I}_x\dot{\phi} \\ I_y\ddot{\theta} = U_2 - \dot{I}_y\dot{\theta} \\ I_z\ddot{\psi} = U_3 - \dot{I}_z\dot{\psi} \\ \ddot{x} = -\left(\theta - \dfrac{\theta^3}{6}\right)\left(1 - \dfrac{\phi^2}{2}\right)g - \dfrac{\dot{m}}{m}\dot{x} - \dfrac{W_{fx}}{m} \\ \ddot{y} = \left(\phi - \dfrac{\phi^3}{6}\right)g - \dfrac{\dot{m}}{m}\dot{y} - \dfrac{W_{fy}}{m} \\ m\ddot{z} = -\left(1 - \dfrac{\theta^2}{2}\right)\left(1 - \dfrac{\phi^2}{2}\right)(mg + u_4) + mg - \dot{m}\dot{z} - W_{fz} \end{cases} \tag{3.39}$$

Equation (3.39) depicts the simplified 6-degree-of-freedom (6-DOF) model of a quadcopter, considering variable payload and significant tilt angles, specifically the roll angle (ϕ) and pitch angle (θ).

By employing equations (3.29) and (3.30), we can express equation (3.39) in an alternative form:

$$\begin{cases} (b_1m^2 + b_2m + b_3)\ddot{\phi} = U_1 - (2b_1m\dot{m} + b_2\dot{m})\dot{\phi} \\ (c_1m^2 + c_2m + c_3)\ddot{\theta} = U_2 - (2c_1m\dot{m} + c_2\dot{m})\dot{\theta} \\ (d_1m + d_2)\ddot{\psi} = U_3 - d_1\dot{m}\dot{\psi} \\ \ddot{x} = -g\theta + \dfrac{g}{2}\phi^2\theta + \dfrac{g}{6}\theta^2\theta - \dfrac{\dot{m}}{m}\dot{x} - \dfrac{1}{m}d_x \\ \ddot{y} = g\phi - \dfrac{g}{6}\phi^2\phi - \dfrac{\dot{m}}{m}\dot{y} - \dfrac{1}{m}d_y \\ \rho_1\ddot{z} = \dfrac{1}{2}\phi^2u_4 + \dfrac{1}{2}\theta^2u_4 - u_4 - \dot{m}\dot{z} - d_z \end{cases} \tag{3.40}$$

The LPV model of the quadcopter, derived from equation (3.40), is presented as follows. This model offers a comprehensive representation, capturing the dynamic characteristics of the quadcopter under varying conditions. It serves as a valuable tool for analyzing and predicting the quadcopter's behavior in diverse operational scenarios.

$$\begin{cases} (b_1\rho_1 + b_2 + b_3\rho_2)\,\ddot{\phi} = \rho_2 U_1 - \left(2b_1\dot{\phi} + b_2\rho_2\dot{\phi}\right) d_r \\ (c_1\rho_1 + c_2 + c_3\rho_2)\,\ddot{\theta} = \rho_2 U_2 - \left(2c_1\dot{\theta} + c_2\rho_2\dot{\theta}\right) d_r \\ (d_1\rho_1 + d_2)\,\ddot{\psi} = U_3 - d_1 d_r\dot{\psi} \\ \ddot{x} = -g\theta + \dfrac{g}{2}\rho_3\theta + \dfrac{g}{6}\rho_4\theta - d_r\rho_2\dot{x} - \rho_2 d_x \\ \ddot{y} = g\phi - \dfrac{g}{6}\rho_3\phi - d_r\rho_2\dot{y} - \rho_2 d_y \\ \rho_1\ddot{z} = \dfrac{1}{2}\rho_3 u_4 + \dfrac{1}{2}\rho_4 u_4 - u_4 - d_r\dot{z} - d_z \end{cases} \tag{3.41}$$

where:

$\rho = [\rho_1 \quad \rho_2 \quad \rho_3 \quad \rho_4]^T$ is a time-varying parameters vector. The terms $(\phi^2\theta^2)/4$ and $(\phi^2\theta^3)/12$ are neglected because of their higher power and relatively modest contribution.

$\begin{bmatrix} d_x & d_y & d_z & d_r \end{bmatrix}^T$ denote the bounded disturbances and are given as:

$$\begin{cases} d_x = W_{fx} \\ d_y = W_{fy} \\ d_z = W_{fz} - \dfrac{mg\phi^2}{2} - \dfrac{mg\theta^2}{2} \\ d_r = \dot{m} \end{cases} \tag{3.42}$$

The scheduling parameters of the quadcopter LPV model are:

$$\begin{cases} \rho_1 = m \in \begin{bmatrix} 1.05e-1 & 7.3e-2 \end{bmatrix} = \begin{bmatrix} \overline{\rho_1} & \underline{\rho_1} \end{bmatrix} \\ \rho_2 = \dfrac{1}{m} \in \begin{bmatrix} 13.71 & 9.51 \end{bmatrix} = \begin{bmatrix} \overline{\rho_2} & \underline{\rho_2} \end{bmatrix} \\ \rho_3 = \phi^2 \in \begin{bmatrix} (\frac{\pi}{3})^2 & 0 \end{bmatrix} = \begin{bmatrix} \overline{\rho_3} & \underline{\rho_3} \end{bmatrix} \\ \rho_4 = \theta^2 \in \begin{bmatrix} (\frac{\pi}{3})^2 & 0 \end{bmatrix} = \begin{bmatrix} \overline{\rho_4} & \underline{\rho_4} \end{bmatrix} \end{cases} \tag{3.43}$$

The significant contributions of the proposed model, distinguishing it from prior research, can be summarized as follows:

1. A novel 6 DOF LPV model is introduced, accommodating variable mass, variable inertia, mass flow rate, large tilt angles, and wind disturbances for the quadcopter system.

2. Model equations for variable mass and variable Moment of Inertia (MOI) are meticulously developed utilizing a curve fitting tool. Notably, a triangle polytope is chosen over a rectangular polytope to reduce the number of vertices in the LPV control system. This strategic choice aims to minimize computational load and conservatism in the LPV control strategy.

3.3.2 Linear Model of Quadcopter

The nonlinear model is linearized around hovering condition, allowing the system nonlinear dynamics to be effectively described by a linearized model when operating around the hovering state [27, 60–62]. The following assumptions are considered to obtain the simplified model of the quadcopter.

$$\begin{cases} \sin(\phi) \approx \phi \\ \cos(\phi) \approx 1 \\ \sin(\theta) \approx \theta \\ \cos(\theta) \approx 1 \\ \psi \approx 0 \\ U_4 \approx m_{avg} g + u_4 \end{cases} \tag{3.44}$$

TABLE 3.5: Nominal parameters of the quadcopter.

Symbol	**Value**	**Unit**
m_{avg}	$1.0497e-1 \times 10^{-1}$	kg
I_{xavg}	1.1568×10^{-4}	kgm^2
I_{yavg}	1.1378×10^{-4}	kgm^2
$\mathrm{I_{zavg}}$	1.2595×10^{-4}	kgm^2

Using the above assumptions, the linearized model for the quadcopter is obtained, which is as follows:

$$\begin{cases} \ddot{\phi} = \frac{u_1}{I_{xavg}} \\ \ddot{\theta} = \frac{u_2}{I_{yavg}} \\ \ddot{\psi} = \frac{u_3}{I_{zavg}} \\ \ddot{x} = -g\theta \\ \ddot{y} = g\phi \\ \ddot{z} = -\frac{u_4}{m_{avg}} \end{cases} \tag{3.45}$$

Equation (3.45) represent the 6-DOF linearized model of the quadcopter.
Table. 3.5 provides the values of the parameters used in the linearized model.

3.4 Model Validation

Model validation is a crucial step in the modeling process.It involves assessing the accuracy, reliability, and predictive capability of a model. It aims to determine whether the model adequately captures the behavior of the real system it represents. The procedure for validating an approximate model using a nonlinear model as a benchmark is given as:

1. **Define the Nonlinear Model:**

   Define the nonlinear model that represents the actual system. This model should capture all the nonlinearities and complexities of the system's behavior that is under study.

2. **Develop the Approximate Model:**

   Create the approximate model that you intend to validate. This could be a simplified linear model, reduced-order model, or any other approximation technique used to simplify the system's complexity.

3. **Simulate Both Models:**

   Simulate both the nonlinear model and the approximate model under identical conditions. This could involve providing the same inputs or initial conditions to both models.

4. **Compare Model Responses:**

   Compare the responses of the nonlinear model and the approximate model. This could involve providing the same input or initial condition to both models.

5. **Model Accuracy:**

   Assess the accuracy of the approximate model by analyzing the differences with the nonlinear model. Consider both qualitative and quantitative aspects such as the overall trends, transient behaviour, steady-state behaviour, and Root Mean Squared Error (RMSE).

To assess the precision of both the LPV model and the linear model of the quadcopter, their outputs are compared to those of the nonlinear model. This comparison is illustrated in Figures 3.3 and 3.4. It is evident that the LPV model's response closely aligns with the nonlinear model, outperforming the linear model.

The RMSE and the percentage (%) improvement values can be found in Table. 3.6. The RMSE is a widely used metric to measure the accuracy of the approximate model. It effectively indicates the model's fidelity. Smaller RMSE values indicate

TABLE 3.6: Comparative analysis: Accuracy of LPV model versus nonlinear model.

Model Outputs	$\mathbf{RMSE_{LPV}}$	$\mathbf{RMSE_{LM}}$	% **Improvement**
Roll	0.79377	5.1669	84.637
Pitch	0.41115	4.4792	90.821
Yaw	0.19917	1.2704	84.322
x-position	0.99186	4.6561	78.698
y-position	1.2572	4.4406	71.689
z-position	2.152	14.477	85.135

a better quality of approximation (i.e,. lower the RMSE, the better the model's accuracy).

The RMSE decreases by upto 90.82% when utilizing the LPV model in comparison to the linear model.

The formula used to compute the %RMSE is given as:

$$\%\text{Improvement} = \left(1 - \frac{\text{RMSE}_{\text{LPV}}}{\text{RMSE}_{\text{LM}}}\right) \times 100\% \tag{3.46}$$

Within this equation, RMSELPV and RMSELM denote the root mean squared error values associated with the LPV model and the linear model. These values signify the disparities between each model and the full nonlinear model of the quadcopter, which accounts for variable payload conditions. The comparison provides insights into the accuracy and performance of both the LPV and linear models under dynamic variations in quadcopter payload.

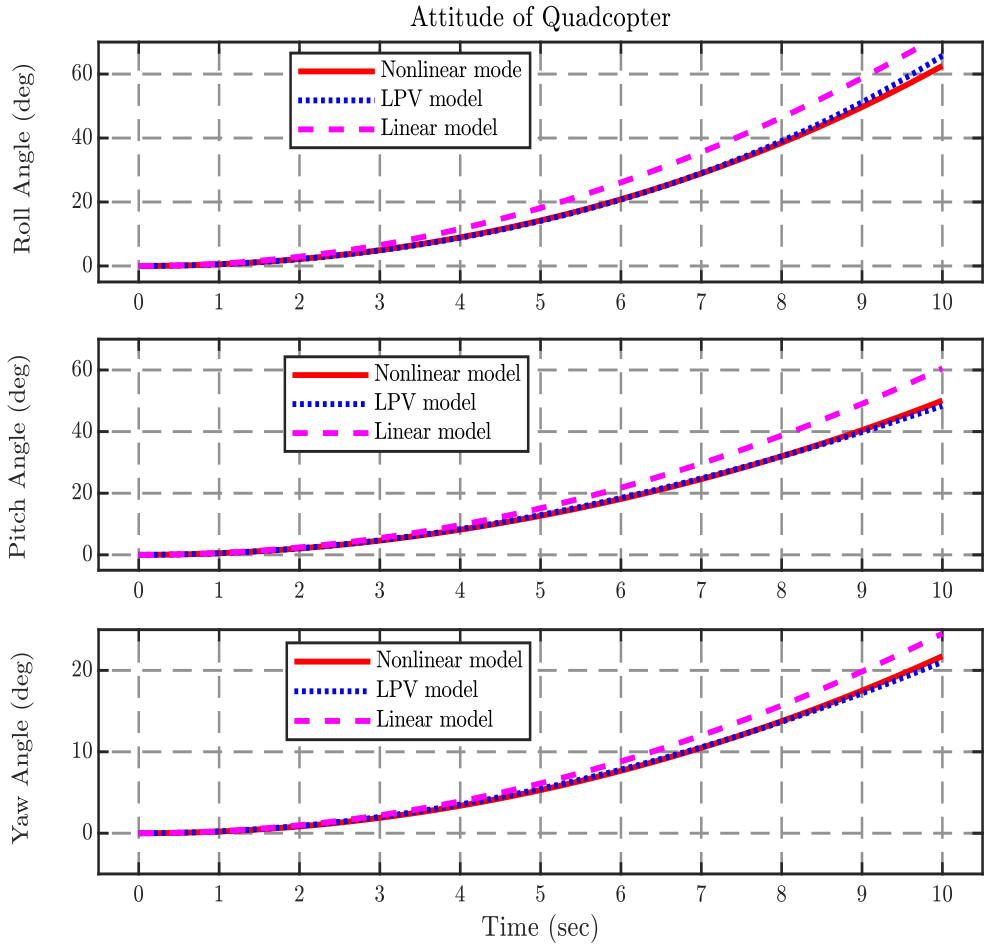

FIGURE 3.3: Quadcopter's response to a step input, showing changes in roll (ϕ), pitch (θ), and yaw (ψ) with time.

3.5 Bode Plots

Bode plots are crucial tools in the field of control systems engineering due to their significance in analyzing and designing control systems. These plots are useful in visualizing how a system's characteristics change across different frequencies, providing essential information about the gain margin (GM), phase margin (PM) and gain crossover frequency (w_{cp}). GM is a measure used to assess the stability of a system. It is related to the gain of the system at the frequency where the phase of the system is -180^o. The GM is expressed in decibels (dB) and represents the amount by which the system's gain can be increased before the system becomes unstable. PM is the amount by which the phase of system at the gain crossover frequency falls short of -180^o. It is expressed in degrees. A positive phase margin

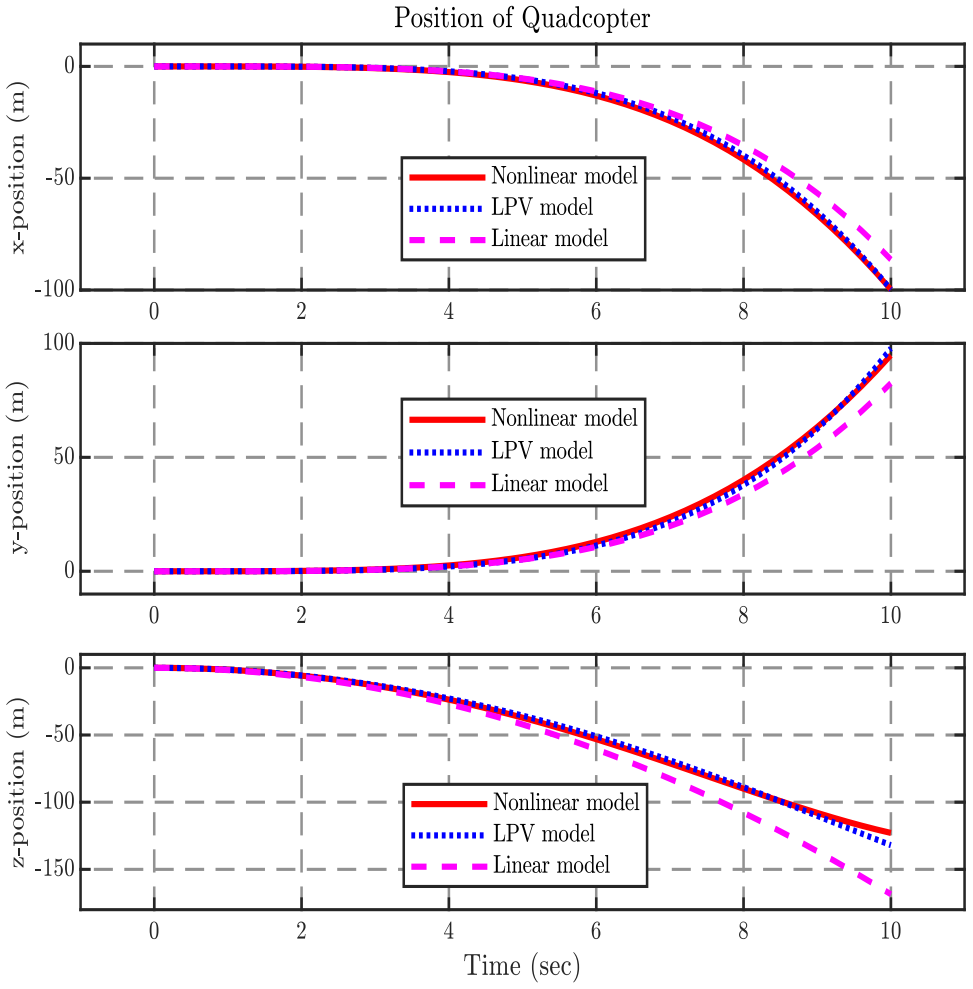

FIGURE 3.4: Quadcopter's response to a step input, illustrating changes in positions (x, y, z) with time.

signifies system stability, indicating there is a margin of safety before instability occurs. Conversely, a negative phase margin suggests proximity to instability, where further gain increases could lead to system instability. w_{cp} is the frequency at which system's gain is equal to 0 dB. It is used to measure the PM of the system. To assess the impact of parameter variations on system behavior, we have compared the Bode plots of the LPV model with the linear model. Bode plots for both the 6-DOF LPV model and the linear model of the quadcopter are given below.

Figure 3.5 (a) illustrates the Bode plots of LPV models representing the altitude dynamics of the quadcopter at different operating points (i.e., vertices of the polytope). These plots depict how the magnitude and phase of the altitude dynamics

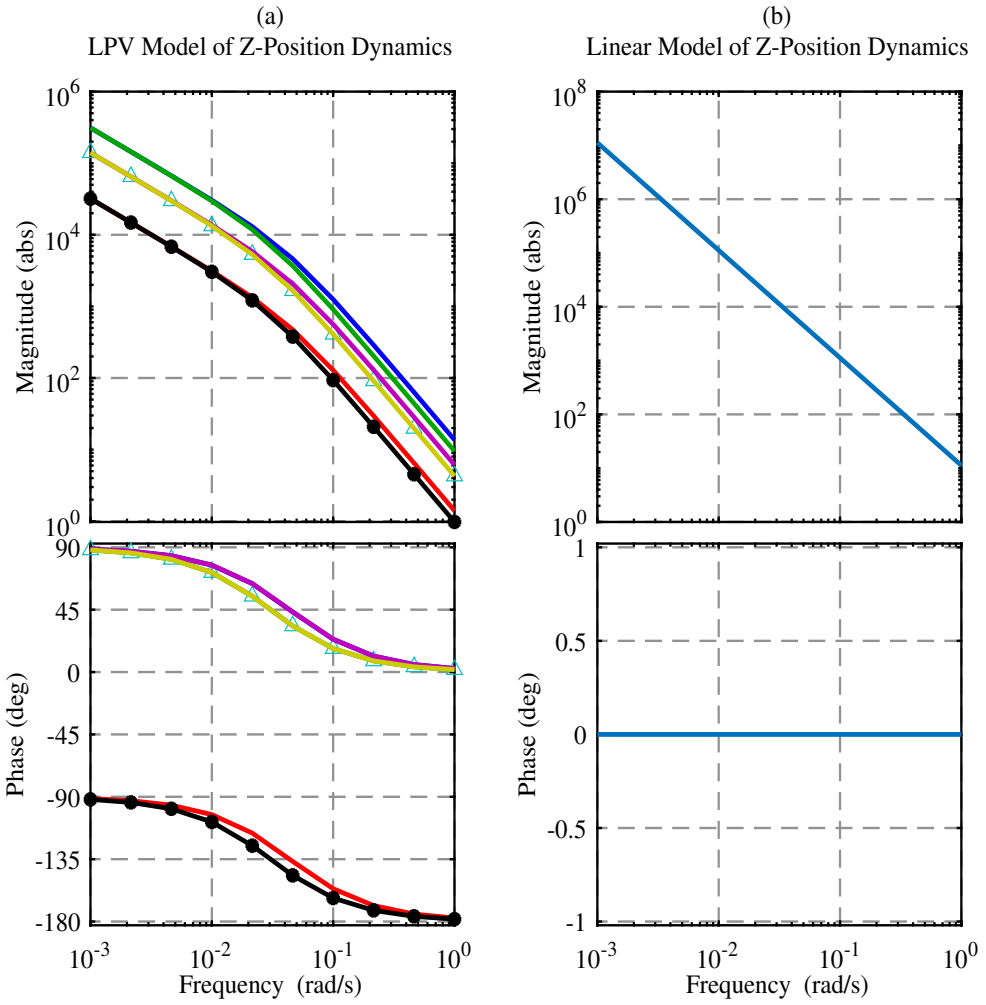

FIGURE 3.5: (**a**) Bode plot of LPV model of z-position dynamics; (**b**) Bode plot of linear model of z-position dynamics.

change with varying frequencies, considering variations in both mass and tilt angles. In contrast, Figure 3.5 (b), showing the Bode plot of linear models obtained at the hovering point (i.e., equilibrium point), fails to capture these variations. The values of GM, PM and w_{cp} are given in Table 3.7. It can be seen that the w_{cp} varies from 3.701 to 0.9878 with the variation in the operating point. It means that linear controller will not be able to provide the desired results.

Similarly, the bode plots of x-position, y-position, roll, pitch, and yaw dynamics of quadcopter are shown in Figures 3.6, 3.7, 3.8, 3.9, and 3.10, respectively. It can be seen from the figures that, when the operating point shifts, the system's magnitude and phase variation with frequencies also alter, which are prominent in

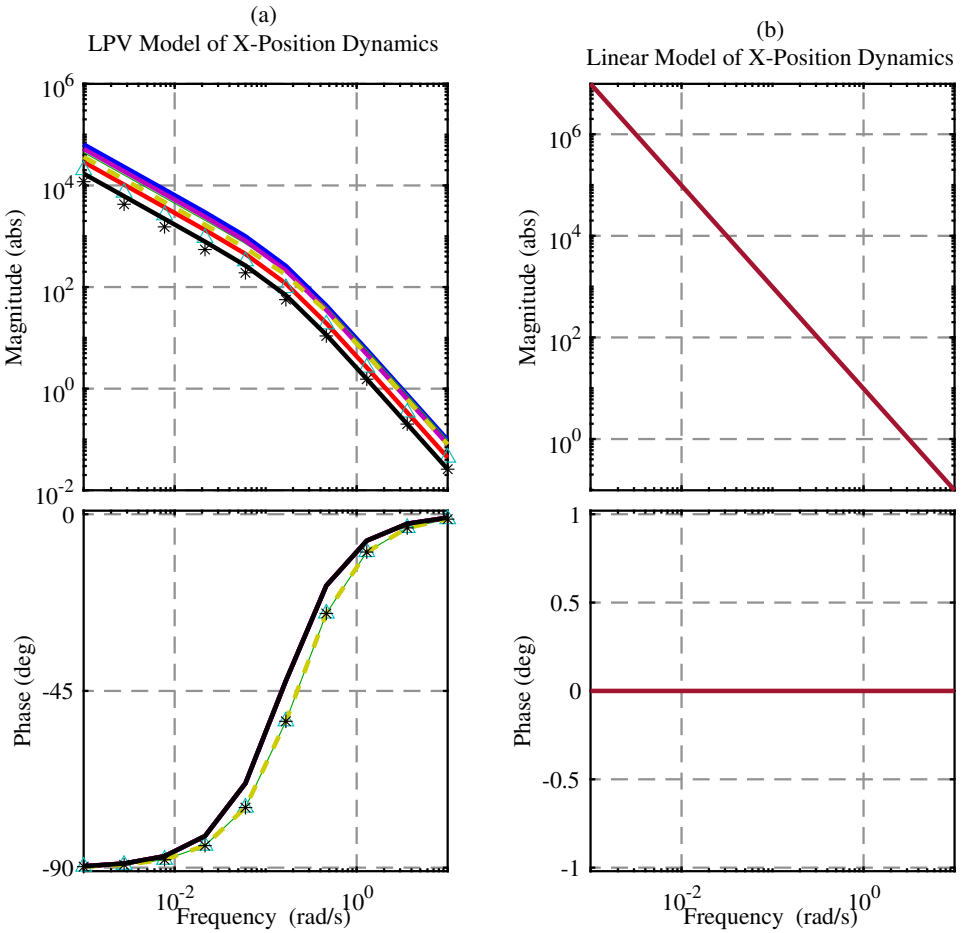

FIGURE 3.6: (**a**) Bode plot of LPV model of x-position dynamics; (**b**) Bode plot of linear model of x-position dynamics.

TABLE 3.7: The GM, PM and w_{cp} of z-position dynamics.

Dynamic Model		**GM**	**PM**	w_{cp}
LPV Model	@ *vertex*-1	inf	179.3214	3.7010
	@ *vertex*-2	inf	179.4342	3.0860
	@ *vertex*-3	inf	178.9870	2.4792
	@ *vertex*-4	inf	179.1554	2.0672
	@ *vertex*-5	inf	178.9870	2.4792
	@ *vertex*-6	inf	179.1554	2.0672
	@ *vertex*-7	inf	-2.1193	1.1845
	@ *vertex*-8	inf	-1.7672	0.9878
Linear Model		inf	-180	3.3520

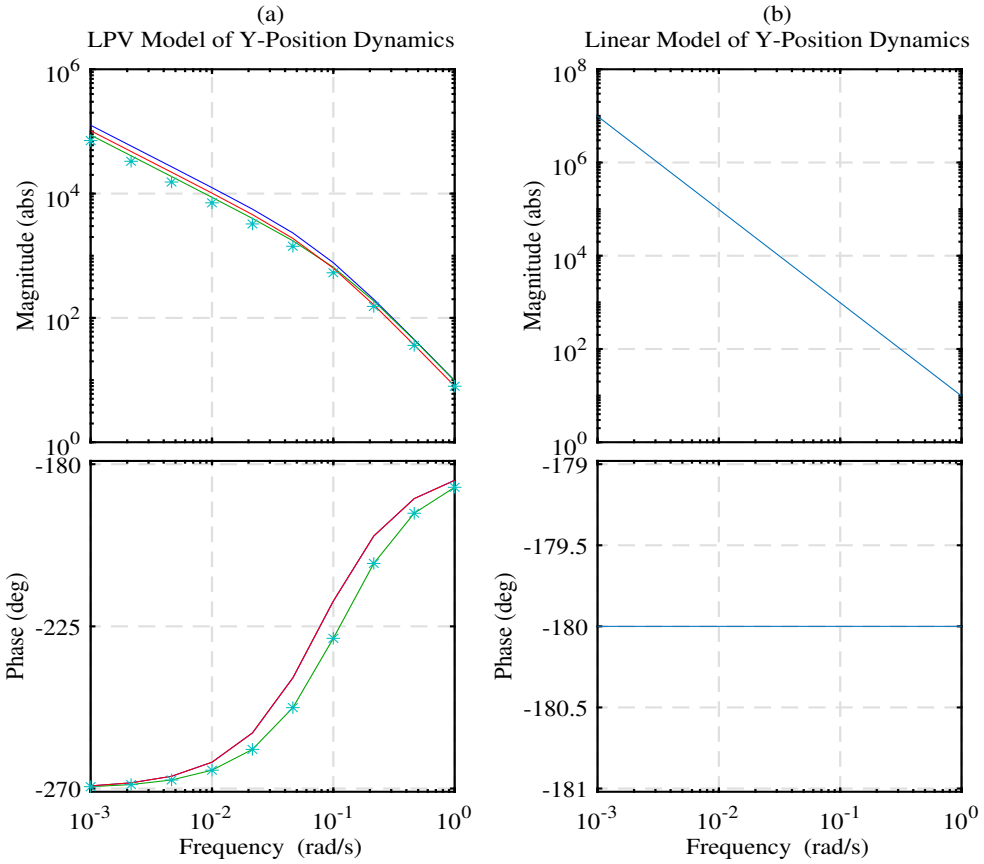

FIGURE 3.7: (**a**) Bode plot of LPV model of y-position dynamics; (**b**) Bode plot of linear model of y-position dynamics.

TABLE 3.8: The GM, PM and w_{cp} of y-position dynamics.

Dynamic Model		**GM**	**PM**	w_{cp}
LPV Model	@ *vertex*-1	Inf	-1.4285	3.1316
	@ *vertex*-2	Inf	-2.0546	3.1311
	@ *vertex*-3	Inf	-1.5812	2.8292
	@ *vertex*-4	Inf	-2.2741	2.8286
Linear Model		1	0	3.1321

the bode plots of LPV models. The fluctuations in the Bode magnitude and phase plots signify that the model's response is affected by varying parameters such as mass and inertia, as well as deviations from the equilibrium point due to changes in tilt angles. Moreover, the variation in the GM, PM and w_{cp} are listed in the Tables 3.8, 3.9, 3.10, 3.11, and 3.12.

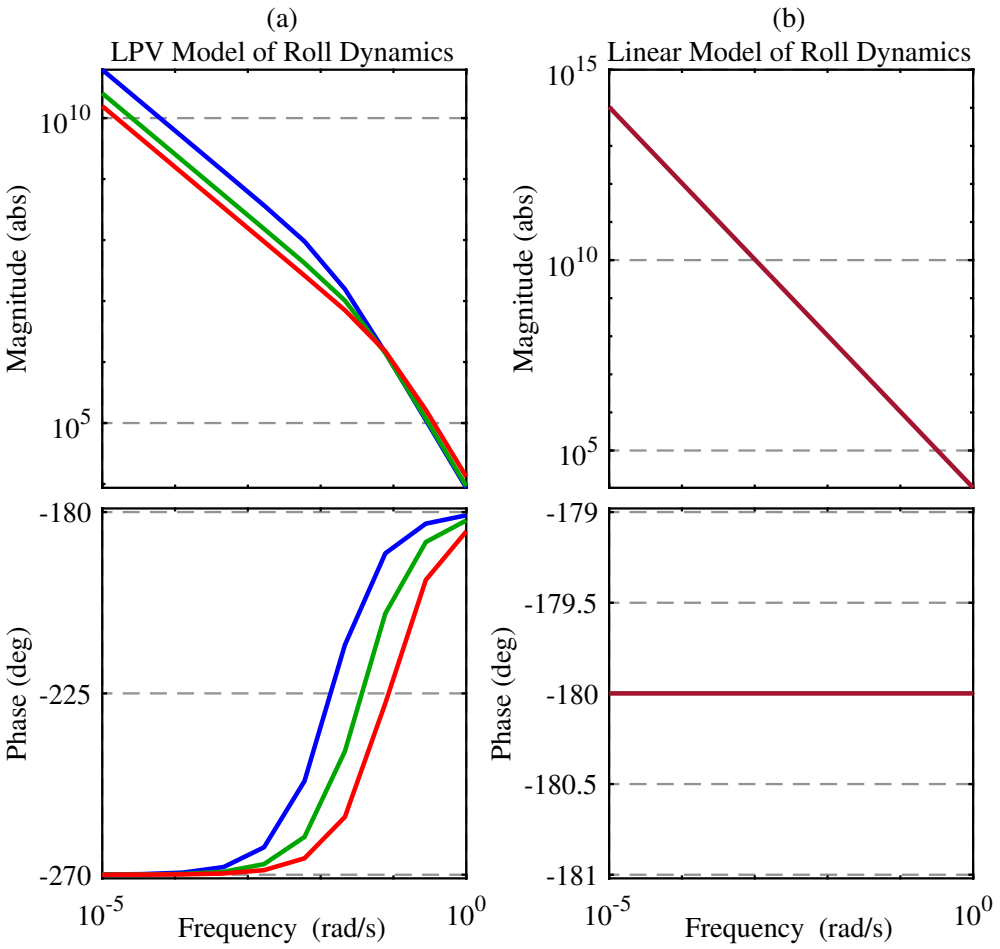

FIGURE 3.8: (**a**) Bode plot of LPV model of roll dynamics; (**b**) Bode plot of linear model of roll dynamics.

TABLE 3.9: The GM, PM and w_{cp} of x-position dynamics.

Dynamic Model		**GM**	**PM**	w_{cp}
LPV Model	@ *vertex*-1	inf	177.2130	3.1302
	@ *vertex*-2	inf	175.9921	3.1282
	@ *vertex*-3	inf	175.8406	2.0953
	@ *vertex*-4	inf	174.0200	2.0924
	@ *vertex*-5	inf	176.9153	2.8277
	@ *vertex*-6	inf	175.5643	2.8254
	@ *vertex*-7	inf	174.5889	1.6087
	@ *vertex*-8	inf	172.2231	1.6049
Linear Model		inf	-180.0000	3.1321

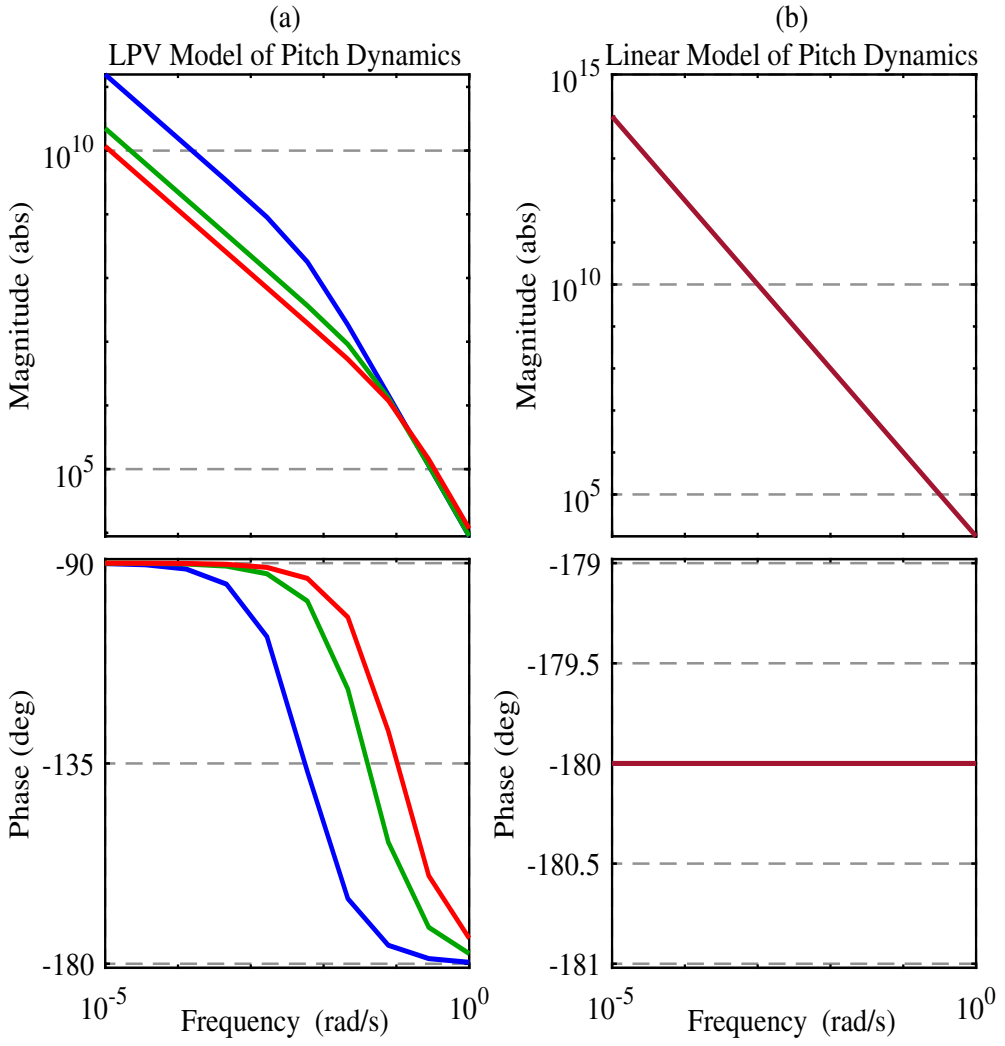

FIGURE 3.9: (**a**) Bode plot of LPV model of pitch dynamics; (**b**) Bode plot of linear model of pitch dynamics.

TABLE 3.10: The GM, PM and w_{cp} of Roll dynamics.

Dynamic Model		**GM**	**PM**	w_{cp}
LPV Model	@ *vertex*-1	inf	-0.0086	93.1309
	@ *vertex*-2	inf	-0.0216	96.2588
	@ *vertex*-3	inf	-0.0419	115.1200
Linear Model		1	0	102.3953

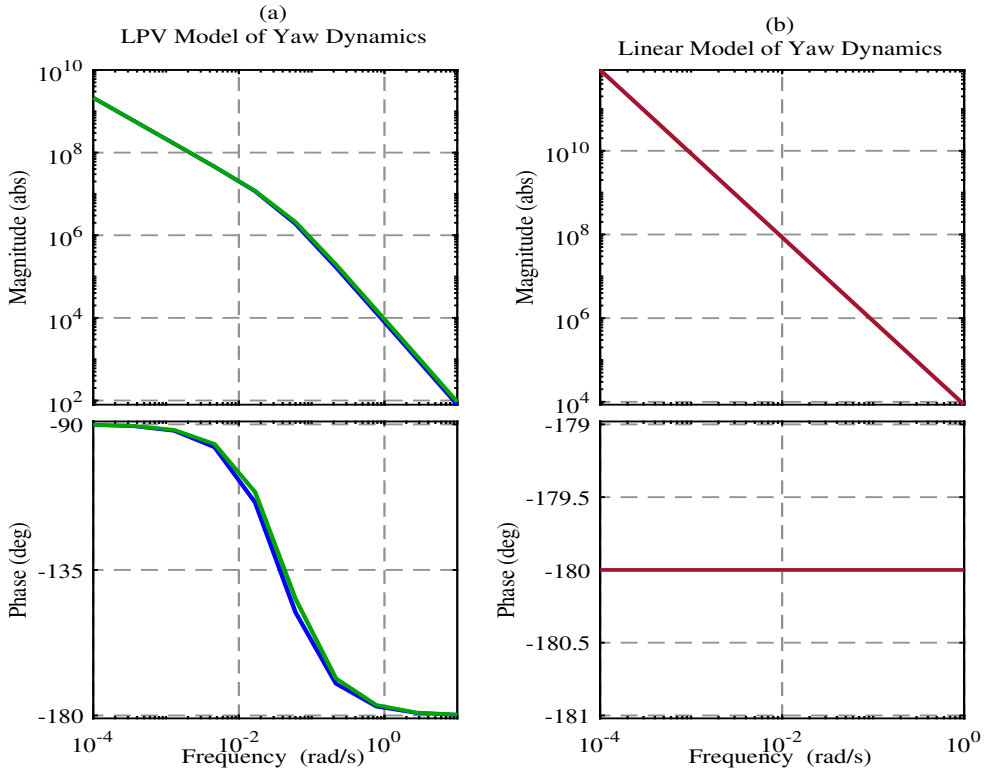

FIGURE 3.10: (**a**) Bode plot of LPV model of yaw dynamics; (**b**) Bode plot of linear model of yaw dynamics.

TABLE 3.11: The GM, PM and w_{cp} of Pitch dynamics.

Dynamic Model		**GM**	**PM**	$\mathbf{w}_{cp}$
LPV Model	@ *vertex*-1	inf	-0.0021	93.8619
	@ *vertex*-2	inf	-0.0149	94.4586
	@ *vertex*-3	inf	-0.0326	108.2865
Linear Model		1	0	100.3045

TABLE 3.12: The GM, PM and w_{cp} of Yaw dynamics.

Dynamic Model		**GM**	**PM**	w_{cp}
LPV Model	@ *vertex*-1	inf	0.0240	89.0703
	@ *vertex*-2	inf	0.0260	96.3610
Linear Model		1	0	92.5008

3.6 Chapter Summary

This chapter starts with the nonlinear modeling of quadcopter with varying payload, which will be used to derive the LPV model. In the next section, the varying parameters of the quadcopter with variable payload are computed. After that, the LPV model derivation of the nonlinear model is presented. This model will be used in designing an LPV control technique to control the position of the quadcopter. Moreover, the linear model of the quadcopter is also presented, which will be used in designing a linear controller for the quadcopter. Finally, in the last section, model validation is presented. The RMSE is used as a performance index to show the accuracy of the LPV model and the linear model compared to the nonlinear model. The response of the LPV model is much closer to the nonlinear model as compared to the linear model. In the next chapter, an LMIs-based LPV control scheme and linear control methodology are discussed for the position control of quadcopter.

Chapter 4

Control Design

This chapter discusses multiple objective control designs using LMI techniques. Many practical control systems require the ability to fit simultaneously different and often conflicting performance objectives as best as possible. Therefore, multiple objective control designs are very important in control system applications. The advantage of this type of approach is that a globally optimal and numerically reliable solution can always be obtained as long as the finally formulated LMI problem has a solution. In this chapter, LMIs-based LPV control for the position control of a quadcopter in the presence of time-varying parameters and wind disturbance is presented. This technique is based on the LPV model presented in the preceding chapter. Moreover, the design of H_∞ design with the desired LMI pole region is also presented for the linear model presented in Chapter 3.

4.1 LPV Control

Linear parameter varying (LPV) control is a relatively recent development in the field of control systems, combining elements of both linear control theory and nonlinear control theory. It emerged in the late 1980s and early 1990s as a response to the increasing need for control techniques that can handle systems with time-varying parameters or operating conditions. One of the significant milestones in

LPV control history was the introduction of the so-called Linear Matrix Inequality (LMI) framework. This framework, pioneered by researchers like Boyd, Ghaoui, and Feron, provided a powerful and systematic approach to solving control synthesis problems for LPV systems [63]. The LMI framework allowed for the design of controllers that guaranteed stability and performance over the entire parameter space of the system. Since then, LPV control has continued to evolve and has found applications in various fields, including aerospace [64, 65], vehicle [66, 67], automotive [68], robotics [69], and renewable energy systems [70]. Today, LPV control remains an active area of research, with ongoing developments in both theory and applications.

The LPV concept is derived from the gain scheduling approach [71–73]. It is viewed as a viable alternative to classical gain-scheduling designs for controlling nonlinear systems. Classical gain-scheduling control is a technique where multiple linear controllers are designed for different operating points or regions of the system and are switched or interpolated based on the current operating conditions. It can handle systems with nonlinearities and time-varying parameters by switching between linear controllers. The stability, performance, and robustness properties are generally difficult to achieve with the classical gain-scheduling control methodologies. Moreover, adhoc methods of interpolation are needed for gains switching. LPV controllers are automatically gain-scheduled, and no adhoc methods of interpolation of gains are needed for gain switching.In summary, gain-scheduling control switches between pre-designed linear controllers based on the operating conditions, while LPV control explicitly models the system dynamics as a function of time-varying parameters and designs controllers that adapt to changes in these parameters.

Some key elements of LPV control are listed below.

- **Parameter Dependency:**

  LPV methodologies explicitly account for the system's time-varying parameters and represents the system's dynamics as a function of these varying

parameters. These parameters could include operating conditions, external disturbances, or other factors influencing the system behavior.

- **LPV Models:**
  LPV techniques are based on LPV models, which mathematically describe the relationship between system parameters and the system dynamics. These models allow for a more accurate representation of the system's behavior under varying parameters and operating conditions.

- **Experimental and Analytical Techniques:**
  LPV modeling can be done using analytical methods if reliable nonlinear equations describing system dynamics are available. Alternatively, experimental identification methods can be employed to construct LPV models based on real-world data, enabling practical implementation of LPV control strategies.

- **Controller Adaptability:**
  LPV controllers are designed to adapt to changes in system parameters. This adaptability ensures that the control system maintains stability and performance even when the system parameters change.

- **Controller Synthesis:**
  LPV methodologies provide systematic techniques for synthesizing controllers that can handle parameter variations. These methods often involve solving mathematical optimization problems, ensuring that the control system meets certain performance criteria under varying conditions.

- **Stability Analysis:**
  LPV methodologies offer systematic ways to analyze the stability of the control system across the entire parameter space. Stability analysis is crucial to ensure that the control system remains stable under all possible operating conditions.

- **Performance Analysis:**

  LPV methods allow for the analysis of control system performance concerning various criteria, such as settling time, overshoot, and steady-state error, across different parameter values. This analysis ensures that the control system meets desired performance specifications under varying conditions.

- **Robustness:** LPV control designs often exhibit robustness, meaning they can handle uncertainties and disturbances in the system. Robust LPV controllers are capable of maintaining stability and performance even when there are uncertainties in the system parameters.

- **Real-time Implementation:**

  LPV methodologies provide control laws that are implementable in real-time systems. The computed control gains can be updated continuously based on the varying parameters, allowing the control system to adapt dynamically to changing conditions.

- **Computational Complexity:**

  In the LPV techniques, controller gains are computed offline using well known LMIs but implemented online, leading to a reduction in computational burden [74, 75].

- **Multivariable Systems:**

  LPV methodologies can handle multivariable systems where multiple parameters influence the system behavior simultaneously. This capability is valuable in complex systems where interactions between parameters can significantly impact the system's dynamics.

LPV systems offer advantages in handling parameter variations and providing robustness, they introduce complexities in terms of design, analysis, and computational requirements as compared to the linear control techniques.

The general LPV control system configuration is depicted in Figure 4.1. $P(\rho)$ shows the generalized LPV plant, and $K(\rho)$ depicts the LPV controller gains. The generalized LPV plant's state-space realization is as follows [76, 77]:

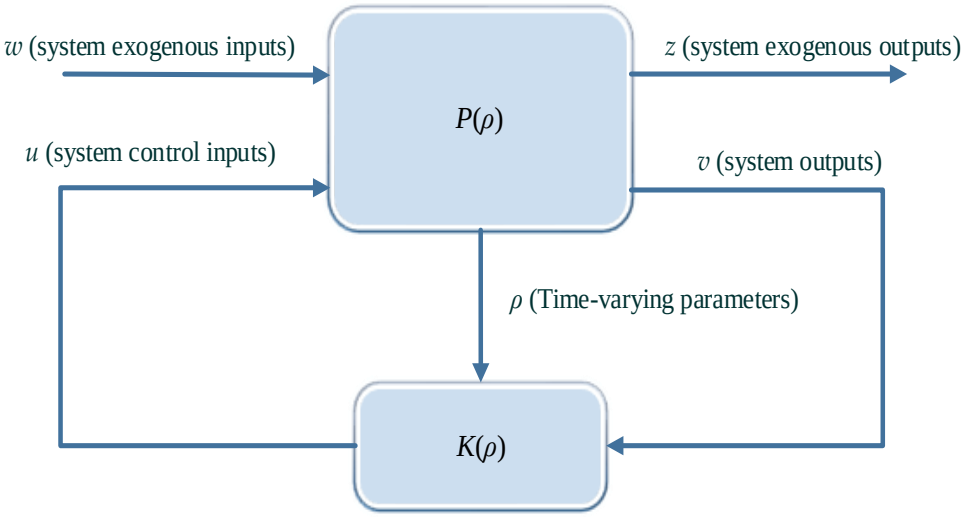

FIGURE 4.1: The structure of closed-loop LPV system.

$$P(\rho) \; : \begin{cases} \dot{\chi} = \mathcal{A}(\rho)\,\chi + \mathcal{B}_1(\rho)\,w + \mathcal{B}_2(\rho)\,u \\ z = \mathcal{C}_z(\rho)\,\chi + \mathcal{D}_{11}(\rho)\,w + \mathcal{D}_{12}(\rho)\,u \\ v = \mathcal{C}_v(\rho)\,\chi + \mathcal{D}_{21}(\rho)\,w + \mathcal{D}_{22}(\rho)\,u \end{cases} \tag{4.1}$$

where

(1) $\chi \in R^n$, $w \in R^{n_w}$, $u \in R^{n_u}$, $z \in R^{n_z}$ and $v \in R^{n_v}$ are the system states, exogenous inputs (i.e., reference signals and disturbances), control signals, exogenous outputs (i.e., error signals which are to be minimized in order to fulfill control objectives), and sensed outputs, respectively.

(2) $\mathcal{A}(\rho)$, $\mathcal{B}_1(\rho)$, $\mathcal{B}_2(\rho)$, $\mathcal{C}_z(\rho)$, $\mathcal{D}_{11}(\rho)$, $\mathcal{D}_{12}(\rho)$, $\mathcal{C}_v(\rho)$, $\mathcal{D}_{21}(\rho)$ and $\mathcal{D}_{22}(\rho)$ are parameter dependent state-space matrices of appropriate dimensions.

(3) ρ is a time-varying parameters vector that varies in a convex polytope of vertices $\rho_{vi}\,(i = 1, 2, \ldots, N)$. N represents the number of vertices.

The LPV control law is given as:

$$u(t) = K(\rho)v(t) \tag{4.2}$$

In the LPV polytopic form, the matrices of $P(\rho)$ can be written as

$$\begin{bmatrix} \mathcal{A}(\rho) & \mathcal{B}_1(\rho) & \mathcal{B}_2(\rho) \\ \mathcal{C}_z(\rho) & \mathcal{D}_{11}(\rho) & \mathcal{D}_{12}(\rho) \\ \mathcal{C}_v(\rho) & \mathcal{D}_{21}(\rho) & \mathcal{D}_{22}(\rho) \end{bmatrix} = \sum_{i=1}^{N} \alpha_i \begin{bmatrix} A_i & B_{1i} & B_{2i} \\ C_{zi} & D_{11i} & D_{12i} \\ C_{vi} & D_{21i} & D_{22i} \end{bmatrix} \tag{4.3}$$

In the polytopic form, LPV controller gains $K(\rho)$ can be expressed as:

$$K(\rho) = \sum_{i=1}^{N} \alpha_i K_i \tag{4.4}$$

$\alpha_i\,(i = 1, 2, \ldots, N)$ represent the barycentric weights (for details, see [78, 79]). The time-varying parameter vector ρ can be expressed as:

$$\rho = \left\{ \alpha_i \rho_{vi}, \quad \alpha_i \geq 0, \quad \textstyle\sum_{i=1}^{N} \alpha_i = 1 \right\} \tag{4.5}$$

To design an LPV controller, a mixed sensitivity control approach is adopted [80, 81]. The weighted closed-loop system for mixed sensitivity control design is shown in Figure 4.2. $G_P(\rho)$ shows the LPV model of the dynamic system to the control signal u and the disturbance signal w_2, W_e is the weighting filter that is chosen to impose meaningful requirements on the closed-loop system, such as trajectory tracking and disturbance rejection, W_u is the sensitivity weight that is chosen to shape the control sensitivity and limit the control effort to stay within the physical limit of the actuator, V_u and V_d are the static weights that represent the maximum values of control signal and disturbance signal, respectively.

The state-space realization of $G_P(\rho)$, W_e, and W_u is given by

$$G_P(\rho): \quad \begin{bmatrix} \dot{x}_p \\ \hline y_p \end{bmatrix} = \left[\begin{array}{c|cc} A_p(\rho) & B_w(\rho)V_d & B_p(\rho) \\ \hline C_p(\rho) & 0 & 0 \end{array}\right] \begin{bmatrix} x_p \\ w_2 \\ u \end{bmatrix} \tag{4.6}$$

$$W_e: \quad \begin{bmatrix} \dot{x}_{We} \\ \hline z_1 \end{bmatrix} = \left[\begin{array}{c|c} A_{We} & B_{We} \\ \hline C_{We} & D_{We} \end{array}\right] \begin{bmatrix} x_{We} \\ \hline e \end{bmatrix} \tag{4.7}$$

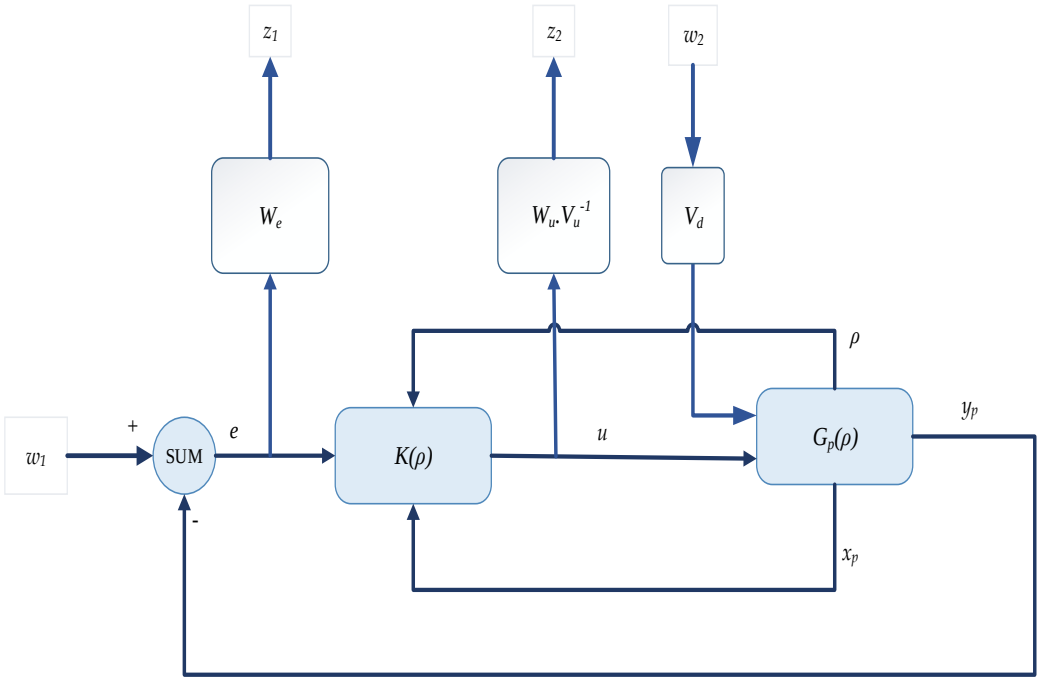

FIGURE 4.2: The mixed sensitivity control problem.

$$W_u: \quad \left[\begin{array}{c} \dot{x}_{Wu} \\ \hline z_2 \end{array}\right] = \left[\begin{array}{c|c} A_{Wu} & B_{Wu} \\ \hline C_{Wu} & D_{Wu} \end{array}\right] \left[\begin{array}{c} x_{Wu} \\ \hline V_u^{-1}u \end{array}\right] \tag{4.8}$$

The weighting sensitivity filter W_u is set to unity. The state-space realization for LPV controller synthesis is given as:

$$\left[\begin{array}{c} \dot{x}_p \\ \dot{x}_{We} \\ \hline z_1 \\ z_2 \end{array}\right] = \left[\begin{array}{ccc|cc} A_p(\rho) & 0 & 0 & B_w(\rho)V_d & B_p(\rho)V_u \\ -B_{We}C_p(\rho) & A_{We} & B_{We} & 0 & 0 \\ \hline -D_{We}C_p(\rho) & C_{We} & D_{We} & 0 & 0 \\ 0 & 0 & 0 & 0 & 1 \end{array}\right] \left[\begin{array}{c} x_p \\ x_{We} \\ \hline w_1 \\ w_2 \\ \hat{u} \end{array}\right] \tag{4.9}$$

The scaled control input $\hat{u}$ is given by:

$$\hat{u} = V_u^{-1}u \tag{4.10}$$

The LPV controller is designed using the LMI approach. The LMI approach is based on the well-known lemmas, which are formalized in the following

Lemma 1 (Condition for Quadratic $\mathcal{L}_2$-Gain Performance):
The $\mathcal{L}_2$-gain of closed-loop LPV system from exogenous inputs w to exogenous outputs z will be lower than a positive scalar γ, if and only if there exists a positive-definite symmetric matrix $X(\rho)$ of $n \times n$, and a non-zero matrix $Y(\rho)$ of $1 \times n$ for all the admissible values of time-varying parameter vector ρ satisfying [82]

$$\begin{cases} \min & \gamma \\ \text{s.t.} & X(\rho) > 0 \\ & \begin{bmatrix} \mathcal{A}(\rho) X(\rho) + X(\rho)\mathcal{A}(\rho)^T + \mathcal{B}_2(\rho) Y(\rho) + Y(\rho)^T \mathcal{B}_2(\rho)^T & \mathcal{B}_1(\rho) & a_{13} \\ \mathcal{B}_1(\rho)^T & -\gamma I & \mathcal{D}_{11}(\rho)^T \\ \mathcal{C}_z(\rho) X(\rho) + \mathcal{D}_{12}(\rho) Y(\rho) & \mathcal{D}_{11}(\rho) & -\gamma I \end{bmatrix} < 0 \end{cases} \tag{4.11}$$

where,

$$a_{13} = X(\rho)\mathcal{C}_z(\rho)^T + Y(\rho)^T \mathcal{D}_{12}(\rho)^T \tag{4.12}$$

In the $\mathcal{L}_2$-gain LPV controller synthesis the objective is to find an LPV controller such that the $\mathcal{L}_2$-gain of the closed-loop system is minimized. $\mathcal{L}_2$-gain of the closed-loop system is an alternate to $\mathcal{H}_\infty$-norm in the LPV framework.

Lemma 2 (Constraints for Pole Placement):
The closed-loop LPV system's eigenvalues will be located in the desirable LMI region $D_{(\alpha,\beta,\varphi)}$, if the following LMIs are feasible [83]. The LMI regions $D_{(\alpha,\beta,\varphi)}$ is shown in Figure 4.3.

- The closed-loop LPV system's eigenvalues will be located in the LMI region $D_{(\alpha,\beta)}$, if and only if there exist $X(\rho)$, and $Y(\rho)$, such that

$$\begin{cases} X(\rho) > 0 \\ 2\alpha X(\rho) + \mathcal{A}(\rho) X(\rho) + \mathcal{B}_2(\rho) Y(\rho) + X(\rho)\mathcal{A}(\rho)^T + Y(\rho)^T \mathcal{B}_2(\rho)^T < 0 \\ 2\beta X(\rho) + \mathcal{A}(\rho) X(\rho) + \mathcal{B}_2(\rho) Y(\rho) + X(\rho)\mathcal{A}(\rho)^T + Y(\rho)^T \mathcal{B}_2(\rho)^T > 0 \end{cases} \tag{4.13}$$

The sub-LMI region $D_{(\alpha,\beta)}$ represented by the LMI given in equation (4.13) is shown in Figure 4.4.

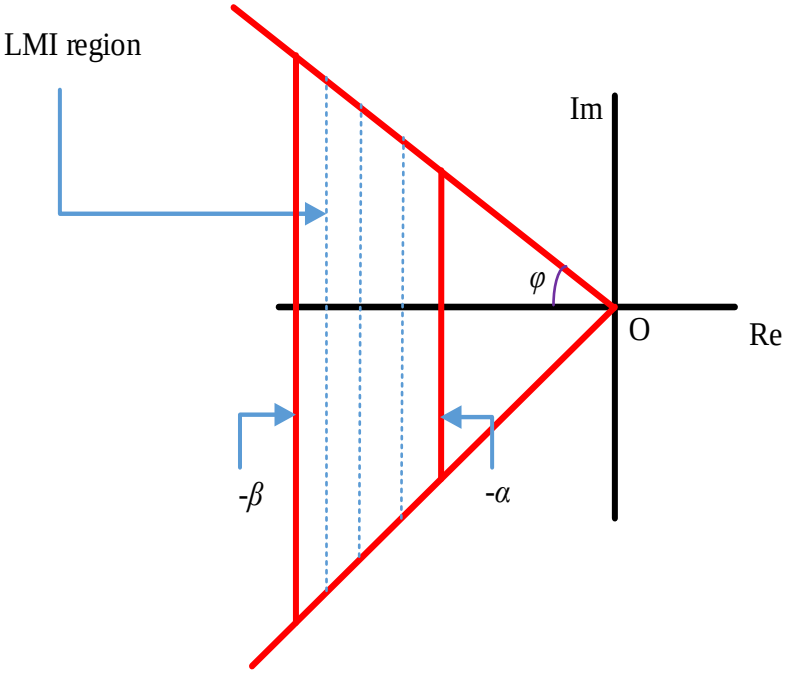

FIGURE 4.3: LMI region $D_{(\alpha,\beta,\varphi)}$.

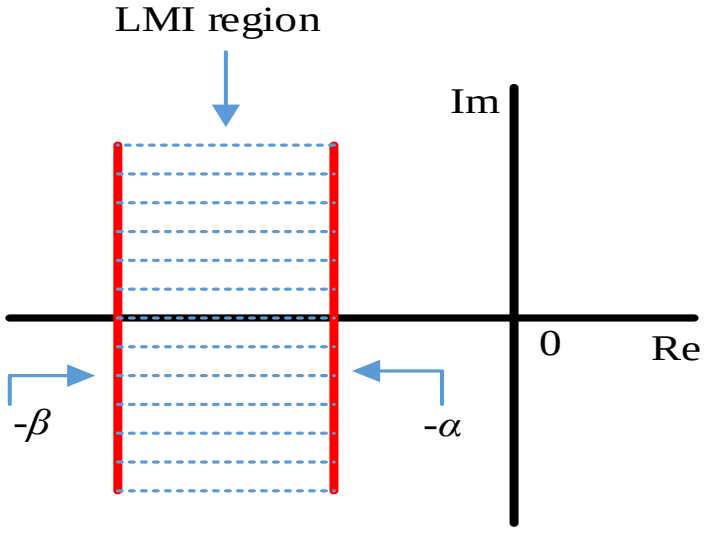

FIGURE 4.4: Strip region $D_{(\alpha,\beta)}$.

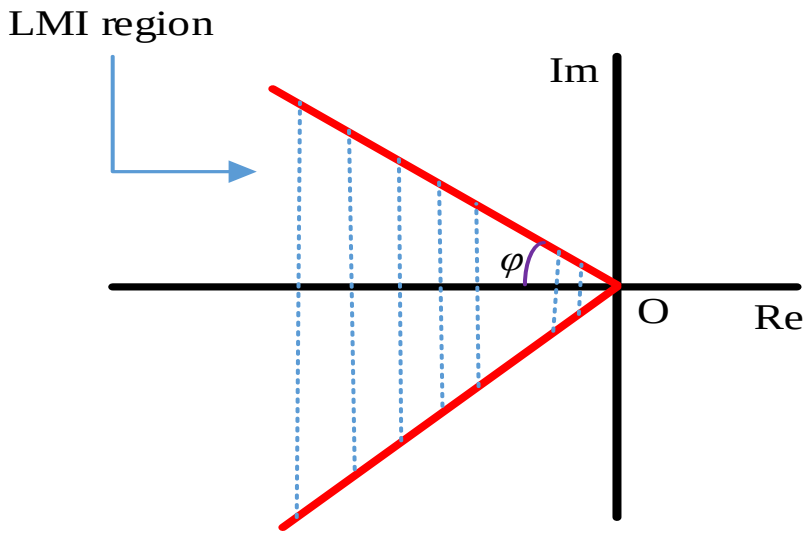

FIGURE 4.5: Conic sector $D_{(\varphi)}$.

- The closed-loop LPV system's eigenvalues will be located in the LMI region $D_{(\varphi)}$, if and only if there exist $X(\rho)$, and $Y(\rho)$, such that

$$\begin{bmatrix} a_{11} & a_{12} \\ a_{21} & a_{22} \end{bmatrix} < 0 \tag{4.14}$$

where,

$$\begin{cases} a_{11} = \left(X(\rho)\mathcal{A}(\rho)^T + \mathcal{A}(\rho) X(\rho) + Y(\rho)^T \mathcal{B}_2(\rho)^T + \mathcal{B}_2(\rho) Y(\rho) \right) sin\varphi \\ a_{12} = \left(X(\rho)\mathcal{A}(\rho)^T - \mathcal{A}(\rho) X(\rho) - \mathcal{B}_2(\rho) Y(\rho) + Y(\rho)^T \mathcal{B}_2(\rho)^T \right) cos\varphi \\ a_{21} = \left(\mathcal{A}(\rho) X(\rho) - X(\rho)\mathcal{A}(\rho)^T + \mathcal{B}_2(\rho) Y(\rho) - Y(\rho)^T \mathcal{B}_2(\rho)^T \right) cos\varphi \\ a_{22} = \left(\mathcal{A}(\rho) X(\rho) + X(\rho)\mathcal{A}(\rho)^T + \mathcal{B}_2(\rho) Y(\rho) + Y(\rho)^T \mathcal{B}_2(\rho)^T \right) sin\varphi \end{cases} \tag{4.15}$$

The sub-LMI region $D_{(\varphi)}$ represented by the LMI given in equation (4.14) is shown in Figure 4.5. The closed-loop LPV system will be D-stable, if both conditions (4.13) and (4.14) are satisfied. The LPV controller gains $K(\rho)$ can be determined as follows:

$$K(\rho) = Y(\rho)X(\rho)^{-1} \tag{4.16}$$

Equations (4.11)–(4.14) impose an unlimited number of LMIs that are difficult to solve. The total number of LMIs can be squeezed to a finite set using a polytopic LPV system. Using convexity, (4.11)–(4.14) will hold if it holds at the vertices of the polytope.

4.1.1 LPV Control Design for Quadcopter

In this section, we present an LMIs-based LPV control design for position tracking of the quadcopter. The goal is that the state variables $[x,\ \ y,\ \ z]$ follow the desired reference trajectories $(x_{ref},\ \ y_{ref},\ \ z_{ref})$, while the yaw angle ψ is required to remain at $\angle 0^0$. All the state variables $(x,\ \ y,\ \ z,\ \ \phi,\ \ \theta,\ \ \psi,\ \ \dot{\phi},\ \ \dot{\theta},\ \ \dot{\psi},\ \ \dot{x},\ \ \dot{y},\ \ \dot{z})$ and the water level in the liquid tank are considered as measurable. The overall control design requirements are as follows:

1. The system response should exhibit minimal or no overshoot.
2. The desired reference positions $(x_{\text{ref}}, y_{\text{ref}}, z_{\text{ref}})$ should be achieved within 4 seconds.
3. The robustness index, denoted by γ, should be less than 4.
4. The disturbance should be rejected within 3 seconds.
5. The motor speed should be within the limits (i.e., 500 rad/sec).

The closed loop block diagram of quadcopter system is shown in Figure 4.6. Based on the system dynamics, the control system is split into subsystems.

(1) The fully actuated subsystem dynamics that consist of $\ddot{z}$ and $\ddot{\psi}$.

(2) The under-actuated subsystem dynamics made up of $\ddot{\phi}$, $\ddot{\theta}$, $\ddot{x}$, and $\ddot{y}$.

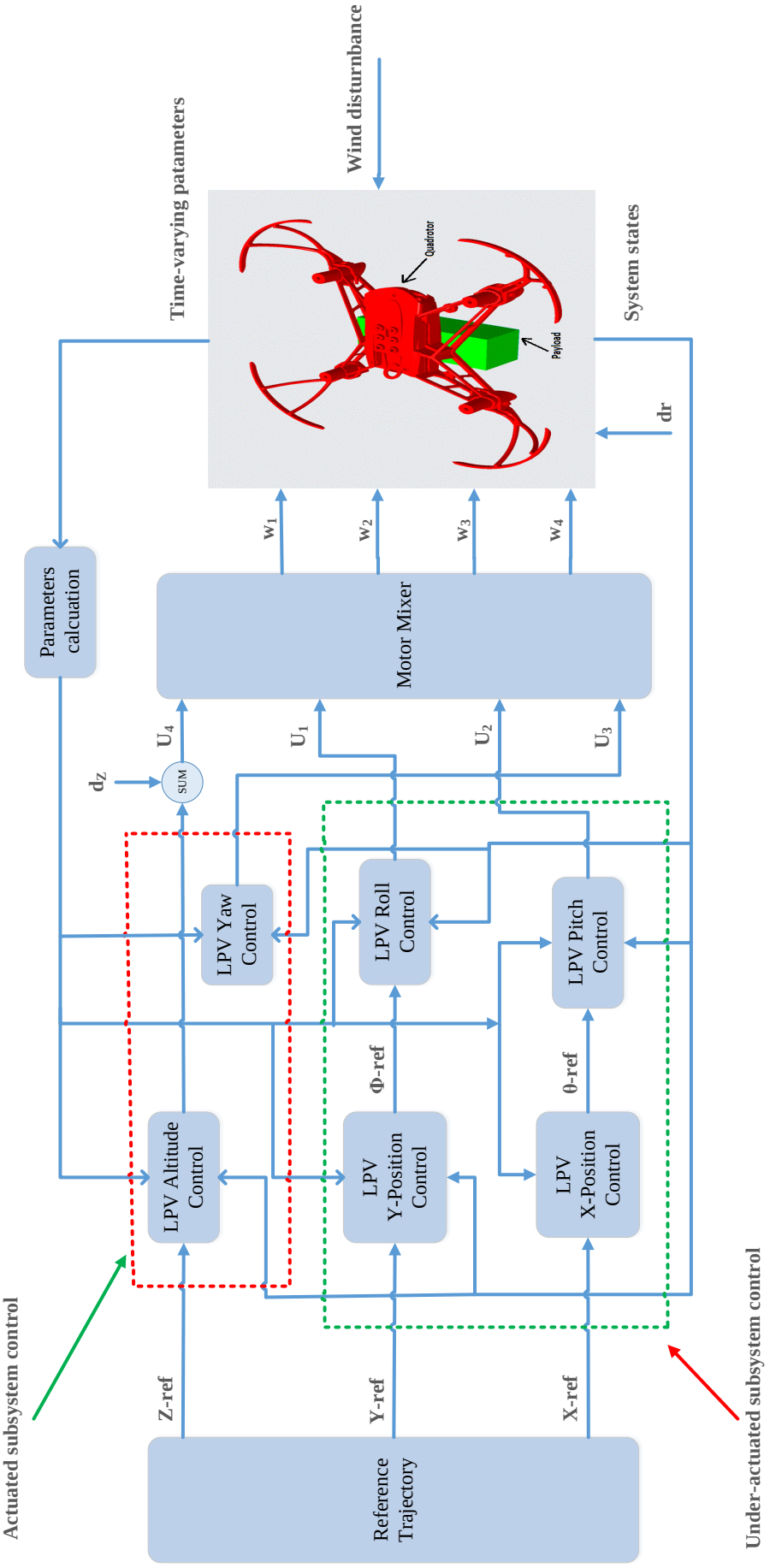

FIGURE 4.6: Closed-loop block diagram of quadcopter system

4.1.2 LPV Control for Fully Actuated Subsystem

LPV controller is devised for the fully actuated subsystem dynamics by solving the LMIs given in (4.11)–(4.14) at each vertex of the rectangular polytope using the LMI control toolbox [59].

The descriptor LPV form of altitude dynamics is:

$$\begin{cases} E_z(\rho_z)\begin{bmatrix}\dot{z}\\ \ddot{z}\end{bmatrix} = \begin{bmatrix}0 & 1\\ 0 & -\dot{m}\end{bmatrix}\begin{bmatrix}z\\ \dot{z}\end{bmatrix} + B_z(\rho_z)\,u_4 \\ y_z = \begin{bmatrix}1 & 0\end{bmatrix}\begin{bmatrix}z\\ \dot{z}\end{bmatrix} \end{cases} \tag{4.17}$$

where,

$$E_z(\rho_z) = \begin{bmatrix}1 & 0\\ 0 & 0\end{bmatrix} + \rho_1\begin{bmatrix}0 & 0\\ 0 & 1\end{bmatrix} + \rho_3\begin{bmatrix}0 & 0\\ 0 & 0\end{bmatrix} + \rho_4\begin{bmatrix}0 & 0\\ 0 & 0\end{bmatrix} \tag{4.18}$$

$$B_z(\rho_z) = \begin{bmatrix}0\\ -1\end{bmatrix} + \rho_3\begin{bmatrix}0\\ \frac{1}{2}\end{bmatrix} + \rho_4\begin{bmatrix}0\\ \frac{1}{2}\end{bmatrix} \tag{4.19}$$

The descriptor LPV form of yaw dynamics is:

$$\begin{cases} E_\psi(\rho_\psi)\begin{bmatrix}\dot{\psi}\\ \ddot{\psi}\end{bmatrix} = \begin{bmatrix}0 & 1\\ 0 & -d_1\dot{m}\end{bmatrix}\begin{bmatrix}\psi\\ \dot{\psi}\end{bmatrix} + \begin{bmatrix}0\\ 1\end{bmatrix}U_3 \\ y_\psi = \begin{bmatrix}1 & 0\end{bmatrix}\begin{bmatrix}\psi\\ \dot{\psi}\end{bmatrix} \end{cases} \tag{4.20}$$

where,

$$E_{\psi}\left(\rho_{\psi}\right)=\begin{bmatrix}1 & 0\\ 0 & d_2\end{bmatrix}+\rho_1\begin{bmatrix}0 & 0\\ 0 & d_1\end{bmatrix} \tag{4.21}$$

The weighting filters W_{ez} and $W_{e\psi}$ are selected as follows,

$$\left[\begin{array}{c}\dot{x}_{Wez}\\ \hline z_{1z}\end{array}\right]=\left[\begin{array}{c|c}-5.6\times10^{-6} & 0.56\\ \hline 1 & 0.5\end{array}\right]\left[\begin{array}{c}x_{Wez}\\ \hline e_z\end{array}\right] \tag{4.22}$$

$$\left[\begin{array}{c}\dot{x}_{We\psi}\\ \hline z_{1\psi}\end{array}\right]=\left[\begin{array}{c|c}-4.5\times10^{-4} & 0.45\\ \hline 1 & 1\end{array}\right]\left[\begin{array}{c}x_{We\psi}\\ \hline e_{\psi}\end{array}\right] \tag{4.23}$$

The static weights V_{uz} and $V_{u\psi}$ are expected to be 0.5 and 1, respectively. The static weight $d_z = 0.5$ is taken into consideration. The bounded disturbance d_r is assumed as $3.2\times10^{-3}\ kg/sec$. The parameters associated with the desired LMI regions are chosen on the basis of the desired control objective given in Section 4.1.1. Based on the desired control objectives, These parameter values are as follows:

$$\alpha_z=-0.5,\quad \beta_z=-30,\quad \angle\varphi_z=50^{\circ} \tag{4.24}$$

$$\alpha_{\psi}=-0.5,\quad \beta_{\psi}=-5,\quad \angle\varphi_{\psi}=50^{\circ} \tag{4.25}$$

The LPV controller gains are:

$$K_z\left(\rho_z\right)=\sum_{i=1}^{8}\alpha_{z_i}K_{z_i} \tag{4.26}$$

$$K_{\psi}\left(\rho_{\psi}\right)=\sum_{i=1}^{2}\alpha_{\psi_i}K_{\psi_i} \tag{4.27}$$

where $K_{z_i}\,(i = 1, 2, \ldots, 8)$ and $K_{\psi_i}\,(i = 1, 2)$ represent the state feedback gains, $\alpha_{z_i}\,(i = 1, 2, \ \ldots, 8)$ and $\alpha_{\psi_i}\,(i = 1, 2)$ represent the barycentric weights, and $\rho_z = [\rho_1, \rho_3, \rho_4]$ and $\rho_\psi = \rho_1$ are the time-varying parameters.

The robust closed-loop system stability and quadratic $\mathcal{H}_\infty$ performance γ of the LPV system are tested by using the functions *pdlstab* and *quadperf* from the MATLAB LMI Toolbox's. The LPV system will be stable, if the quantity t_{min} returned by the *pdlstab* function is negative (i.e., $t_{min} < 0$). The values achieved using the functions are given in Table 4.1.

TABLE 4.1: t_{min} and γ values of fully actuated LPV subsystem.

Name	**z-position**	**Yaw Angle**
t_{min}	-0.0512	-0.0158
γ	1.95	0.02

The quantity $t_{min} < 0$, which ensures the closed-loop system's robust stability. The Controller gains and the positive-definite symmetric matrix X at each vertex for the altitude control and yaw control are shown in the Table 4.3, and Table 4.2, respectively.

TABLE 4.2: Controller gains and X matrix of yaw control

Vertex	**Controller Gains**	$X > 0$
@ *vertex*-1	$\begin{bmatrix} -0.0080 & -0.0013 & -0.0084 \end{bmatrix}$	$\begin{bmatrix} 0.2627 & -0.9667 & -0.0797 \\ -0.9667 & 10.9236 & 0.0283 \\ -0.0797 & 0.0283 & 0.0686 \end{bmatrix}$
@ *vertex*-2	$\begin{bmatrix} -0.0069 & -0.0011 & -0.0072 \end{bmatrix}$	$\begin{bmatrix} 0.2624 & -0.9661 & -0.0792 \\ -0.9665 & 10.9236 & 0.0281 \\ -0.0791 & 0.0281 & 0.0681 \end{bmatrix}$

TABLE 4.3: Controller gains and X matrix of altitude control.

Vertex	**Controller Gains**	$X > 0$
@ *vertex*-1	$\begin{bmatrix} 7.1586 & 2.3208 & -9.7133 \end{bmatrix}$	$\begin{bmatrix} 25.0316 & -17.3795 & 14.3073 \\ -17.3795 & 19.3877 & -8.3387 \\ 14.3073 & -8.3387 & 8.5537 \end{bmatrix}$
@ *vertex*-2	$\begin{bmatrix} 8.6006 & 3.2495 & -10.8622 \end{bmatrix}$	$\begin{bmatrix} 16.1704 & -10.4017 & 9.7018 \\ -10.4017 & 11.0004 & -5.0557 \\ 9.7018 & -5.0557 & 6.1710 \end{bmatrix}$
@ *vertex*-3	$\begin{bmatrix} 10.8783 & 4.9088 & -12.4656 \end{bmatrix}$	$\begin{bmatrix} 10.0194 & -5.9018 & 6.4293 \\ -5.9018 & 5.7644 & -2.9512 \\ 6.4293 & -2.9512 & 4.4513 \end{bmatrix}$
@ *vertex*-4	$\begin{bmatrix} 13.3529 & 6.9253 & -14.0111 \end{bmatrix}$	$\begin{bmatrix} 6.5871 & -3.6439 & 4.4863 \\ -3.6439 & 3.3826 & -1.8492 \\ 4.4863 & -1.8492 & 3.3655 \end{bmatrix}$
@ *vertex*-5	$\begin{bmatrix} 10.8783 & 4.9088 & -12.4656 \end{bmatrix}$	$\begin{bmatrix} 10.0194 & -5.9018 & 6.4293 \\ -5.9018 & 5.7644 & -2.9512 \\ 6.4293 & -2.9512 & 4.4513 \end{bmatrix}$
@ *vertex*-6	$\begin{bmatrix} 13.3529 & 6.9253 & -14.0111 \end{bmatrix}$	$\begin{bmatrix} 6.5871 & -3.6439 & 4.4863 \\ -3.6439 & 3.3826 & -1.8492 \\ 4.4863 & -1.8492 & 3.3655 \end{bmatrix}$
@ *vertex*-7	$\begin{bmatrix} -27.697 & -21.087 & 21.025 \end{bmatrix}$	$\begin{bmatrix} 1.8839 & -0.9442 & 1.542 \\ -0.9442 & 0.7476 & -0.509 \\ 1.5420 & -0.5093 & 1.525 \end{bmatrix}$

Continued on next page

Continued from previous page

Vertex	**Controller Gains**	$X > 0$
@ *vertex*-8	$\begin{bmatrix} -35.304 & -29.917 & 23.698 \end{bmatrix}$	$\begin{bmatrix} 1.3114 & -0.6577 & 1.130 \\ -0.6577 & 0.4823 & -0.383 \\ 1.1303 & -0.3834 & 1.203 \end{bmatrix}$

4.1.3 LPV Control for Under-Actuated Subsystem

To address the under-actuation, a multi-loop control strategy is adopted. An inner-loop LPV scheme is suggested for roll and pitch dynamics, while an outer-loop LPV strategy is proposed for the y-position and x-position dynamics to generate the roll and pitch commands. The inner-loop receives the roll and pitch commands $[\phi_{ref}, \quad \theta_{ref}]$ from the outer-loop to track the desired reference positions $[y_{ref}, \quad x_{ref}]$. The scheduling parameters ρ_1 and ρ_2 are not independent, which leads to conservatism. To reduce conservatism, we use a triangle polytope, BED, rather than a rectangular polytope, ABCD, as shown in Figure 4.7 (for details, see [68, 84]). The roll dynamics in descriptor LPV form is:

$$\begin{cases} E_\phi(\rho_\phi) \begin{bmatrix} \dot{\phi} \\ \ddot{\phi} \end{bmatrix} = A_\phi(\rho_\phi) \begin{bmatrix} \phi \\ \dot{\phi} \end{bmatrix} + B_\phi(\rho_\phi) U_1 \\ y_\phi = \begin{bmatrix} 1 & 0 \end{bmatrix} \begin{bmatrix} \phi \\ \dot{\phi} \end{bmatrix} \end{cases} \tag{4.28}$$

where,

$$E_\phi(\rho_\phi) = \begin{bmatrix} 1 & 0 \\ 0 & b_2 \end{bmatrix} + \rho_1 \begin{bmatrix} 0 & 0 \\ 0 & b_1 \end{bmatrix} + \rho_2 \begin{bmatrix} 0 & 0 \\ 0 & b_3 \end{bmatrix} \tag{4.29}$$

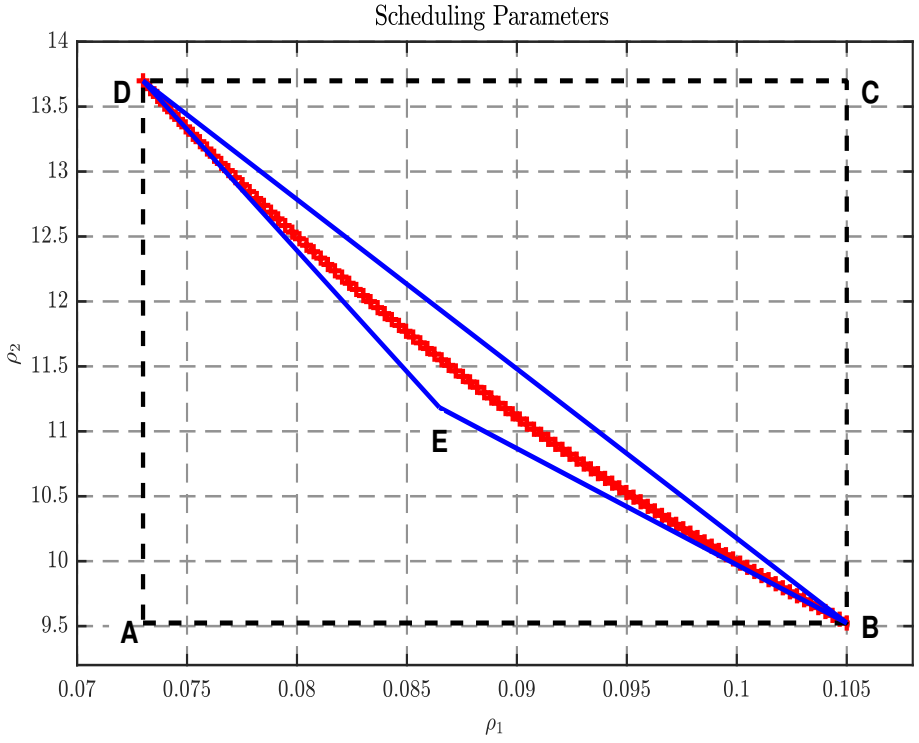

FIGURE 4.7: The structure of the polytope.

$$A_\phi(\rho_\phi) = \begin{bmatrix} 0 & 1 \\ 0 & -2b_1\dot{m} \end{bmatrix} + \rho_1 \begin{bmatrix} 0 & 0 \\ 0 & 0 \end{bmatrix} + \rho_2 \begin{bmatrix} 0 & 0 \\ 0 & -b_2\dot{m} \end{bmatrix} \tag{4.30}$$

$$B_\phi(\rho_\phi) = \begin{bmatrix} 0 \\ 0 \end{bmatrix} + \rho_1 \begin{bmatrix} 0 \\ 0 \end{bmatrix} + \rho_2 \begin{bmatrix} 0 \\ 1 \end{bmatrix} \tag{4.31}$$

The descriptor LPV form of pitch dynamics is given by:

$$\begin{cases} E_\theta(\rho_\theta) \begin{bmatrix} \dot{\theta} \\ \ddot{\theta} \end{bmatrix} = A_\theta(\rho_\theta) \begin{bmatrix} \theta \\ \dot{\theta} \end{bmatrix} + B_\theta(\rho_\theta) U_2 \\ y_\theta = \begin{bmatrix} 1 & 0 \end{bmatrix} \begin{bmatrix} \theta \\ \dot{\theta} \end{bmatrix} \end{cases} \tag{4.32}$$

where,

$$E_\theta(\rho_\theta) = \begin{bmatrix} 1 & 0 \\ 0 & c_2 \end{bmatrix} + \rho_1 \begin{bmatrix} 0 & 0 \\ 0 & c_1 \end{bmatrix} + \rho_2 \begin{bmatrix} 0 & 0 \\ 0 & c_3 \end{bmatrix} \tag{4.33}$$

$$A_\theta(\rho_\theta) = \begin{bmatrix} 0 & 1 \\ 0 & -2c_1\dot{m} \end{bmatrix} + \rho_1 \begin{bmatrix} 0 & 0 \\ 0 & 0 \end{bmatrix} + \rho_2 \begin{bmatrix} 0 & 0 \\ 0 & -c_2\dot{m} \end{bmatrix} \tag{4.34}$$

$$B_\theta(\rho_\theta) = \begin{bmatrix} 0 \\ 0 \end{bmatrix} + \rho_1 \begin{bmatrix} 0 \\ 0 \end{bmatrix} + \rho_2 \begin{bmatrix} 0 \\ 1 \end{bmatrix} \tag{4.35}$$

The LPV form of x-position dynamics is given by:

$$\begin{cases} \begin{bmatrix} \dot{x} \\ \ddot{x} \end{bmatrix} = A_x(\rho_x) \begin{bmatrix} x \\ \dot{x} \end{bmatrix} + B_x(\rho_x)\, u_x \\ \\ y_x = \begin{bmatrix} 1 & 0 \end{bmatrix} \begin{bmatrix} x \\ \dot{x} \end{bmatrix} \end{cases} \tag{4.36}$$

where,

$$A_x(\rho_x) = \begin{bmatrix} 0 & 1 \\ 0 & 0 \end{bmatrix} + \rho_2 \begin{bmatrix} 0 & 0 \\ 0 & -\dot{m} \end{bmatrix} + \rho_3 \begin{bmatrix} 0 & 0 \\ 0 & 0 \end{bmatrix} + \rho_4 \begin{bmatrix} 0 & 0 \\ 0 & 0 \end{bmatrix} \tag{4.37}$$

$$B_x(\rho_x) = \begin{bmatrix} 0 \\ -g \end{bmatrix} + \rho_2 \begin{bmatrix} 0 \\ 0 \end{bmatrix} + \rho_3 \begin{bmatrix} 0 \\ \frac{g}{2} \end{bmatrix} + \rho_4 \begin{bmatrix} 0 \\ \frac{g}{6} \end{bmatrix} \tag{4.38}$$

The descriptor LPV form of y-position dynamics is given by:

$$\begin{cases} \begin{bmatrix} \dot{y} \\ \ddot{y} \end{bmatrix} = A_y(\rho_y) \begin{bmatrix} y \\ \dot{y} \end{bmatrix} + B_y(\rho_y) u_y \\ \\ y_y = \begin{bmatrix} 1 & 0 \end{bmatrix} \begin{bmatrix} y \\ \dot{y} \end{bmatrix} \end{cases} \tag{4.39}$$

where,

$$A_y(\rho_y) = \begin{bmatrix} 0 & 1 \\ 0 & 0 \end{bmatrix} + \rho_2 \begin{bmatrix} 0 & 0 \\ 0 & -\dot{m} \end{bmatrix} + \rho_3 \begin{bmatrix} 0 & 0 \\ 0 & 0 \end{bmatrix} \tag{4.40}$$

$$B_y(\rho_y) = \begin{bmatrix} 0 \\ g \end{bmatrix} + \rho_2 \begin{bmatrix} 0 \\ 0 \end{bmatrix} + \rho_3 \begin{bmatrix} 0 \\ -\frac{g}{6} \end{bmatrix} \tag{4.41}$$

Weighting filters $W_{e\psi}$, $W_{e\theta}$, W_{ex}, and W_{ey} are chosen as follows:

$$\left[\begin{array}{c} \dot{x}_{We\phi} \\ \hline z_{1\psi} \end{array}\right] = \left[\begin{array}{c|c} -7.5 \times 10^{-4} & 7.45 \\ \hline 1 & 0.5 \end{array}\right] \left[\begin{array}{c} x_{We\phi} \\ \hline e_\phi \end{array}\right] \tag{4.42}$$

$$\left[\begin{array}{c} \dot{x}_{We\theta} \\ \hline z_{1\theta} \end{array}\right] = \left[\begin{array}{c|c} -7.5 \times 10^{-4} & 7.45 \\ \hline 1 & 0.5 \end{array}\right] \left[\begin{array}{c} x_{We\theta} \\ \hline e_\theta \end{array}\right] \tag{4.43}$$

$$\left[\begin{array}{c} \dot{x}_{Wex} \\ \hline z_{1x} \end{array}\right] = \left[\begin{array}{c|c} -9.5 \times 10^{-5} & 0.95 \\ \hline 1 & 0.83 \end{array}\right] \left[\begin{array}{c} x_{Wex} \\ \hline e_x \end{array}\right] \tag{4.44}$$

$$\left[\begin{array}{c} \dot{x}_{Wey} \\ \hline z_{1y} \end{array}\right] = \left[\begin{array}{c|c} -9.1 \times 10^{-5} & 0.90 \\ \hline 1 & 0.83 \end{array}\right] \left[\begin{array}{c} x_{Wey} \\ \hline e_y \end{array}\right] \tag{4.45}$$

The values of weights $V_{u\psi} = 1$, $V_{u\theta} = 1$, $V_{ux} = \frac{\pi}{3}$, and $V_{uy} = \frac{\pi}{3}$are considered. The values of static weights $V_{dx} = 0.5$ and $V_{dy} = 0.5$ are assumed. The values of the parameters associated with the LMI regions selected on the basis of control

TABLE 4.4: t_{min} and γ values of under-actuated LPV subsystem.

Name	**Roll Angle**	**Pitch Angle**	**x-position**	**y-position**
t_{min}	-0.04	-0.032	-0.1042	-0.0433
γ	1.0	1.0	1.718	1.292

objectives are:

$$\alpha_\phi = -5, \quad \beta_\phi = -30, \quad \angle\varphi_\phi = 50^\circ \tag{4.46}$$

$$\alpha_\theta = -5, \quad \beta_\theta = -30, \quad \angle\varphi_\theta = 50^\circ \tag{4.47}$$

$$\alpha_x = -0.5, \quad \beta_x = -4.5, \quad \angle\varphi_x = 50^\circ \tag{4.48}$$

$$\alpha_y = -0.5, \quad \beta_y = -4.5, \quad \angle\varphi_y = 50^\circ \tag{4.49}$$

The following are the gains of the LPV controllers designed using conditions (4.11)–(4.14):

$$K_\phi(\rho_\phi) = \sum_{i=1}^{3} \alpha_{\phi i} K_{\phi i} \tag{4.50}$$

$$K_\theta(\rho_\theta) = \sum_{i=1}^{3} \alpha_{\theta_i} K_{\theta_i} \tag{4.51}$$

$$K_x(\rho_x) = \sum_{i=1}^{8} \alpha_{x_i} K_{x_i} \tag{4.52}$$

$$K_y(\rho_y) = \sum_{i=1}^{4} \alpha_{yi} K_{yi} \tag{4.53}$$

$K_{\phi_i}\,(i = 1, 2, 3)$, $K_{\theta_i}\,(i = 1, 2, 3)$, $K_{x_i}\,(i = 1, 2, \ldots, 8)$, and $K_{y_i}\,(i = 1, 2, \ldots, 4)$ represent the feedback gains, $\alpha_{\phi_i}\,(i = 1, 2, 3)$, $\alpha_{\theta_i}\,(i = 1, 2, 3)$, $\alpha_{x_i}\,(i = 1, 2, \ldots, 8)$, and $\alpha_{y_i}\,(i = 1, 2, \ldots, 4)$ represent the barycentric weights, and ρ_ϕ=$[\rho_1, \rho_2]$, $\rho_\theta = [\rho_1, \rho_2]$, $\rho_x = [\rho_2, \rho_3, \rho_4]$, and $\rho_y = [\rho_2, \rho_3]$ are the scheduling parameters.

The values of t_{min} and γ achieved using the MATLAB functions for the under-actuated subsystem are presented in Table 4.4. The condition $t_{min} < 0$ ensures robust stability of the closed-loop system, and $\gamma < 4$, which is a requirement in the H_∞ control scheme. The controller gains and the positive-definite symmetric

matrix X at each vertex for the roll angle controller, pitch angle controller, x-position controller, and y-position controller are presented in Tables 4.5, 4.6, 4.7, and 4.8, respectively.

TABLE 4.5: Controller gains and X matrix of roll control

Vertex	**Controller Gains**	$X > 0$
@ *vertex*-1	$\begin{bmatrix} -0.3417 & -0.0086 & 0.4788 \end{bmatrix}$	$10^6 \begin{bmatrix} 0.028 & -0.426 & 0.014 \\ -0.426 & 6.493 & -0.211 \\ 0.014 & -0.211 & 0.007 \end{bmatrix}$
@ *vertex*-2	$\begin{bmatrix} -0.3210 & -0.0080 & 0.4503 \end{bmatrix}$	$10^6 \begin{bmatrix} 0.032 & -0.489 & 0.016 \\ -0.489 & 7.434 & -0.243 \\ 0.016 & -0.243 & 0.008 \end{bmatrix}$
@ *vertex*-3	$\begin{bmatrix} -0.2247 & -0.0056 & 0.3151 \end{bmatrix}$	$10^7 \begin{bmatrix} 0.006 & -0.102 & 0.003 \\ -0.102 & 1.545 & -0.051 \\ 0.003 & -0.051 & 0.001 \end{bmatrix}$

TABLE 4.6: Controller gains and X matrix of pitch control

Vertex	**Controller Gains**	$X > 0$
@ *vertex*-1	$\begin{bmatrix} -0.3364 & -0.0084 & 0.4715 \end{bmatrix}$	$10^6 \begin{bmatrix} 0.029 & -0.441 & 0.014 \\ -0.441 & 6.716 & -0.219 \\ 0.014 & -0.219 & 0.007 \end{bmatrix}$

Continued on next page

Continued from previous page

Vertex	**Controller Gains**	$X > 0$
@ *vertex*-2	$\begin{bmatrix} -0.3322 & -0.0083 & 0.4657 \end{bmatrix}$	$10^6 \begin{bmatrix} 0.030 & -0.453 & 0.015 \\ -0.453 & 6.896 & -0.225 \\ 0.015 & -0.225 & 0.007 \end{bmatrix}$
@ *vertex*-3	$\begin{bmatrix} -0.2560 & -0.0064 & 0.3600 \end{bmatrix}$	$10^7 \begin{bmatrix} 0.005 & -0.080 & 0.002 \\ -0.080 & 1.211 & -0.039 \\ 0.002 & -0.039 & 0.001 \end{bmatrix}$

TABLE 4.7: Controller gains and X matrix of x-position control.

Vertex	**Controller Gains**	$X > 0$
@ *vertex*-1	$\begin{bmatrix} 2.2456 & 0.7551 & -2.9107 \end{bmatrix}$	$\begin{bmatrix} 47.185 & -42.758 & 25.510 \\ -42.758 & 62.821 & -19.381 \\ 25.510 & -19.381 & 14.603 \end{bmatrix}$
@ *vertex*-2	$\begin{bmatrix} 1.5114 & 0.6723 & -1.0850 \end{bmatrix}$	$\begin{bmatrix} 12.5559 & -8.8900 & 12.0704 \\ -8.8900 & 10.5232 & -6.8530 \\ 12.0704 & -6.8530 & 12.5194 \end{bmatrix}$
@ *vertex*-3	$\begin{bmatrix} 3.3447 & 1.4922 & -2.3959 \end{bmatrix}$	$\begin{bmatrix} 18.962 & -14.165 & 11.647 \\ -13.965 & 18.899 & -6.556 \\ 11.447 & -6.456 & 7.538 \end{bmatrix}$
@ *vertex*-4	$\begin{bmatrix} 3.5014 & 1.5214 & -3.9611 \end{bmatrix}$	$\begin{bmatrix} 18.762 & -14.465 & 11.147 \\ -14.465 & 18.599 & -6.756 \\ 11.147 & -6.756 & 7.238 \end{bmatrix}$

Continued on next page

Continued from previous page

Vertex	**Controller Gains**	$X > 0$
@ *vertex*-5	$\begin{bmatrix} 2.8091 & 1.0976 & -2.8555 \end{bmatrix}$	$\begin{bmatrix} 35.174 & -30.486 & 19.511 \\ -30.586 & 44.782 & -13.691 \\ 19.511 & -13.691 & 11.484 \end{bmatrix}$
@ *vertex*-6	$\begin{bmatrix} 2.5091 & 0.8976 & -3.1555 \end{bmatrix}$	$\begin{bmatrix} 35.074 & -30.686 & 19.311 \\ -30.686 & 44.682 & -13.791 \\ 19.311 & -13.791 & 11.384 \end{bmatrix}$
@ *vertex*-7	$\begin{bmatrix} 4.1207 & 2.9288 & -4.1713 \end{bmatrix}$	$\begin{bmatrix} 11.1191 & -7.6819 & 7.257 \\ -7.6019 & 8.6191 & -3.740 \\ 7.2176 & -3.79305 & 5.238 \end{bmatrix}$
@ *vertex*-8	$\begin{bmatrix} 4.7202 & 2.4283 & -4.7717 \end{bmatrix}$	$\begin{bmatrix} 11.1991 & -7.6219 & 7.2976 \\ -7.6219 & 8.6496 & -3.7905 \\ 7.2976 & -3.7905 & 5.2889 \end{bmatrix}$

TABLE 4.8: Controller gains and X matrix of y-position control.

Vertex	**Controller Gains**	$X > 0$
@ *vertex*-1	$\begin{bmatrix} -2.4701 & -0.7942 & 3.2797 \end{bmatrix}$	$\begin{bmatrix} 34.981 & -35.581 & 18.182 \\ -35.581 & 58.484 & -15.077 \\ 18.182 & -15.077 & 10.179 \end{bmatrix}$
@ *vertex*-2	$\begin{bmatrix} -1.4098 & -0.5517 & 1.1195 \end{bmatrix}$	$\begin{bmatrix} 24.101 & -25.013 & 12.179 \\ -25.013 & 41.688 & -10.759 \\ 12.371 & -10.157 & 7.912 \end{bmatrix}$

Continued on next page

Continued from previous page

Vertex	**Controller Gains**	$X > 0$
@ *vertex*-3	$\begin{bmatrix} -2.7772 & -0.9471 & 3.5963 \end{bmatrix}$	$\begin{bmatrix} 24.908 & -25.083 & 12.974 \\ -25.083 & 41.629 & -10.256 \\ 12.974 & -10.256 & 7.423 \end{bmatrix}$
@ *vertex*-4	$\begin{bmatrix} -1.6747 - 0.68441.3073 \end{bmatrix}$	$\begin{bmatrix} 24.908 & -25.083 & 12.974 \\ -25.083 & 41.629 & -10.256 \\ 12.974 & -10.256 & 7.423 \end{bmatrix}$

4.2 LMI-based H_∞ Control with Pole Placement Constraints

To design H_∞ control with pole placement constraints, the following steps are followed.

1. **System Modeling:**

   Develop a mathematical model of the system in state-space form:

$$\begin{cases} dx(t)/dt = A_p x(t) + B_p u(t) \\ y(t) = C_p x(t) + D_p u(t) \end{cases} \tag{4.54}$$

   Here, $x(t)$ represents the state vector, $u(t)$ is the control input, $y(t)$ is the output, and A_p, B_p, C_p, and D_p are matrices defining the system dynamics.

2. **Define Performance Specifications:**

   Specify the desired performance objectives for the system, such as settling time, overshoot, and robustness requirements.

3. **LMI Problem Formulation:**

   Formulate the control problem as an LMI problem. The LMI problem consists of a set of linear matrix inequalities that should be satisfied for the controller design. The LMIs are typically constructed using the system matrices A_p, B_p, C_p, and D_p, along with weighting functions that capture the desired trade-offs between performance and robustness.

4. **Solve the LMI Problem:**

   Solve the LMI problem using numerical optimization algorithms available in software tools like MATLAB. The goal is to find a set of matrices that satisfy the LMIs, which correspond to the designed controller.

5. **Controller Implementation:**

   Once the LMI problem is solved, the controller matrices are obtained. Implement the controller in the control system using appropriate hardware or software.

4.2.1 H_∞ State Feedback Control

H_∞ controller is a type of robust control design technique used in control systems engineering. It aims to design a controller that minimizes the effects of disturbances and uncertainties in a system while achieving desired performance specifications. The H_∞ control methodology is based on the concept of optimizing the "H_∞-norm" of a system. By minimizing this norm, the controller is designed to provide the best possible disturbance rejection. It achieves this by optimizing the "H_∞-norm" of the system , which represents the worst-case amplification of disturbances to the controlled output.

The general control system configuration is depicted in Figure 4.8. P shows the generalized plant and K depicts the controller gains. The generalized plant is given in state-space form by [85–87]:

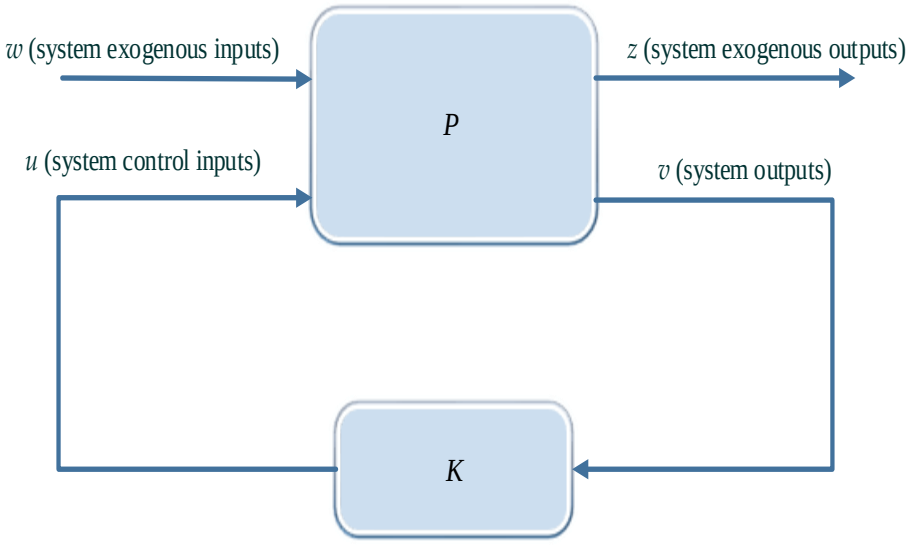

FIGURE 4.8: The structure of closed-loop system.

$$P \ : \begin{cases} \dot{\chi} = \mathcal{A}x + \mathcal{B}_1 w + \mathcal{B}_2 u \\ z = \mathcal{C}_z + \mathcal{D}_{11} w + \mathcal{D}_{12} u \\ v = \mathcal{C}_v \chi + \mathcal{D}_{21} w + \mathcal{D}_{22} u \end{cases} \tag{4.55}$$

The state feedback control law is given as:

$$u = Kv \tag{4.56}$$

The feedback gain can be taken as:

$$K = YX^{-1} \tag{4.57}$$

The LMIs-based linear controller is designed using the following theorems [83, 88, 89].

Theorem 1 (Condition for the $\mathcal{H}_\infty$ Performance):

The $\mathcal{H}_\infty$-norm of closed-loop LPV system from exogenous inputs w to exogenous outputs z will be lower than a positive scalar γ, if and only if there exists a positive-definite symmetric matrix X, and a non-zero matrix Y for all the admissible values of time-varying parameter vector ρ satisfying

$$\begin{cases} \min & \gamma \\ \text{s.t.} & X > 0 \\ & \begin{bmatrix} \mathcal{A}X + X\mathcal{A}^T + \mathcal{B}_2 Y + Y^T \mathcal{B}_2^T & \mathcal{B}_1 & X\mathcal{C}_z^T + Y^T \mathcal{D}_{12}^T \\ \mathcal{B}_1^T & -\gamma I & \mathcal{D}_{11}^T \\ \mathcal{C}_z X + \mathcal{D}_{12} Y & \mathcal{D}_{11} & -\gamma I \end{bmatrix} < 0 \end{cases} \tag{4.58}$$

4.2.2 Pole Placement in LMI Regions

Theorem 2 (Condition for the Closed-Loop Pole Location):
The closed-loop system's eigenvalues will be located in the desirable LMI region $D_{(\alpha,\beta,\varphi)}$, if and only if there exist X, and Y, such that

$$\begin{cases} X > 0 \\ 2\alpha X + \mathcal{A}X + \mathcal{B}_2 Y + X\mathcal{A}^T + Y^T \mathcal{B}_2^T < 0 \\ 2\beta X + \mathcal{A}X + \mathcal{B}_2 Y + X\mathcal{A}^T + Y^T \mathcal{B}_2^T > 0 \end{cases} \tag{4.59}$$

and

$$\begin{bmatrix} \left(X\mathcal{A}^T + \mathcal{A}X + Y^T \mathcal{B}_2^T + \mathcal{B}_2 Y\right) sin\varphi & \left(X\mathcal{A}^T - \mathcal{A}X - \mathcal{B}_2 Y + Y^T \mathcal{B}_2^T\right) cos\varphi \\ \left(\mathcal{A}X - X\mathcal{A}^T + \mathcal{B}_2 Y - Y^T \mathcal{B}_2^T\right) cos\varphi & \left(\mathcal{A}X + X\mathcal{A}^T + \mathcal{B}_2 Y + Y^T \mathcal{B}_2^T\right) sin\varphi \end{bmatrix} < 0 \tag{4.60}$$

where the LMI region $D_{(\alpha,\beta,\varphi)} = D_{(\alpha,\beta)} \cap D_{(\varphi)}$. The system will be D-stable if both conditions (4.59) and (4.60) are satisfied.

4.2.3 H_∞ Design with Desired Pole Region

In many real-world applications, standard H_∞ synthesis cannot adequately capture all design specifications. Pure H_∞ synthesis only enforces closed-loop stability and does not allow for direct placement of the closed-loop poles in more specific regions of the left-half plane. Since the pole location is related to the time response and transient behavior of the feedback system, it is often desirable to impose additional damping and clustering constraints on the closed-loop dynamics. This makes multi-objective synthesis highly desirable in practice, and LMI theory offers powerful tools to attack such problems. In the H_∞ design with a desired LMI pole region, the H_∞ and closed-loop Eigen value performance requirements are satisfied simultaneously.

4.2.4 Linear Control Design for Quadcopter

To design a linear controller for a quadcopter, the linear model given in equation (3.45) is used:
Linear model of fully-actuated subsystem is given by:

$$G: \begin{cases} \ddot{z} = -\frac{u_4}{m_{avg}} \\ \ddot{\psi} = \frac{u_3}{I_{zavg}} \end{cases} \tag{4.61}$$

In state space form, we can write:

$$\begin{bmatrix} \dot{z} \\ \ddot{z} \\ \dot{\psi} \\ \ddot{\psi} \end{bmatrix} = \begin{bmatrix} 0 & 1 & 0 & 0 \\ 0 & 0 & 0 & 0 \\ 0 & 0 & 0 & 1 \\ 0 & 0 & 0 & 0 \end{bmatrix} \begin{bmatrix} z \\ \dot{z} \\ \psi \\ \dot{\psi} \end{bmatrix} + \begin{bmatrix} 0 & 0 \\ -1/m & 0 \\ 0 & 0 \\ 0 & 1/I_{zavg} \end{bmatrix} \begin{bmatrix} u_4 \\ u_3 \end{bmatrix} \tag{4.62}$$

$$\begin{bmatrix} y_1 \\ y_2 \end{bmatrix} = \begin{bmatrix} 1 & 0 & 0 & 0 \\ 0 & 0 & 1 & 0 \end{bmatrix} \begin{bmatrix} z \\ \dot{z} \\ \psi \\ \dot{\psi} \end{bmatrix} \tag{4.63}$$

The representation of the under-actuated subsystem's linear model of quadcopter is expressed as follows:

$$G: \begin{cases} \ddot{\phi} = \dfrac{u_1}{I_{xavg}} \\ \ddot{\theta} = \dfrac{u_2}{I_{yavg}} \\ \ddot{x} = -g\theta = -gu_x \\ \ddot{y} = g\phi = gu_y \end{cases} \tag{4.64}$$

The representation of the state space equations for the 2-degrees-of-freedom linear model of quadcopter is as follows:

$$\begin{bmatrix} \dot{\phi} \\ \ddot{\phi} \\ \dot{\theta} \\ \ddot{\theta} \\ \dot{x} \\ \ddot{x} \\ \dot{y} \\ \ddot{y} \end{bmatrix} = \begin{bmatrix} 0 & 1 & 0 & 0 & 0 & 0 & 0 & 0 \\ 0 & 0 & 0 & 0 & 0 & 0 & 0 & 0 \\ 0 & 0 & 0 & 1 & 0 & 0 & 0 & 0 \\ 0 & 0 & 0 & 0 & 0 & 0 & 0 & 0 \\ 0 & 0 & 0 & 0 & 0 & 1 & 0 & 0 \\ 0 & 0 & 0 & 0 & 0 & 0 & 0 & 0 \\ 0 & 0 & 0 & 0 & 0 & 0 & 0 & 1 \\ 0 & 0 & 0 & 0 & 0 & 0 & 0 & 0 \end{bmatrix} \begin{bmatrix} \phi \\ \dot{\phi} \\ \theta \\ \dot{\theta} \\ x \\ \dot{x} \\ y \\ \dot{y} \end{bmatrix} + \begin{bmatrix} 0 & 0 & 0 & 0 \\ 1/I_{xavg} & 0 & 0 & 0 \\ 0 & 0 & 0 & 0 \\ 0 & 1/I_{yavg} & 0 & 0 \\ 0 & 0 & 0 & 0 \\ 0 & 0 & -g & 0 \\ 0 & 0 & 0 & 0 \\ 0 & 0 & 0 & g \end{bmatrix} \begin{bmatrix} u_1 \\ u_2 \\ u_x \\ u_y \end{bmatrix} \tag{4.65}$$

(4.66)

$$\begin{bmatrix} y_1 \\ y_2 \\ y_3 \\ y_4 \end{bmatrix} = \begin{bmatrix} 1 & 0 & 0 & 0 & 0 & 0 & 0 & 0 \\ 0 & 0 & 1 & 0 & 0 & 0 & 0 & 0 \\ 0 & 0 & 0 & 0 & 1 & 0 & 0 & 0 \\ 0 & 0 & 0 & 0 & 0 & 0 & 1 & 0 \end{bmatrix} \begin{bmatrix} \phi \\ \dot{\phi} \\ \theta \\ \dot{\theta} \\ x \\ \dot{x} \\ y \\ \dot{y} \end{bmatrix} \tag{4.67}$$

4.2.5 Linear Control Design for Fully Actuated Subsystem

Linear controller is devised for the fully actuated subsystem dynamics given in (4.61) by solving the LMIs given in (4.59) and (4.60). Same weighting functions and pole region constraints used in LPV control design are used for the linear control scheme design.

The postive definite matrix X, and the gain matrix, K computed for the altitude and yaw dynamics are given as:

$$X_z = \begin{bmatrix} 30.35 & -18.032 & 21.66 \\ -18.03 & 16.796 & -11.33 \\ 21.66 & -11.333 & 15.88 \end{bmatrix} > 0, \; X_\psi = \begin{bmatrix} 0.26 & -0.96 & -0.079 \\ -0.96 & 10.92 & 0.028 \\ -0.07 & 0.02 & 0.068 \end{bmatrix} > 0 \tag{4.68}$$

$$\begin{bmatrix} K_z \\ K_\psi \end{bmatrix} = \begin{bmatrix} 8.8906 & 2.7924 & -10.1349 \\ -0.0075 & -0.0012 & -0.0078 \end{bmatrix} \tag{4.69}$$

The values of γ for the actuated linear subsystem are given in Table 4.9.

TABLE 4.9: γ values of full actuated linear subsystem.

Name	**Altitude**	**Yaw Angle**
γ	1.0	1.0

The condition $\gamma < 4$ ensures robust performance of the closed-loop system.

4.2.6 Linear Controller for Under-Actuated Subsystem

Linear controller is devised for the under-actuated subsystem dynamics given in (4.64) by solving the LMIs in (4.59) and (4.60). Same weighting functions and pole region constraints are used for the control design. The positive definite matrix X, and the gain matrix K computed for the roll, pitch, x-position, and y-position dynamics are:

$$X_\phi = 10^7 \begin{bmatrix} 0.012 & -0.140 & 0.008 \\ -0.140 & 1.583 & -0.093 \\ 0.008 & -0.093 & 0.005 \end{bmatrix} > 0,\ X_\theta = 10^7 \begin{bmatrix} 0.011 & -0.128 & 0.007 \\ -0.128 & 1.455 & -0.085 \\ 0.007 & -0.085 & 0.005 \end{bmatrix} > 0 \tag{4.70}$$

$$X_x = \begin{bmatrix} 296.16 & -200.63 & 397.17 \\ -200.63 & 168.14 & -262.60 \\ 397.17 & -262.60 & 534.44 \end{bmatrix} > 0,\ X_y = \begin{bmatrix} 172.88 & -128.37 & 205.51 \\ -128.37 & 127.33 & -146.31 \\ 205.51 & -146.31 & 246.01 \end{bmatrix} > 0 \tag{4.71}$$

$$\begin{bmatrix} K_\phi \\ K_\theta \\ K_x \\ K_y \end{bmatrix} = \begin{bmatrix} -0.2601 & -0.0067 & 0.2948 \\ -0.2717 & -0.0070 & 0.3081 \\ 4.7186 & 1.0533 & -2.9967 \\ -4.3824 & -1.0145 & 3.0649 \end{bmatrix} \tag{4.72}$$

The values of γ for the under-actuated subsystem are given in Table 4.10.

TABLE 4.10: γ values of under-actuated linear subsystem.

Name	**Roll Angle**	**Pitch Angle**	**x-position**	**y-position**
γ	1.0	1.0	1.718	1.292

The quantity $\gamma < 4$, which ensures the closed-loop system's robust performance.

4.3 Chapter Summary

This chapter begins with the general formulation of LPV control design scheme. The next section provides the design of LMIs-based LPV control scheme for quadcopter with variable payload. LMIs of H_∞ and pole placement constraints in the LMI region are used to design the LPV control scheme for the quadcopter position control. The robust stability and quadratic H_∞ performance are assessed by LMIs. Finally, in the last section, the formulation and design of H_∞ control design with pole placement constraint is presented. The simulations conducted to assess the effectiveness of the designed control techniques are covered in the next chapter.

Chapter 5

Simulation Results and Discussion

In this chapter, simulation results for three distinct control strategies, namely, the LPV control scheme, the H_∞ control scheme, and the SMC control scheme, designed for precise quadcopter position tracking, are presented. The simulations are performed in MATLAB/SIMULINK for the quadcopter's position tracking in x, y and z direction and yaw angle ψ stabilization. The simulations utilize the nonlinear model of the quadcopter with variable load, as outlined in Equation (3.26). Several factors, such as varying parameters, model uncertainties, step disturbances, wind disturbance, noise, and actuator saturation, are taken into account to evaluate the proposed control schemes' ability to maintain the desired output. The effectiveness of these schemes is assessed using performance parameters such as rise time (t_r), settling time (t_s), overshoot (OS), root mean squared error (RMSE), and robustness.

5.1 Simulation Results of the LPV Scheme

To evaluate the trajectory tracking performance of the LPV scheme in the presence of wind disturbance and variations in payload, wind disturbances are introduced

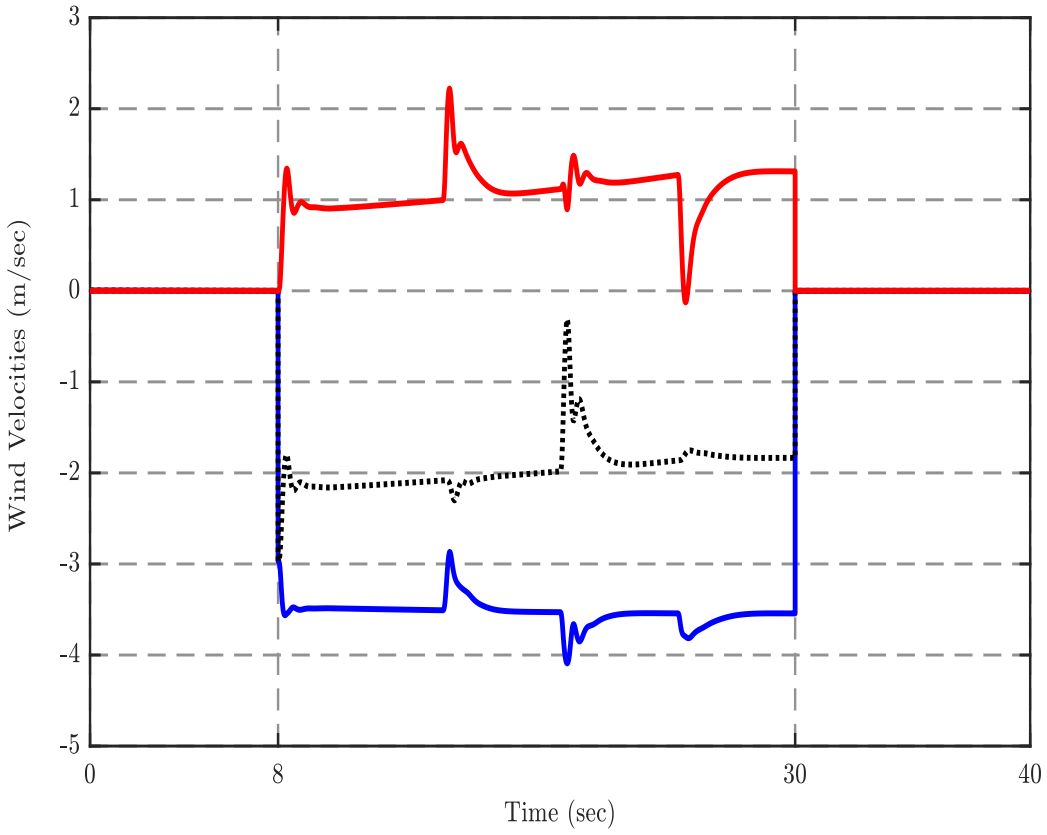

FIGURE 5.1: Variation in the wind velocities with time

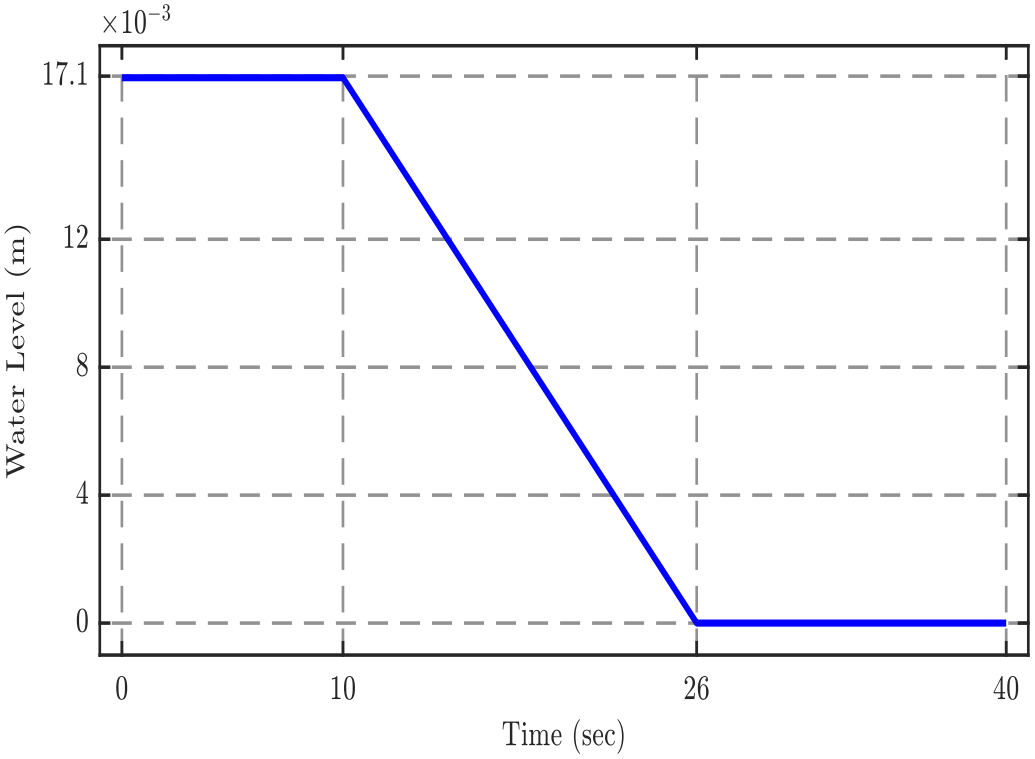

FIGURE 5.2: Variation in the water level with time

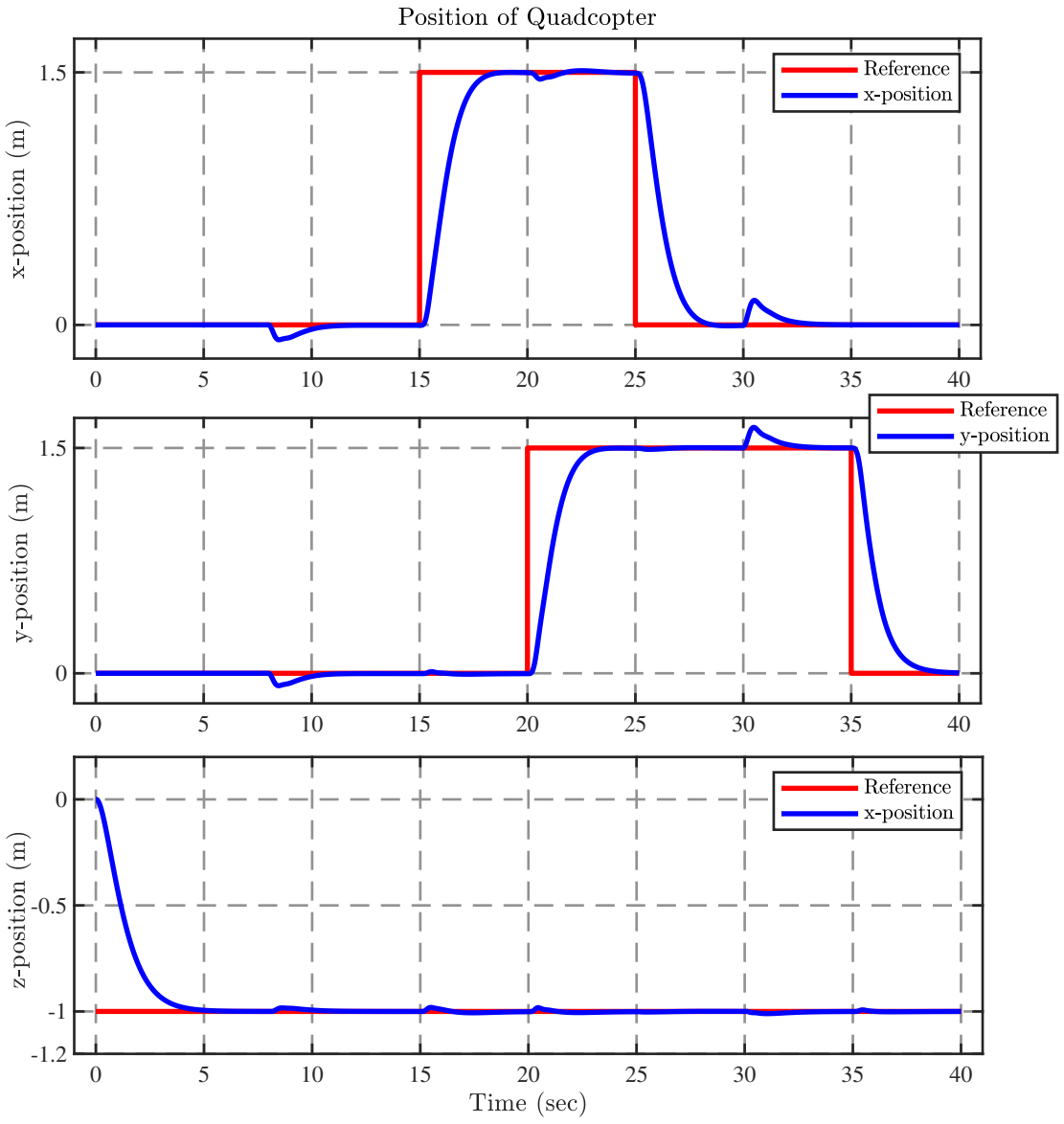

FIGURE 5.3: Quadcopter positions (x, y, z) with wind disturbance and varying payload

at $t = 8$ sec, while payload variation is applied at $t = 10$ sec. The Horizontal Wind Model in SIMULINK is used for wind generation. The wind is specified by wind speed and wind direction in inertial frame. The Horizontal Wind Model block computes the wind velocity in body frame. Using the rotation matrix R_b^i given in equation (3.5), the wind velocities are transformed into inertial frame wind velocities represented in equation (3.15). A constant North-East wind velocity of 4.3 m/s is considered. The wind velocity is set to zero from $t = 0$ to $t = 8$ sec, 4.3 m/s from $t = 8$ to $t = 30$ sec, and back to zero from $t = 30$ to $t = 40$ sec.

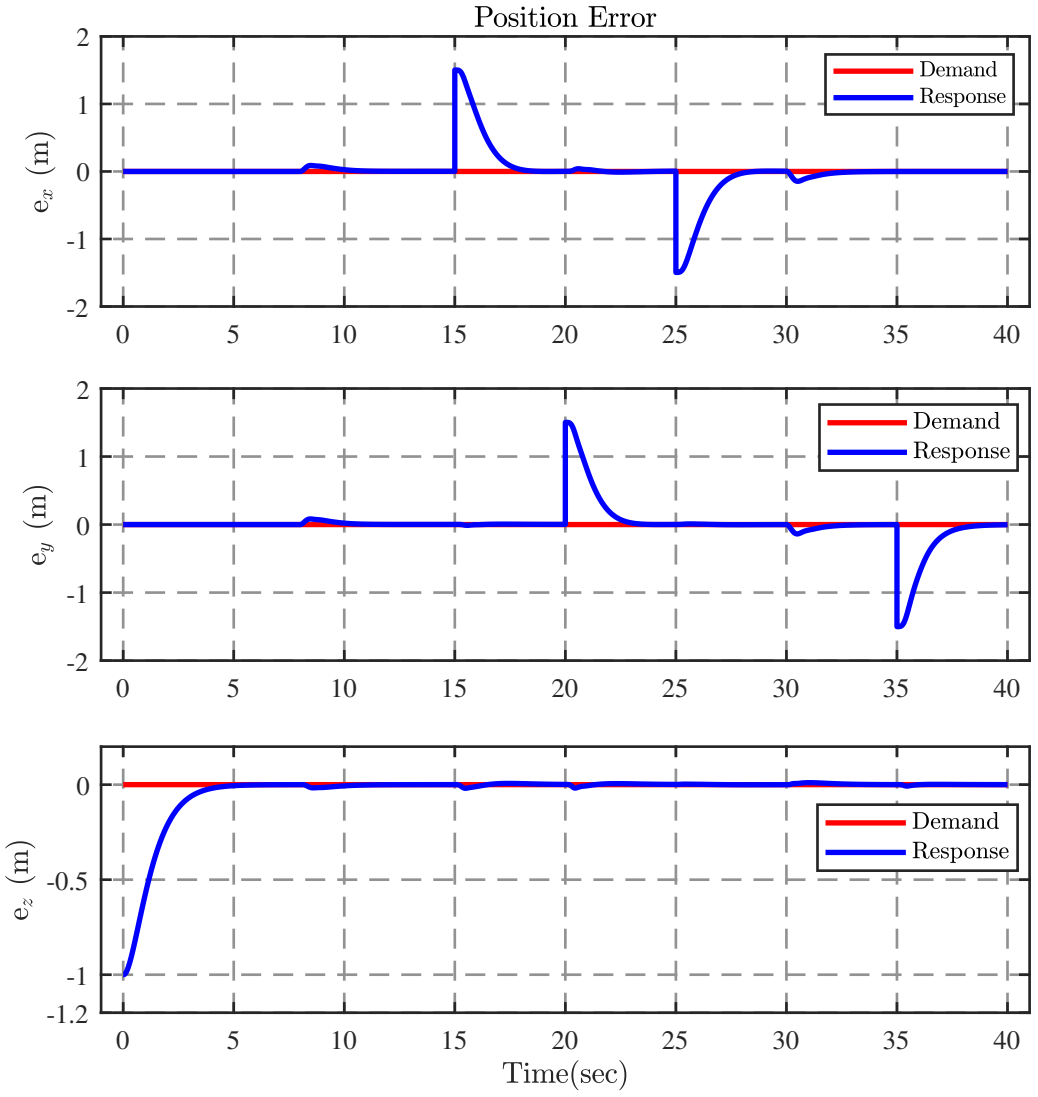

FIGURE 5.4: Error plots (e_x ,e_y, ez) in the presence of wind disturbance and varying payload.

Figure 5.1 displays the wind velocities. Additionally, the variation in the liquid flow rate is assumed to be 0.002 kg/s. Figure 5.2 illustrates the variation in the water level over time.

A square type reference signal is applied to the x and y positions, and a step signal is applied to the z position as reference signals. Figure 5.3 presents these reference signals alongside the quadcopter's positions in the presence of varying payload and wind disturbances. It is observed that the quadcopter efficiently tracks the reference signals, even when large tilt angles are required due to wind

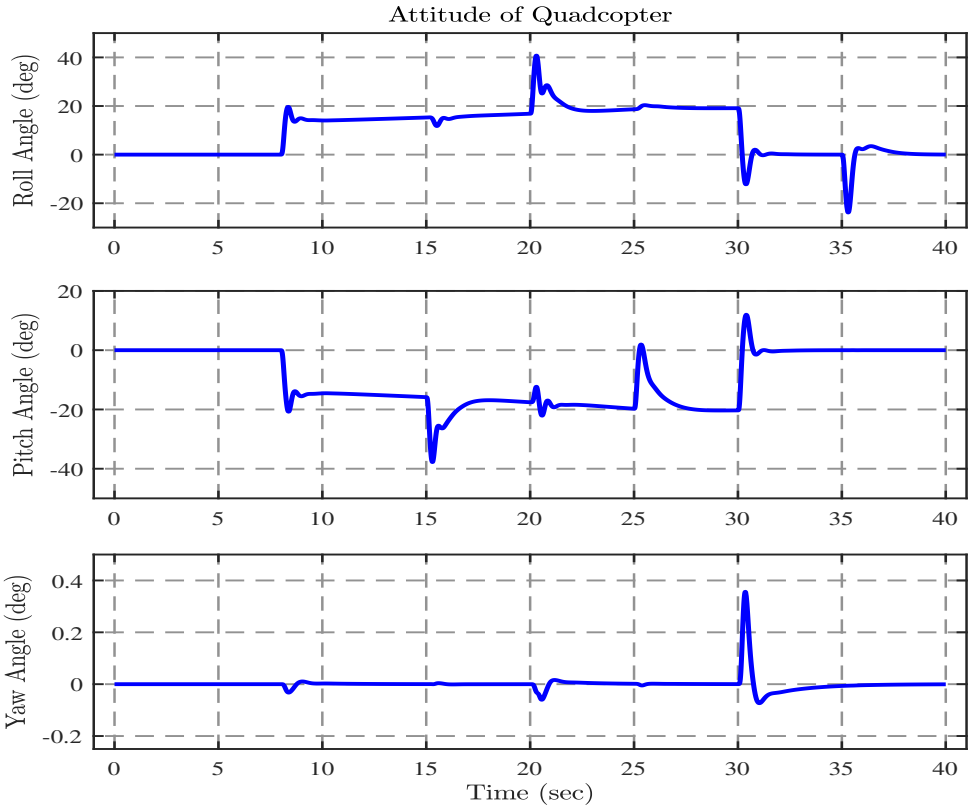

FIGURE 5.5: Attitude (ϕ, θ, ψ) with wind disturbance and varying payload.

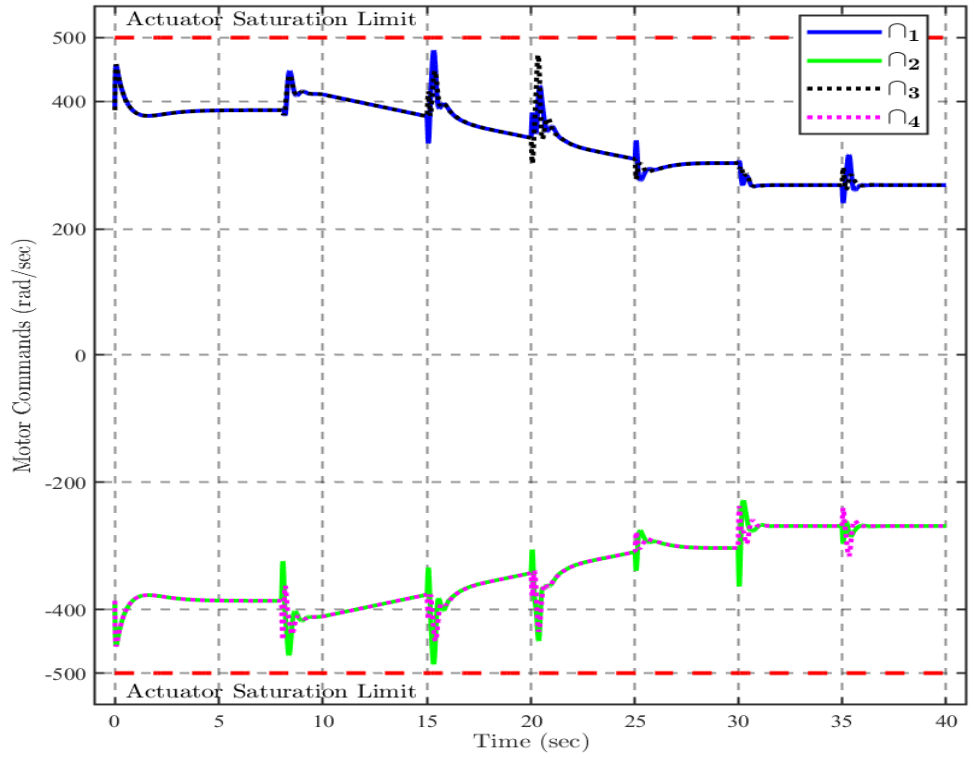

FIGURE 5.6: Motor commands ($\cap_1$, $\cap_2$, $\cap_3$, $\cap_4$) with wind disturbance and varying payload.

disturbances and variable payload. Figure 5.4 shows the error plot, indicating that the proposed scheme drives the error signals to zero in the steady state and is capable of rejecting wind disturbances within 2 sec. The controller generates significant roll and pitch angles to follow the x and y trajectories in the presence of wind disturbances while maintaining the yaw angle at 0°, as shown in Figure 5.5. Figures 5.7 and 5.6 illustrate the control signals and motor reference commands, respectively. It is evident from the control signals that there is no saturation, and the motor commands are within the limits. Actuator saturation occurs if the motor command value reaches 500 rad/sec.

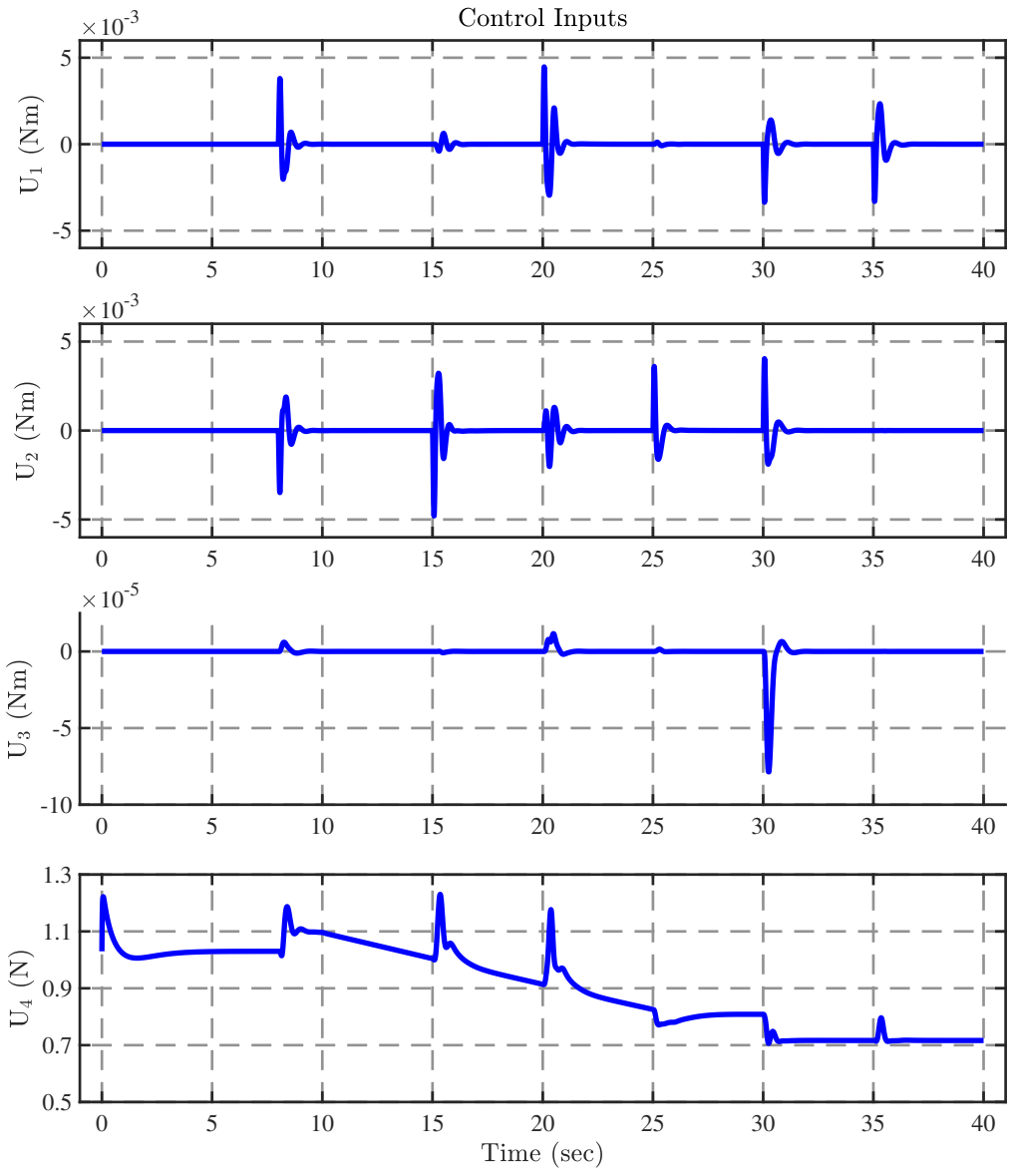

FIGURE 5.7: Control inputs (U_1, U_2, U_3, U_4) with wind disturbance and varying payload.

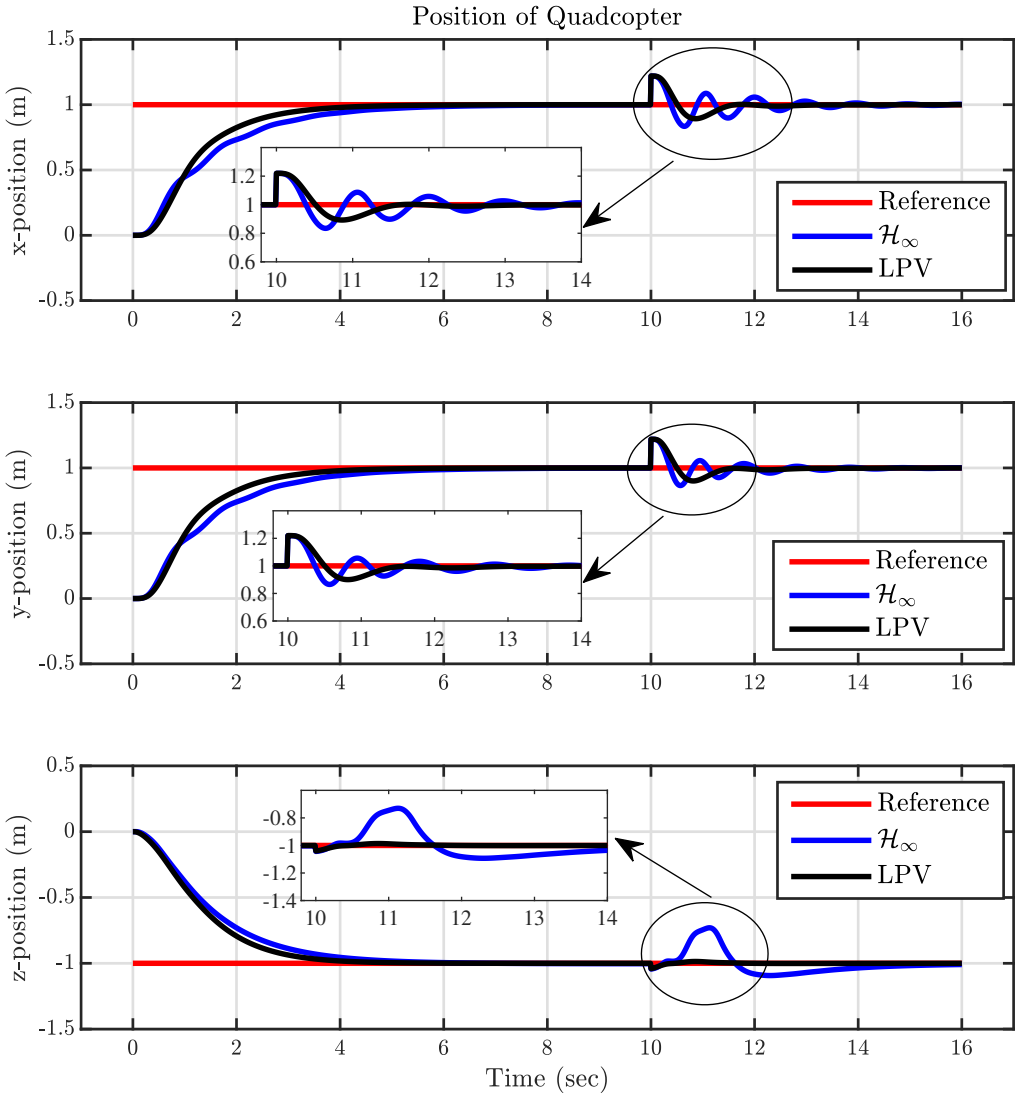

FIGURE 5.8: Response of quadcopter positions (x, y, z) to varying payload in a step input scenario.

5.2 Comparison with H_∞ Controller

In this section, we present a comparison of the simulation outcomes derived from the control strategies we formulated. We compared the response of the LPV controller, specifically designed for the LPV model, with the H_∞ controller designed for the quadcopter's linear model. The latter was obtained using the small angle

assumption and nominal values of mass and inertia parameters. Various scenarios were explored in the simulations. In the first scenario, the control schemes we devised were evaluated for their ability to track the reference position of the quadcopter with variable payload and external output disturbances. The second scenario introduced uncertainty by incorporating fluctuations in the inertia parameters. Wind disturbance was incorporated in the third scenario, and in the fourth scenario, noise was introduced into the system states.

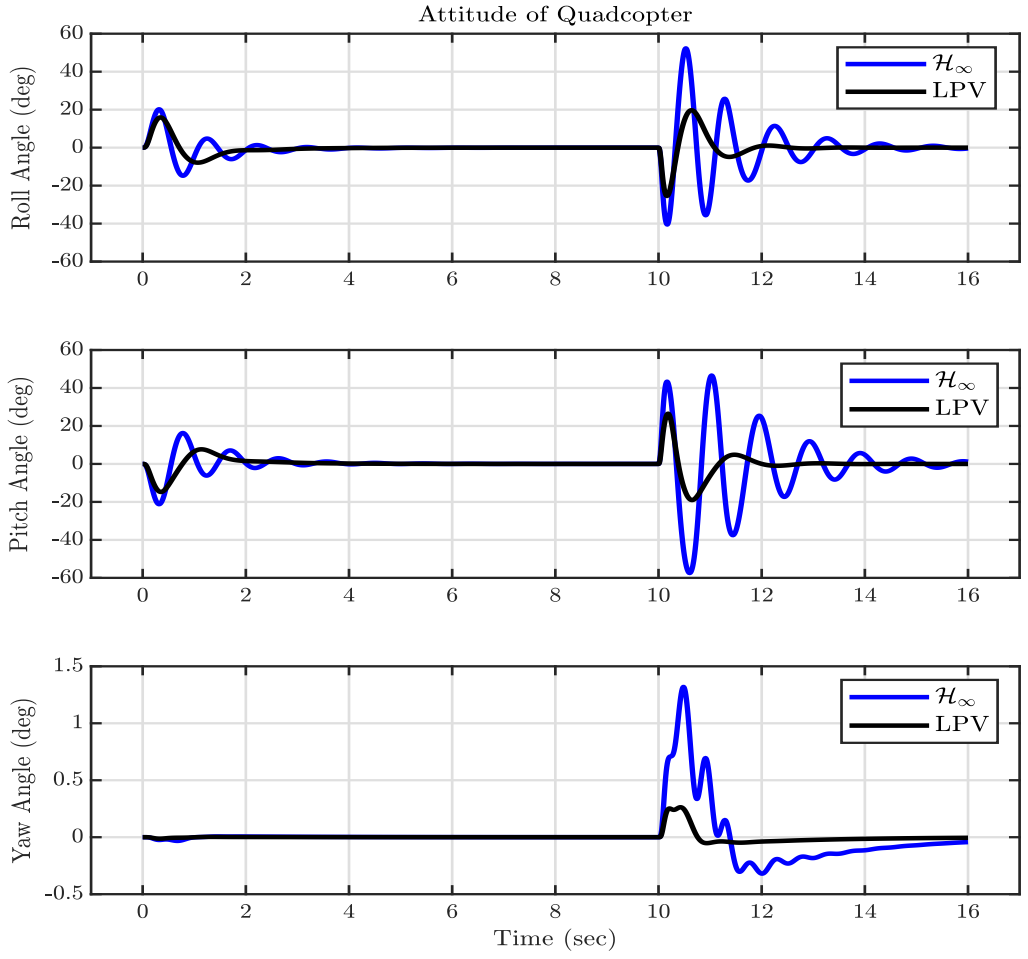

FIGURE 5.9: Attitude angles (ϕ, θ, ψ) of quadcopter with varying payload.

Case 1 (Position Tracking and Yaw Angle Control):

In this case, we assess the quadcopter's ability to track its position and maintain a yaw angle of $\angle 0°$ under varying payload. A step input signal is applied to all three position states (x, y, z) of the quadcopter. The results presented in Figure 5.8

demonstrate precise position tracking without overshoot (OS) for both control techniques, with some differences observed between them.

To analyze the robustness of the controllers, a step disturbance is introduced at 10 sec. The LPV controller robustly rejects the disturbance effects, while the H_∞ controller produces an oscillatory response, particularly evident in the attitude angles, as illustrated in Figure 5.9.

TABLE 5.1: The closed-loop performance parameters with varying payload.

	Performance Parameters	$\boldsymbol{H_\infty}$	**LPV**	% **Improvement**
x-position	t_r	2.8931 *sec*	2.0841 *sec*	27.96
	t_s	5.3687 *sec*	3.9667 *sec*	26.11
	RMSE_{TR}	0.3902 m	0.3775 m	3.25
	RMSE_{SSR}	0.0493 m	0.03765 m	23.63
y-position	t_r	2.8515 *sec*	2.0836 *sec*	26.93
	t_s	5.3132 *sec*	3.9606 *sec*	25.46
	RMSE_{TR}	0.3893 m	0.3725 m	4.32
	RMSE_{SSR}	0.0459 m	0.0367 m	20.04
z-position	t_r	2.7062 *sec*	2.2461 *sec*	17
	t_s	4.9786 *sec*	3.9287 *sec*	21.09
	RMSE_{TR}	0.4039 m	0.3803 m	5.84
	RMSE_{SSR}	0.0739 m	0.0049 m	93.37
Yaw angle	RMSE_{TR}	0.0089 *rad*	0.0024 *rad*	73.03
	RMSE_{SSR}	0.2685 *rad*	0.0674 *rad*	74.9

TABLE 5.2: The RMS comparison of control signals of LPV and H_∞ with varying payload.

Performance Parameters	$\boldsymbol{H_\infty}$	**LPV**	% **Improvement**
RMS of U_1	1.4103×10^{-3}	8.3014×10^{-4}	41
RMS of U_2	1.6362×10^{-3}	7.8155×10^{-4}	52
RMS of U_3	3.5155×10^{-5}	8.9423×10^{-6}	74
RMS of U_4	9.2252×10^{-1}	8.7228×10^{-1}	6

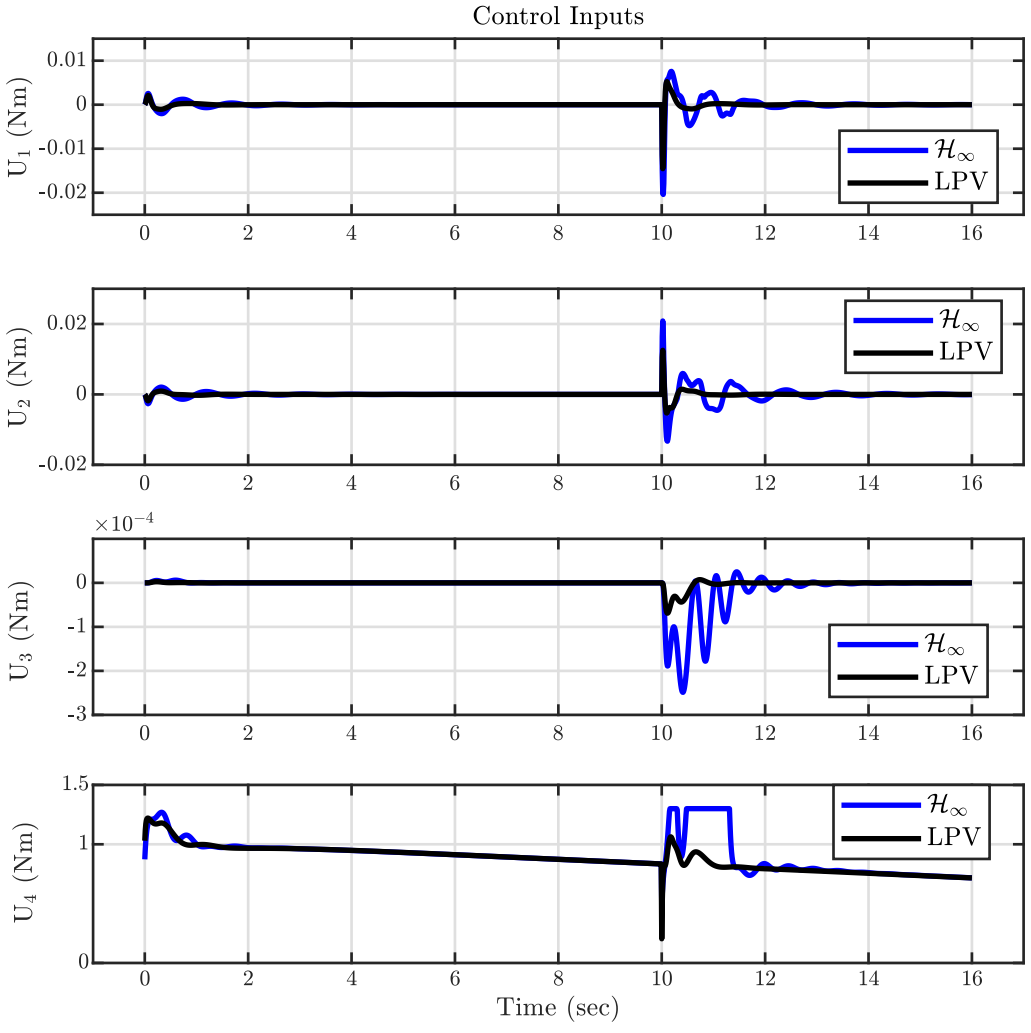

FIGURE 5.10: Control inputs (U_1, U_2, U_3, U_4) with varying payload.

The control inputs are depicted in Figure 5.10. The first three subplots represent the rolling, pitching, and yawing moments as U_1, U_2, and U_3, respectively. U_4 represents the thrust force, which reaches saturation limits for the H_∞ controller. Motor reference commands are illustrated in Figure 5.11, calculated using Equation (3.25) from the control inputs U_1, U_2, U_3, and U_4. For the H_∞ controller, the motor speed reaches its maximum value of 500 rad/sec.

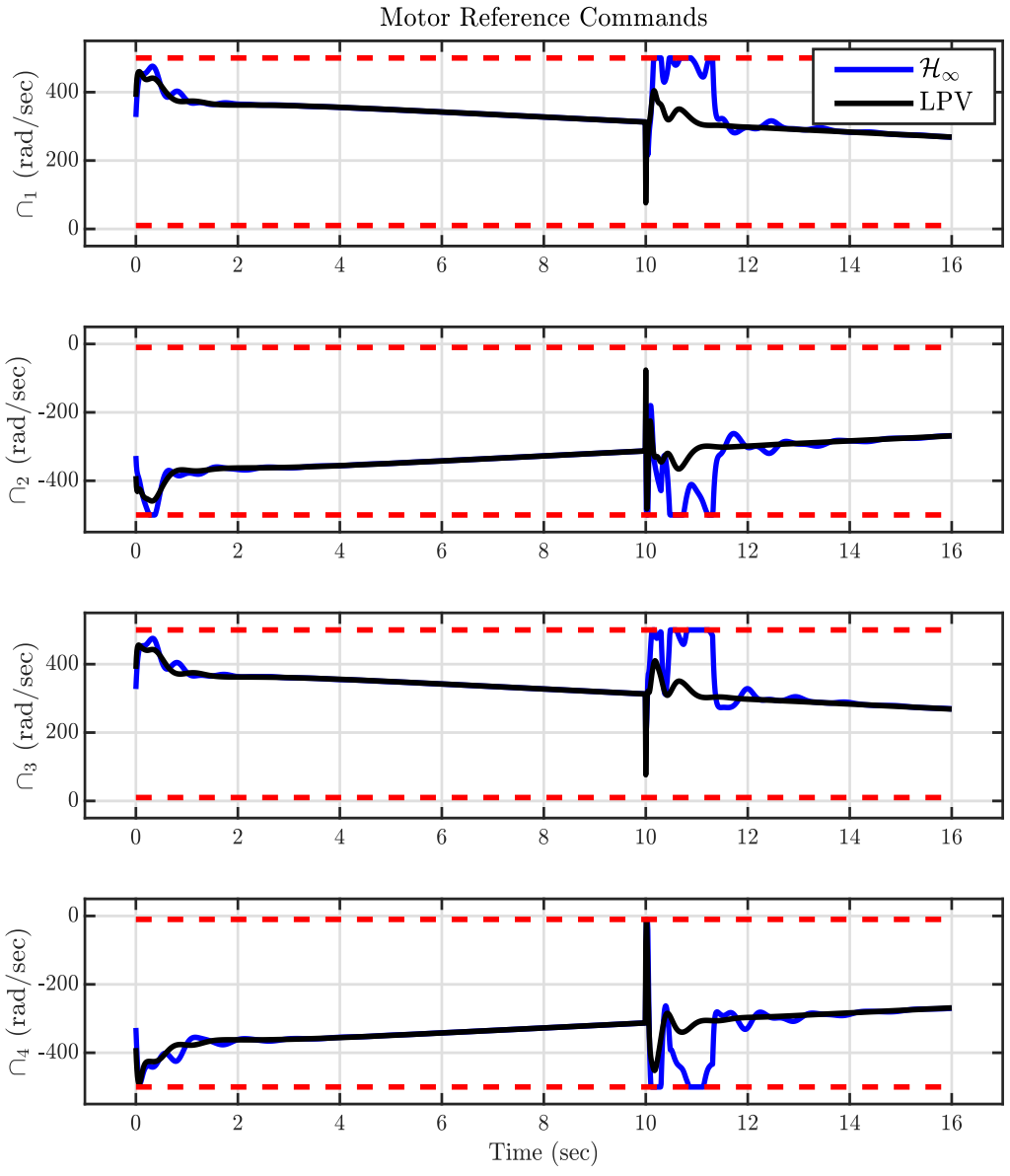

FIGURE 5.11: Motor commands ($\cap_1$, $\cap_2$, $\cap_3$, $\cap_4$) with varying payload.

Furthermore, a quantitative analysis of both techniques is presented in Tables 5.1 and 5.2. System rise time (t_r), system settling time (t_s), root mean squared error during the transient stage (RMSE_{TR}), and RMSE for steady-state response (RMSE_{SSR}) are compared for positions (x, y, z) and yaw angle (ψ). Moreover, the root mean squared values of the control inputs are also compared. The results indicate a significant improvement in t_r, t_s, RMSE_{TR}, RMSE_{SSR}, and RMS, up to 28%, 26%, 73%, 93%, and 74%, respectively, highlighting the effectiveness of the LPV control strategy. This 93% improvement signifies that the RMSE_{SSR} achieved with the LPV approach is 93% lower than that attained with the $H\infty$ controller.

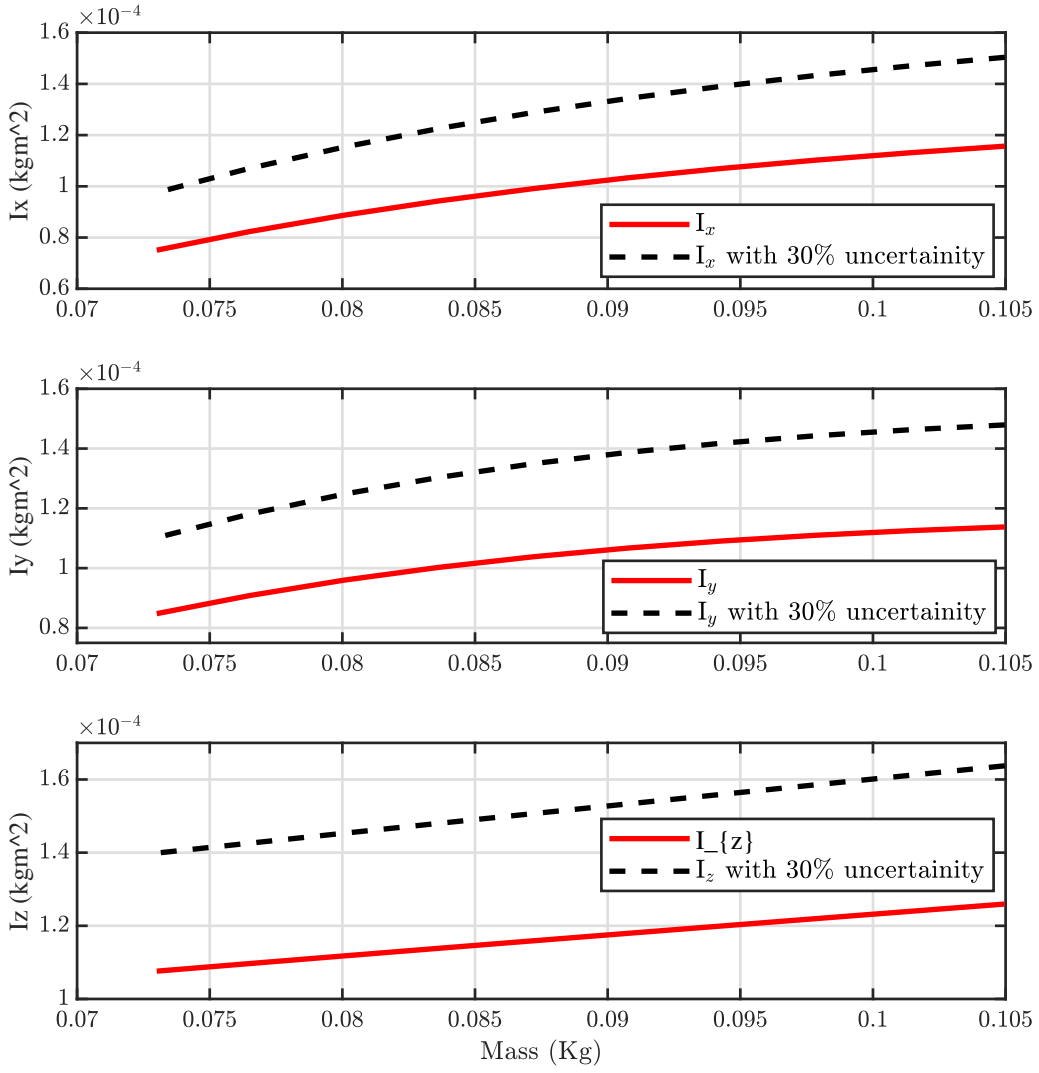

FIGURE 5.12: Variation in the inertia parameters with mass.

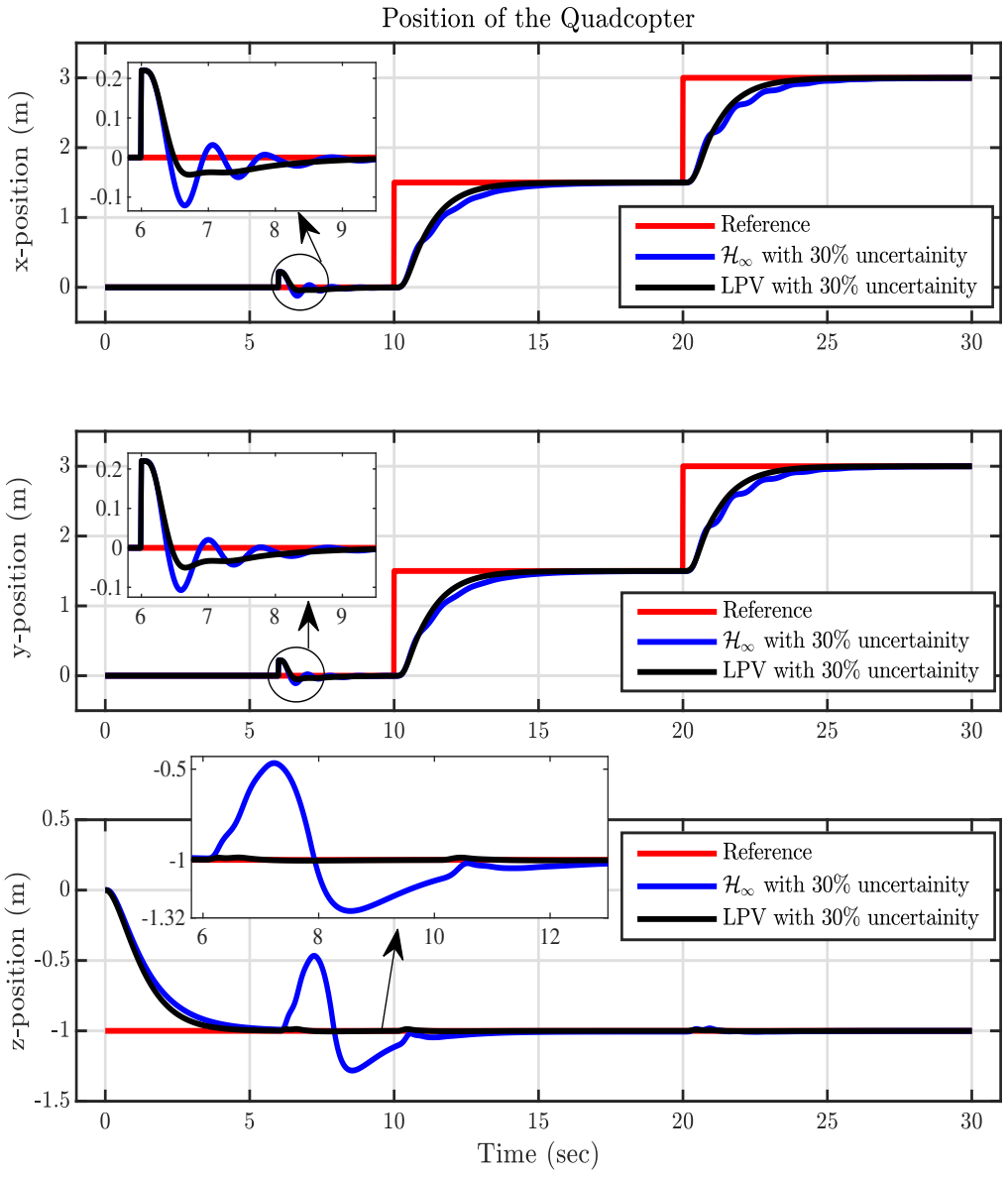

FIGURE 5.13: Positions (x, y, z) of quadcopter with 30% variation in the inertia.

Case 2 (Performance Comparison under Uncertainty in Inertia Parameters):

In the second case, we illustrate the performance comparison of both control techniques in the presence of uncertainty in the inertia parameters (I_x, I_y, I_z) caused by tilt angles (ϕ, θ). The inertia parameters can vary due to the tilting of the quadcopter with a variable payload. A 30% uncertainty is introduced to account

for the change in the inertia parameters during tilting. Figure 5.12 illustrates the variation in inertia due to mass for both untilted and tilted positions.

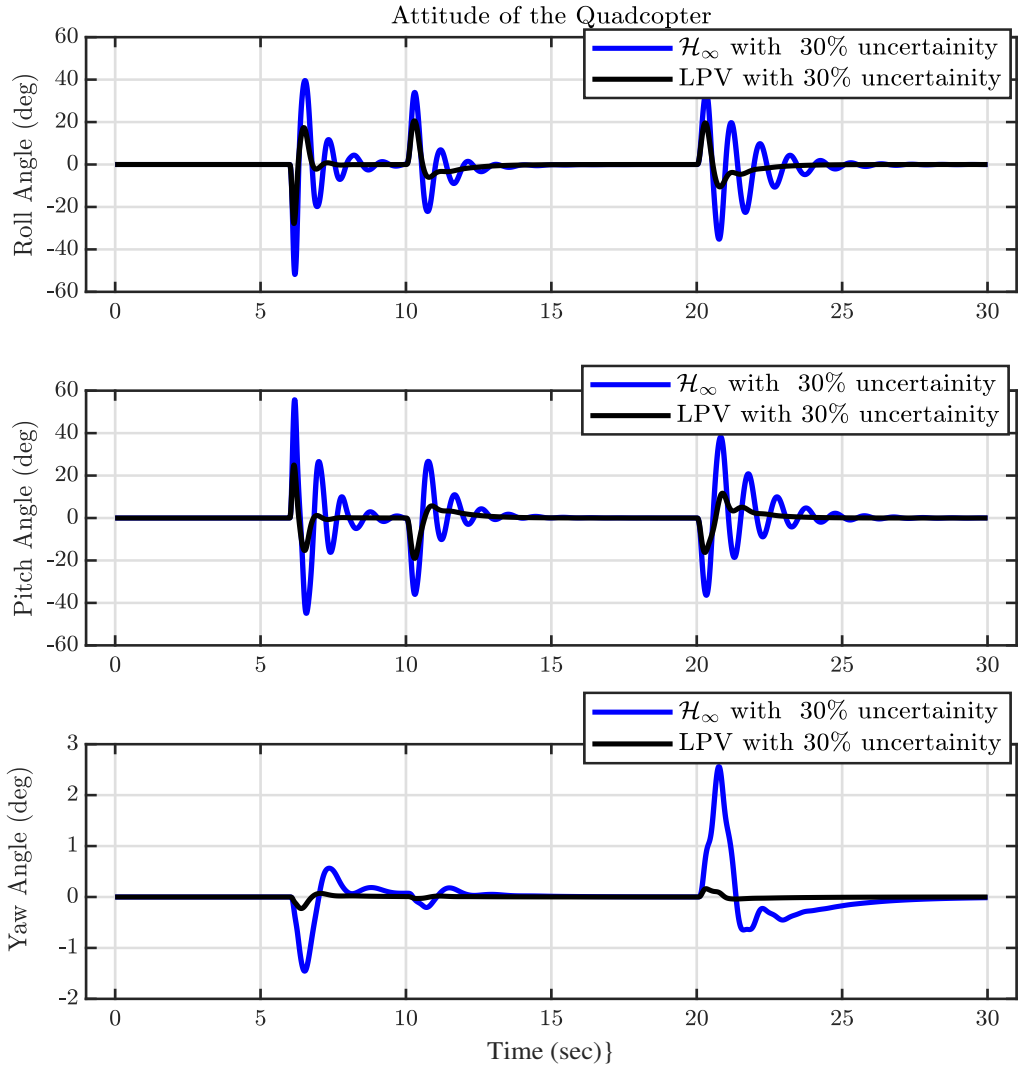

FIGURE 5.14: Attitude angles (ϕ, θ, ψ) of quadcopter with 30% variation in the inertia.

The performance evaluation involves applying a steer case reference signal on the x, y, and z states and introducing a step disturbance in position at 6 sec. Figure 5.13 presents the position tracking and disturbance rejection responses of the controllers. Both techniques adequately track the reference signal. However, the disturbance rejection, especially along the z-axis, is significantly poorer in the H_∞ controller compared to LPV.

TABLE 5.3: The RMSE with 30% uncertainty.

	Performance Parameters	H_∞	**LPV**	% **Improvement**
x-position	RMSE	0.3712 m	0.3524 m	5.06
y-position	RMSE	0.3748 m	0.3516 m	6.19
z-position	RMSE	0.2089 m	0.1701 m	18.57
Yaw angle	RMSE	0.3809 rad	0.032 rad	91.59

TABLE 5.4: The RMS comparison of control signals of LPV and H_∞ with 30% uncertainty.

Performance Parameters	H_∞	**LPV**	% **Improvement**
RMS of U_1	4.5911×10^{-3}	1.1185×10^{-3}	75
RMS of U_2	4.6314×10^{-3}	9.1573×10^{-4}	80
RMS of U_3	5.7893×10^{-5}	4.2431×10^{-6}	92
RMS of U_4	9.1312×10^{-1}	8.7860×10^{-1}	4

Furthermore, Figure 5.14 demonstrates the substantial variation and oscillation in the attitude angles. Additionally, the H_∞ technique requires considerably more control effort compared to LPV, as evident in the Figure 5.15. The Figure 5.16 shows that the motor speeds for the LPV methodology remain well within the maximum range limit.

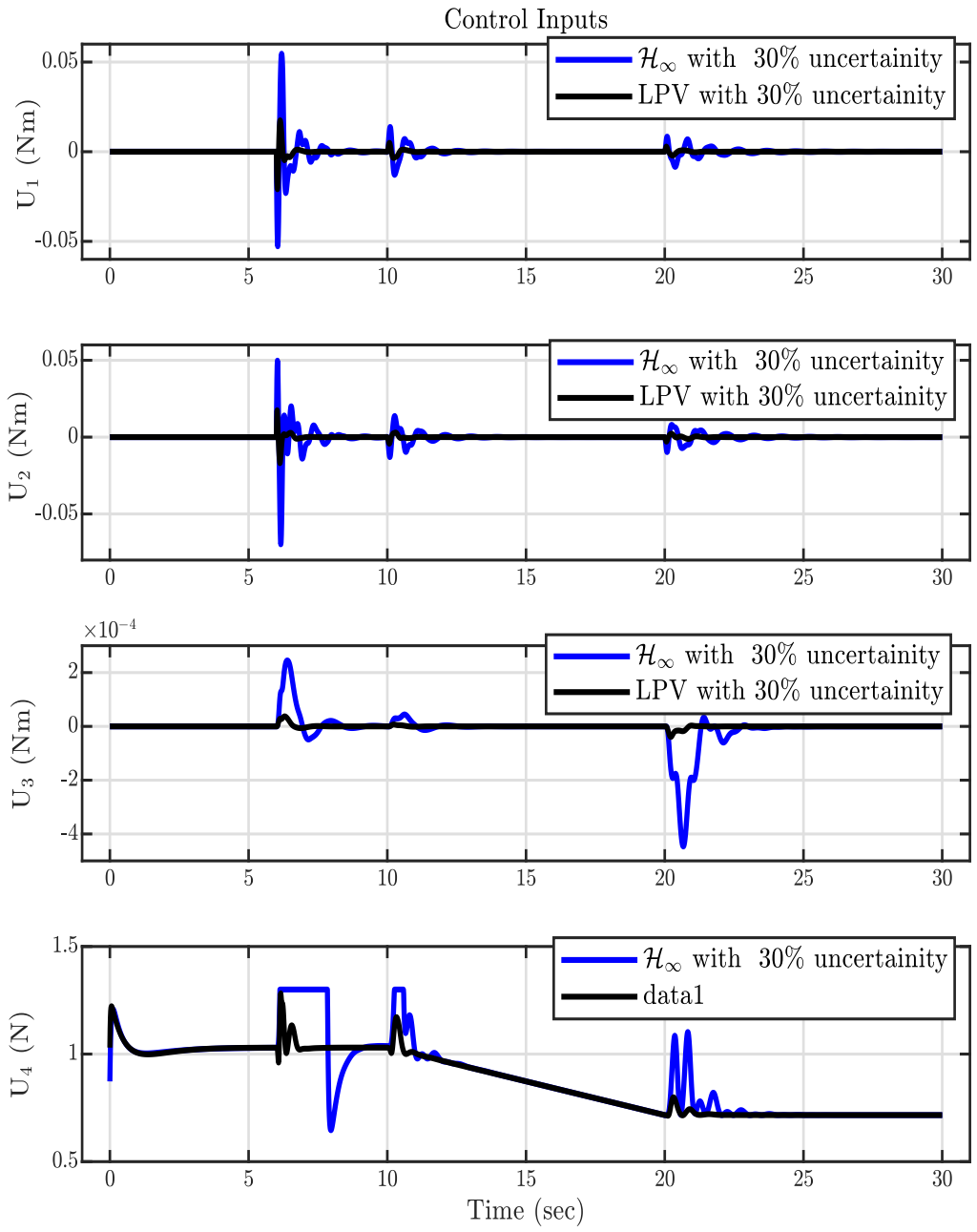

FIGURE 5.15: Control inputs (U_1, U_2, U_3, U_4) with 30% variation in the inertia.

Quantitative analysis of the system response is presented in Tables 5.3 and 5.4. The results reveal a significant improvement in the disturbance rejection ability along the z-axis and yaw angle stabilization for the LPV control as compared to the H_∞ scheme.

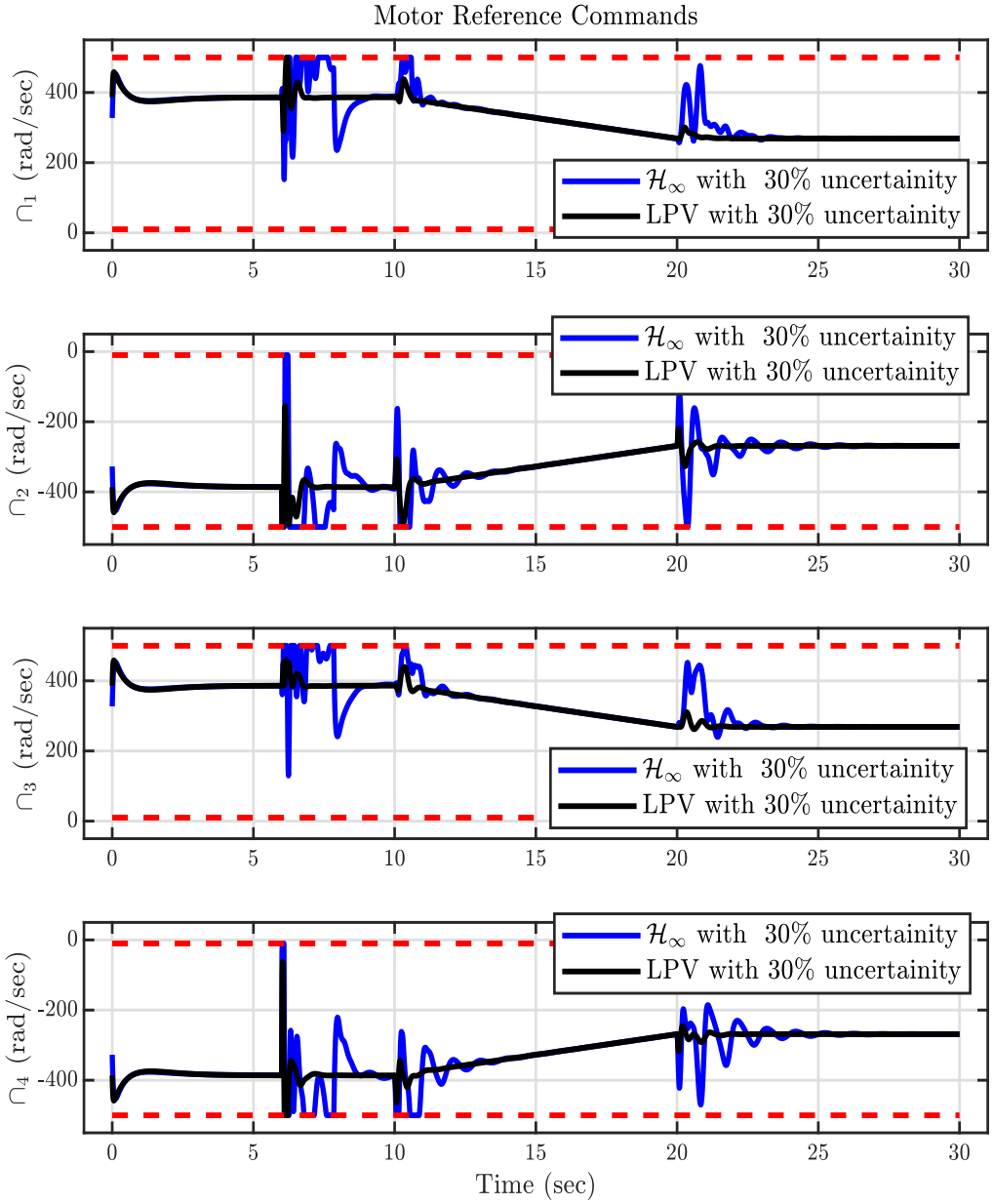

FIGURE 5.16: Motor commands ($\cap_1$, $\cap_2$, $\cap_3$, $\cap_4$) with 30% variation in the inertia.

Case 3 (Position Tracking under Wind Disturbance and Variable Payload:)

In the third case, we conduct a performance comparison of the H_∞ and LPV control schemes for quadcopter position tracking, subject to varying payloads and

wind disturbance. To assess reference tracking performance in the presence of simultaneous wind disturbance and variable payloads, a steer-case reference signal is applied to the longitudinal and latitudinal positions (x, y), and a step signal is applied to the z-position (z). Payload variation is introduced at $t = 7.5$ sec, and wind disturbance is applied at $t = 10$ sec. A constant north-east wind speed of 5.8 m/s is considered, as shown in Figure 5.17. Both control schemes successfully track the reference signals in the presence of wind disturbance and payload variation. However, the LPV scheme outperforms by providing superior tracking and wind disturbance rejection, particularly in altitude tracking, as evident in Figure 5.18. In contrast, the H_∞ controller induces significant oscillations in the quadcopter's attitude, as depicted in Figure 5.19. Figure 5.20 illustrates the control signals, revealing that the H_∞ controller necessitates large control efforts and exhibits pronounced oscillations. Furthermore, the motor commands reach their maximum values, as depicted in Figure 5.21.

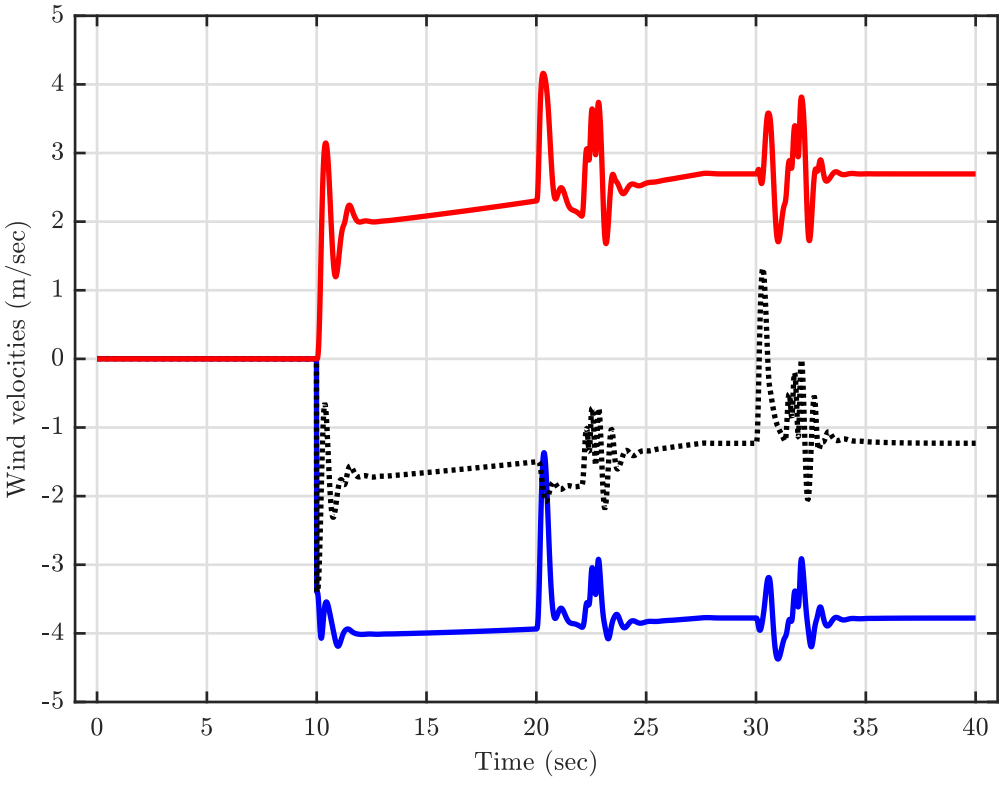

FIGURE 5.17: Variation in the wind velocities with time.

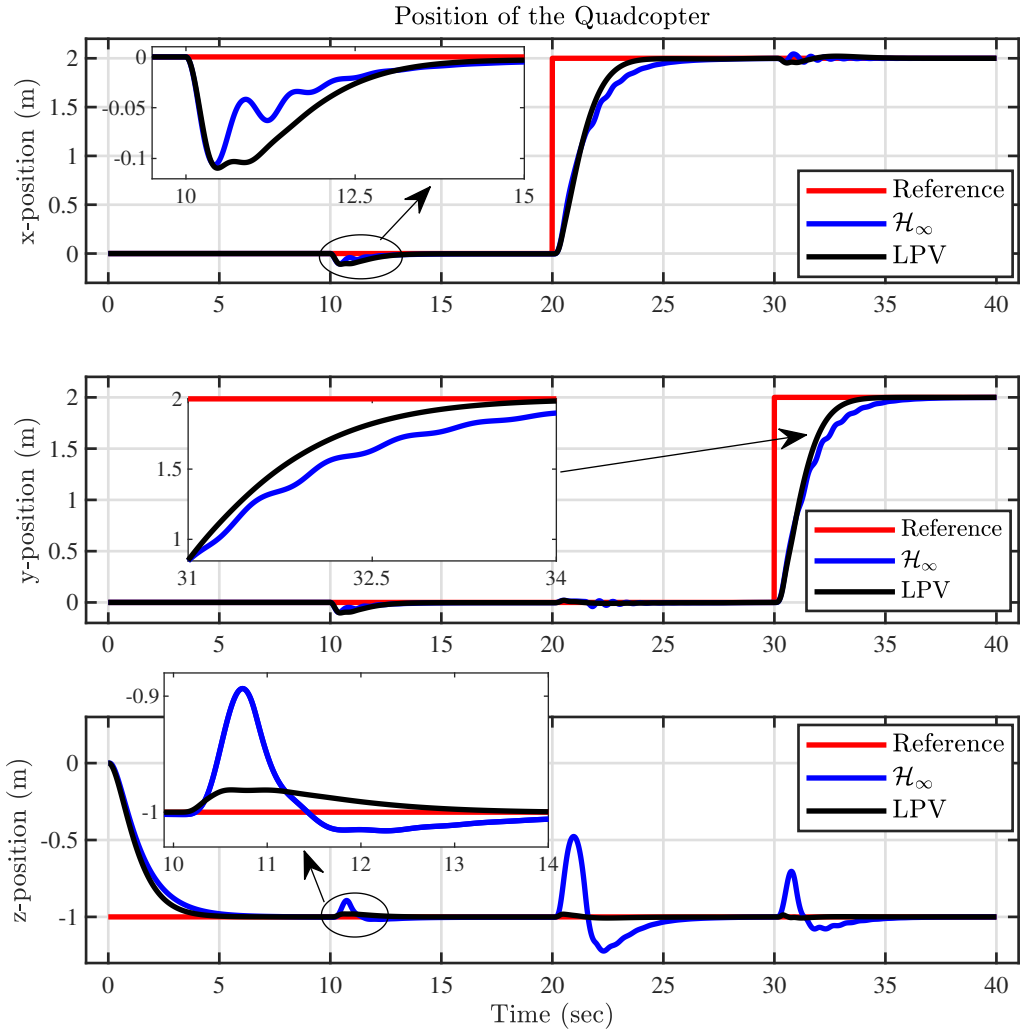

FIGURE 5.18: Positions (x,y,z) of quadcopter with payload variation and wind disturbance.

TABLE 5.5: The RMS comparison of control signals of LPV and H_∞ with wind disturbance and variable payload.

Performance Parameters	$\boldsymbol{H_\infty}$	**LPV**	% **Improvement**
RMS of U_1	4.4891×10^{-4}	2.5151×10^{-4}	44
RMS of U_2	4.9912×10^{-4}	2.8707×10^{-4}	43
RMS of U_3	4.9607×10^{-6}	1.5784×10^{-6}	68
RMS of U_4	1.0689×10^{0}	9.64×10^{-1}	10

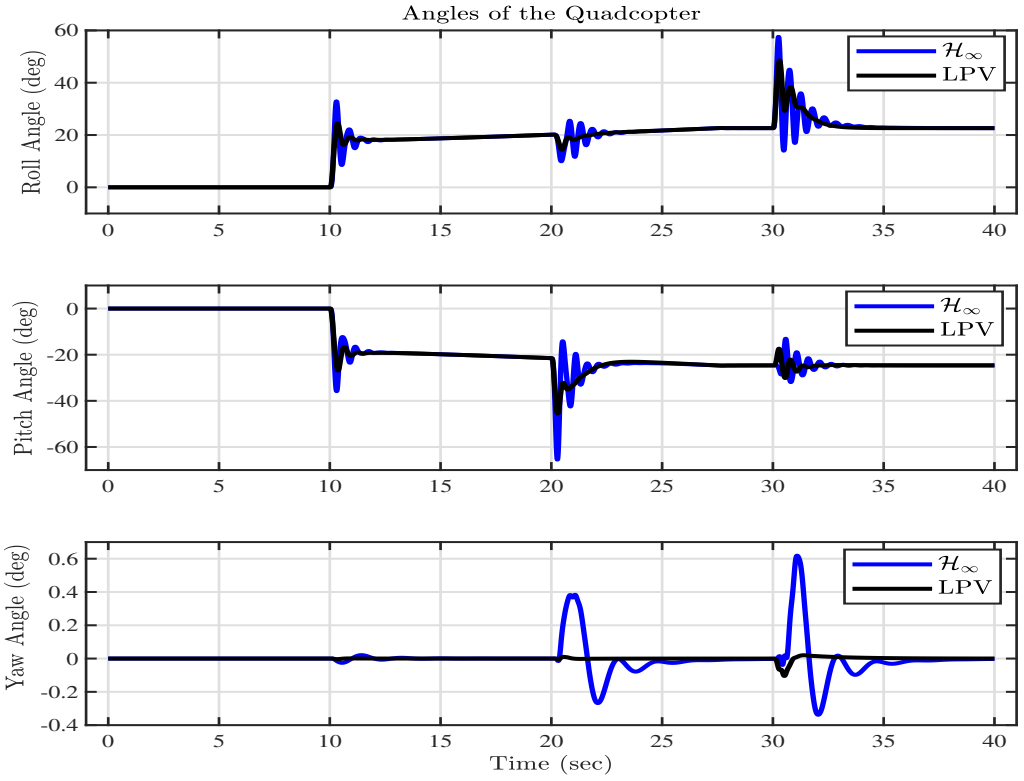

FIGURE 5.19: Attitude angles (ϕ, θ, ψ) of quadcopter with payload variation and wind disturbance.

TABLE 5.6: The RMSE with wind disturbances and variable payload.

	Performance Parameters	$\boldsymbol{H_\infty}$	**LPV**	% **Improvement**
x-position	RMSE	0.3162 m	0.3051 m	3.51
y-position	RMSE	0.3085 m	0.2962 m	3.98
z-position	RMSE	0.1955 m	0.1474 m	24.60
Yaw angle	RMSE	0.054 rad	0.0096 rad	82.22

Tables 5.6 and 5.5 showcase quantitative results, underscoring a significant enhancement in altitude, yaw angle stabilization, and control signals (U_1,U_2,U_3,U_4) performance for the LPV control scheme when compared with the $H\infty$ approach. This implies that the LPV control strategy outperforms the $H\infty$ approach across multiple key parameters, demonstrating its efficacy in the presence of variation in the payload and wind disturbance that are considered simultaneously.

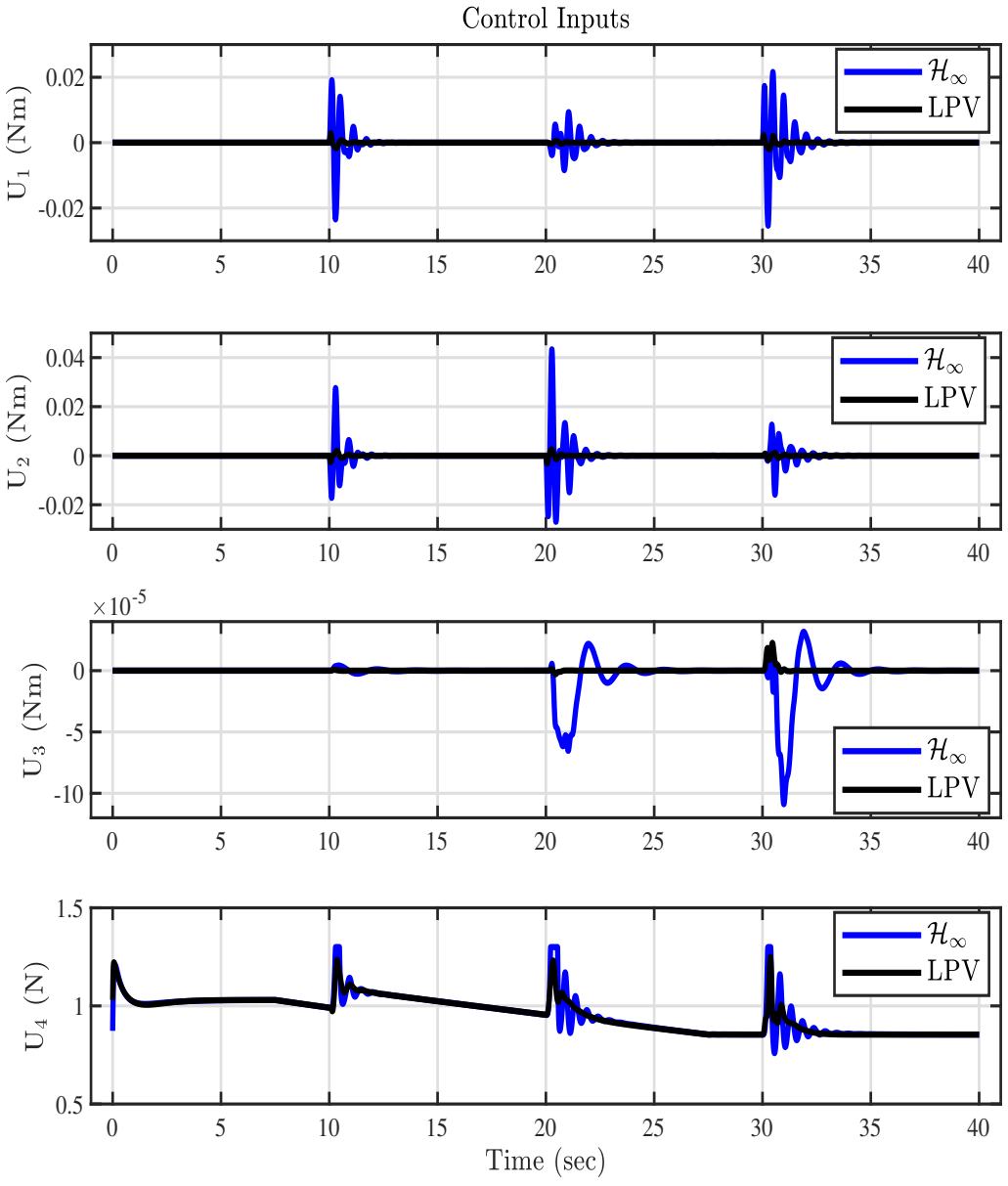

FIGURE 5.20: Control inputs (U_1, U_2, U_3, U_4) with payload variation and wind disturbance.

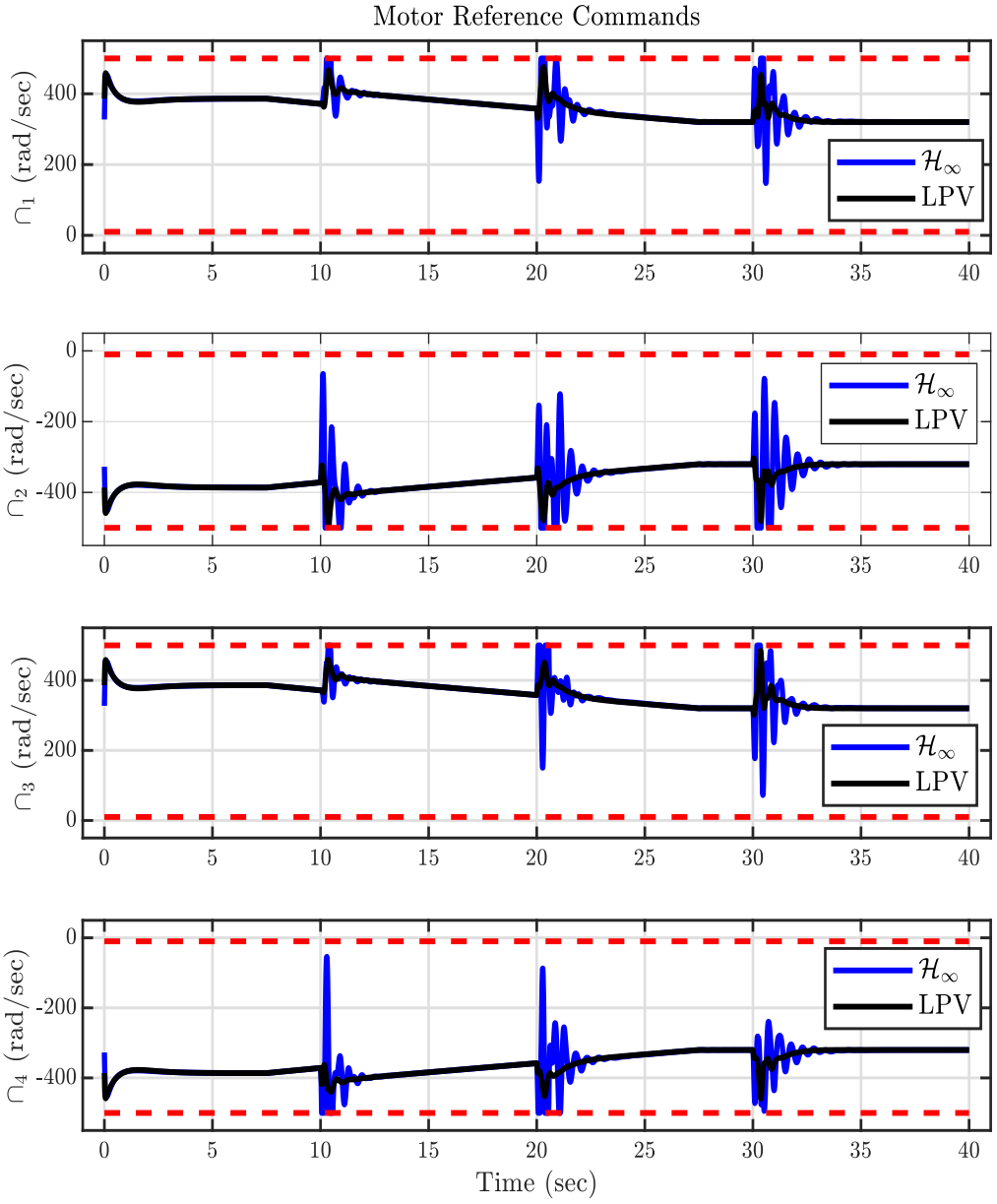

FIGURE 5.21: Motor commands ($\cap_1$, $\cap_2$, $\cap_3$, $\cap_4$) with payload variation and wind disturbance.

Case 4 (Performance Comparison under Noise and Variable Paylaod): In this scenario, Gaussian noise $N(\mu, \sigma^2)$ is introduced into the quadcopter outputs, and results of both control techniques are compared [90]. Noise $N(0, (1\text{ cm})^2)$ is added to the x, y, and z positions, while $N(0, (0.51°)^2)$ is introduced to the yaw, pitch, and roll angles. Figure 5.22 illustrates that both algorithms can track the

steer-type signal in the x and y directions and the step signal in the z-direction. The LPV controller demonstrates better tracking performance. Noticeable deviations from the reference trajectory, particularly in the z-direction, are observed in the case of the H_∞ controller. Figure 5.23 shows attitude angles, indicating significant peaks and oscillations in the H_∞ controller case.

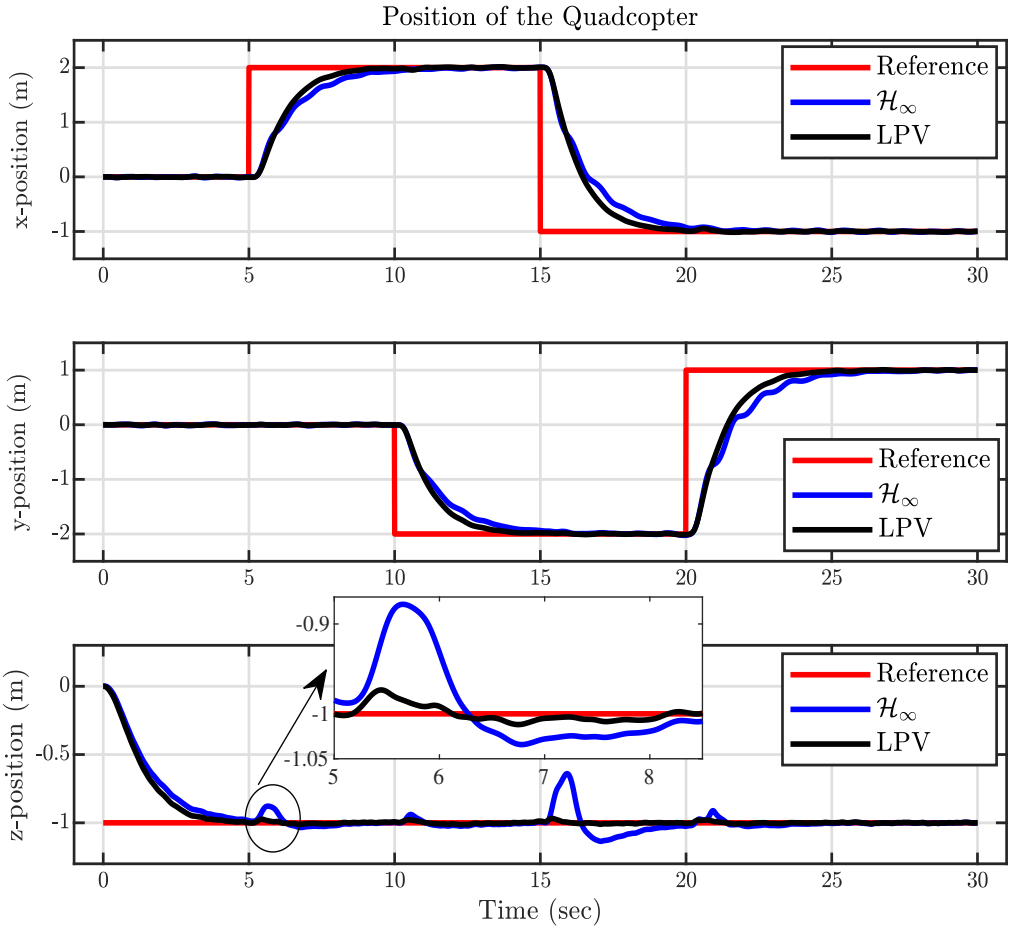

FIGURE 5.22: Positions (x, y, z) of quadcopter with payload variation and noise.

Control signals are presented in Figure 5.24, where saturation can be observed in the control input for the H_∞ controller. Motor reference commands in Figure 5.25 demonstrate that motor commands remain within limits in the case of the LPV controller. Quantitative results are summarized in Tables 5.7 and 5.8 , indicating a substantial improvement in altitude, yaw angle stabilization, and control inputs with the LPV control compared to the H_∞ scheme.

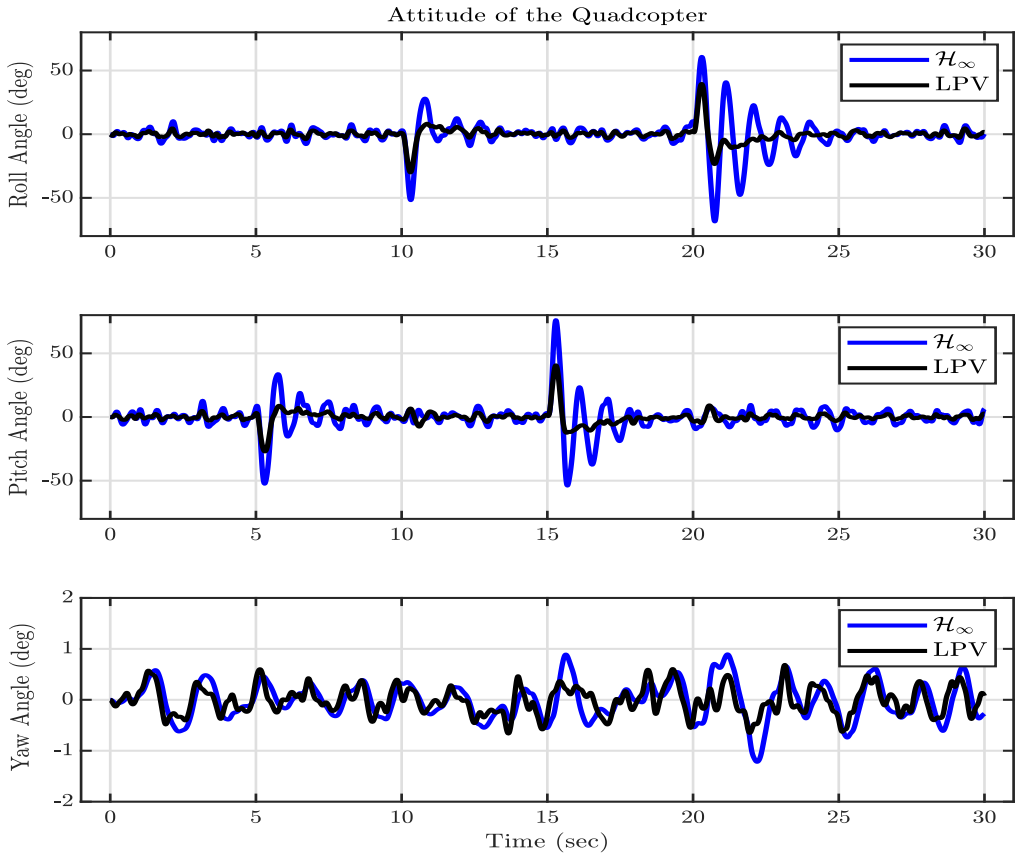

FIGURE 5.23: Attitude of quadcopter with payload variation and noise.

TABLE 5.7: The RMSE with noise and variable payload.

	Performance Parameters	H_∞	**LPV**	% **Improvement**
x-position	RMSE	0.6298 m	0.6072 m	3.59
y-position	RMSE	0.6269 m	0.5985 m	4.53
z-position	RMSE	0.1972 m	0.1701 m	13.74
Yaw angle	RMSE	0.3667 rad	0.02687 rad	26.73

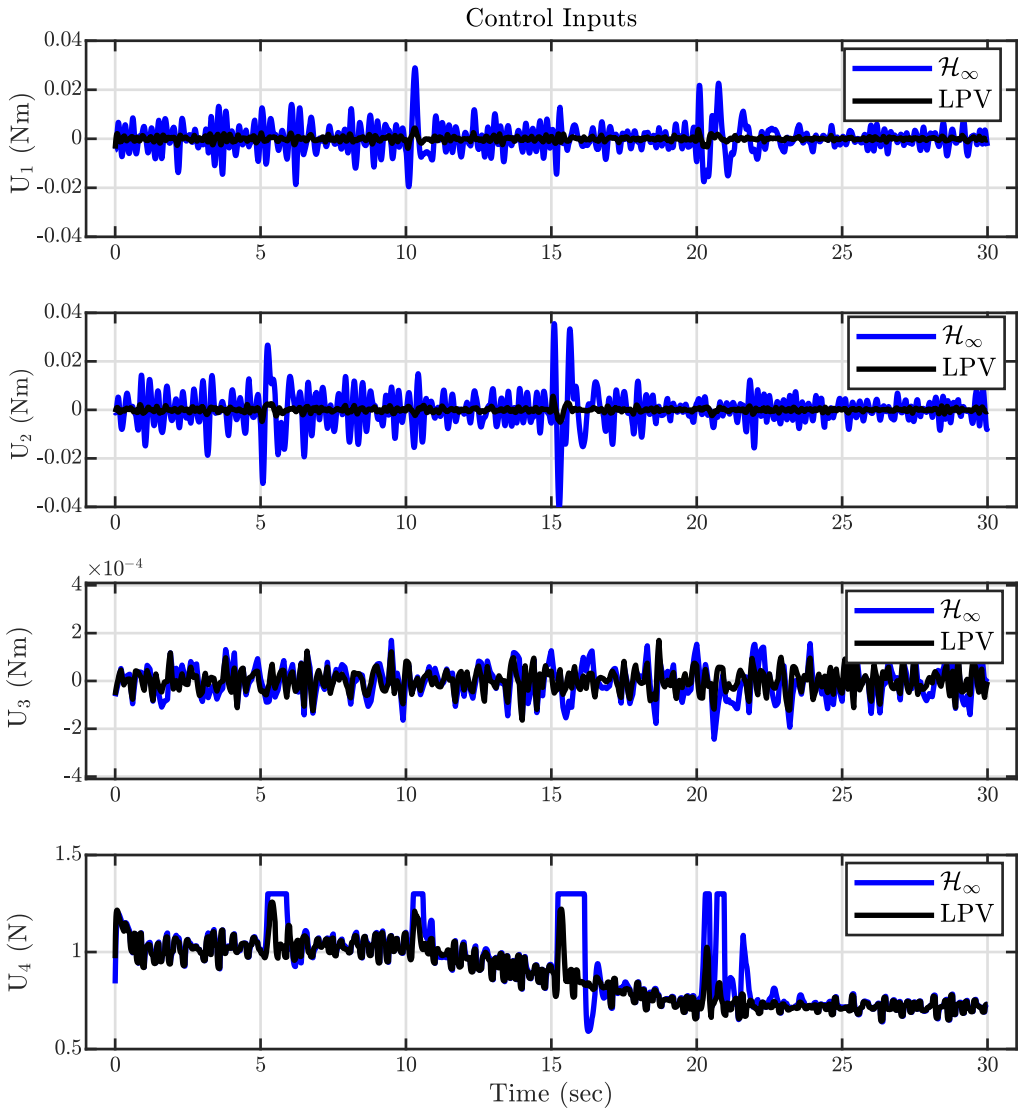

FIGURE 5.24: Control inputs (U_1, U_2, U_3, U_4) with payload variation and noise.

TABLE 5.8: The RMS comparison of control signals of LPV and H_∞ with payload variation and noise.

Performance Parameters	$\boldsymbol{H_\infty}$	**LPV**	**% Improvement**
RMS of U_1	4.5701×10^{-3}	8.2550×10^{-4}	82
RMS of U_2	5.6669×10^{-3}	8.5119×10^{-4}	85
RMS of U_3	5.6954×10^{-5}	4.1134×10^{-5}	28
RMS of U_4	9.2431×10^{-1}	8.9214×10^{-1}	4

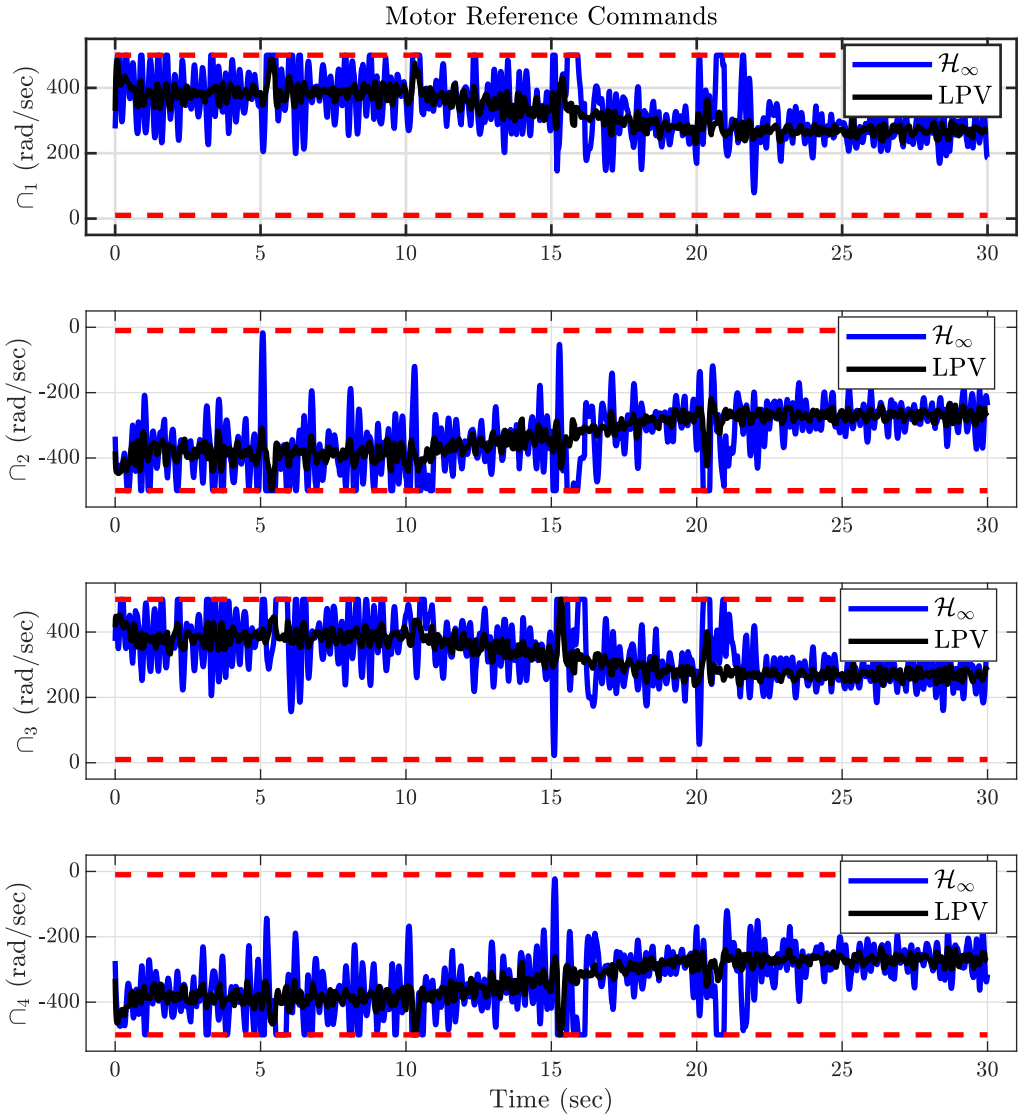

FIGURE 5.25: Motor commands ($\cap_1$, $\cap_2$, $\cap_3$, $\cap_4$) with payload variation and noise.

5.3 Comparison with SMC Controller

This section presents a comparative analysis between the conventional SMC controller proposed in [91] and the suggested LPV scheme applied to a quadcopter experiencing fixed mass, varying mass, and wind disturbance. In Figure 5.26, the outputs (x, y, z) of the quadcopter with fixed mass are depicted in response to a

step reference signal and a step disturbance introduced at t=10 sec. The simulation results reveal that both controllers demonstrate effective position tracking and disturbance rejection. However, the LPV controller exhibits superior performance parameters, as highlighted in Table 5.9. The enhancements in t_r, t_s, RMSE_{TR}, and RMSE_{SSR} are up to 7%, 17%, 25%, and 44%, respectively, attributed to the implementation of the LPV controller. This 44% enhancement indicates that the RMSE_{SSR} obtained through the LPV approach is 44% less than the one achieved with the SMC controller.

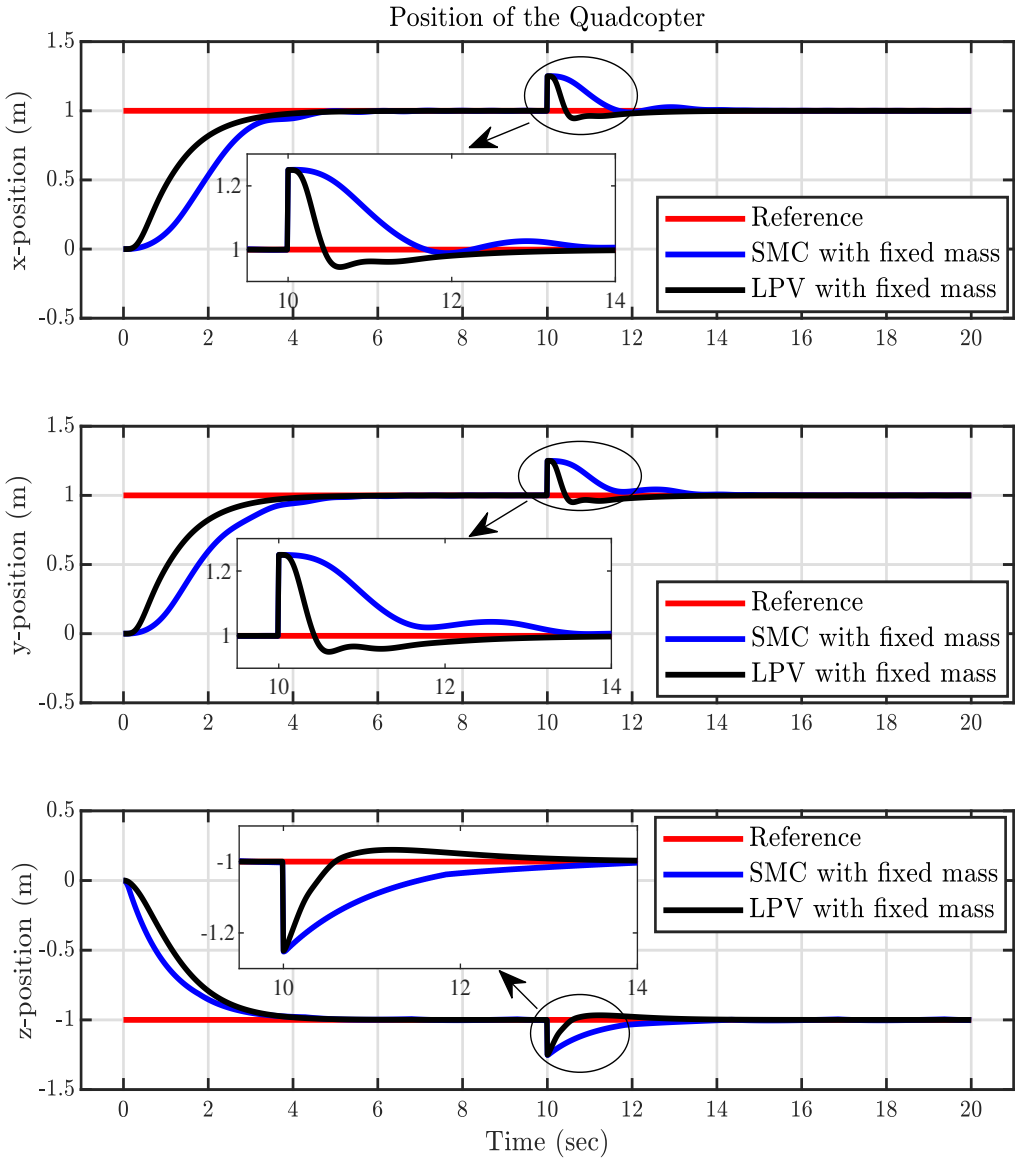

FIGURE 5.26: Positions (x, y, z) of quadcopter with fixed mass.

Figure 5.27 depicts the positions (x, y, z) of the quadcopter with varying mass, responding to a step reference signal and a step disturbance introduced at $t = 10$ sec. The simulation results reveal that the LPV controller outperforms the SMC controller in achieving superior position tracking amidst varying mass and step disturbance. Notably, pronounced oscillations are observed in the x-position and y-positions, while steady-state error is evident in the z-position when employing the SMC controller. The enhancements in t_r, t_s, RMSE_{TR}, and RMSE_{SSR} reach up to 26%, 55%, 19%, and 51%, respectively, as detailed in Table 5.11.

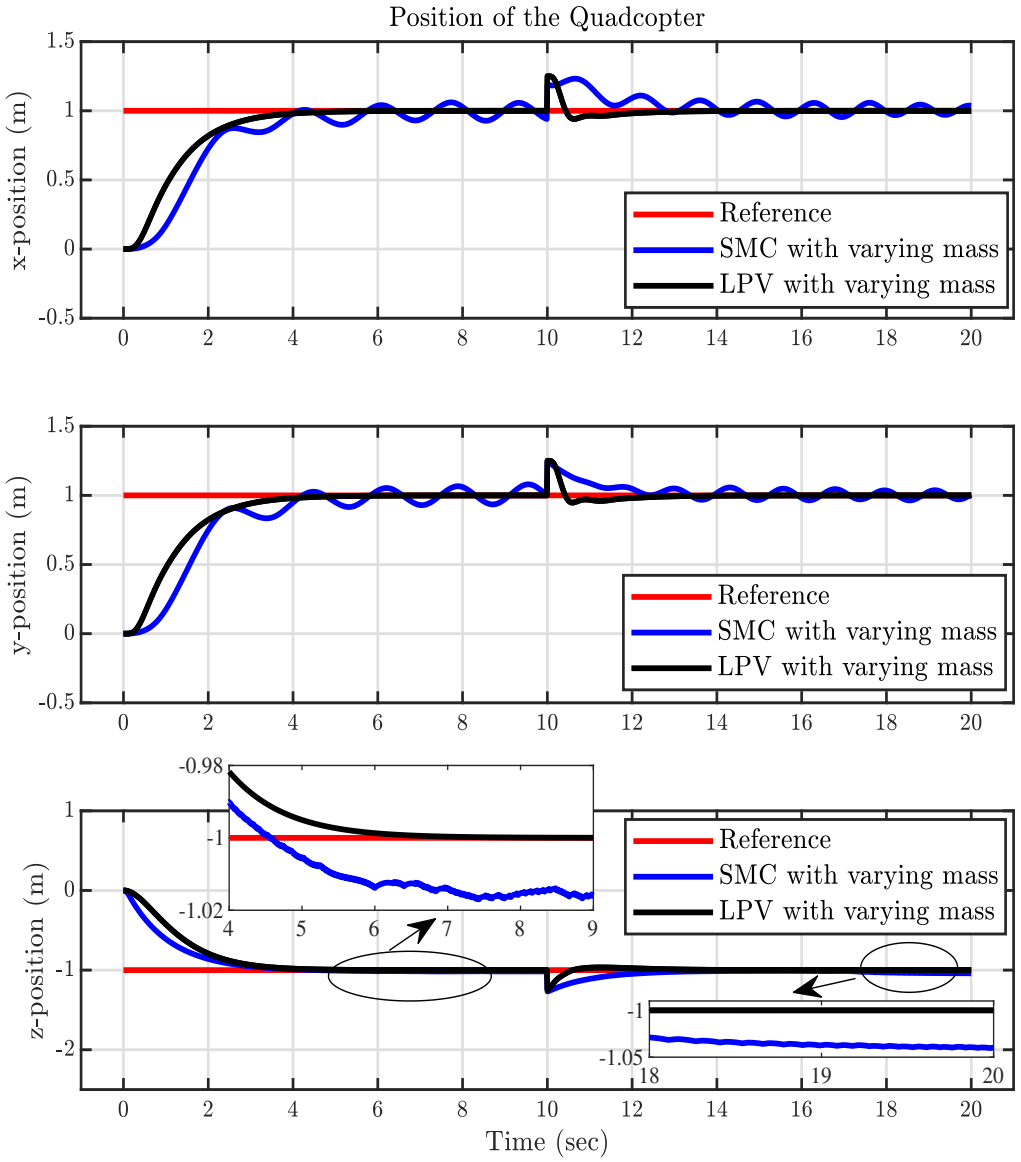

FIGURE 5.27: Positions (x, y, z) of quadcopter with varying mass.

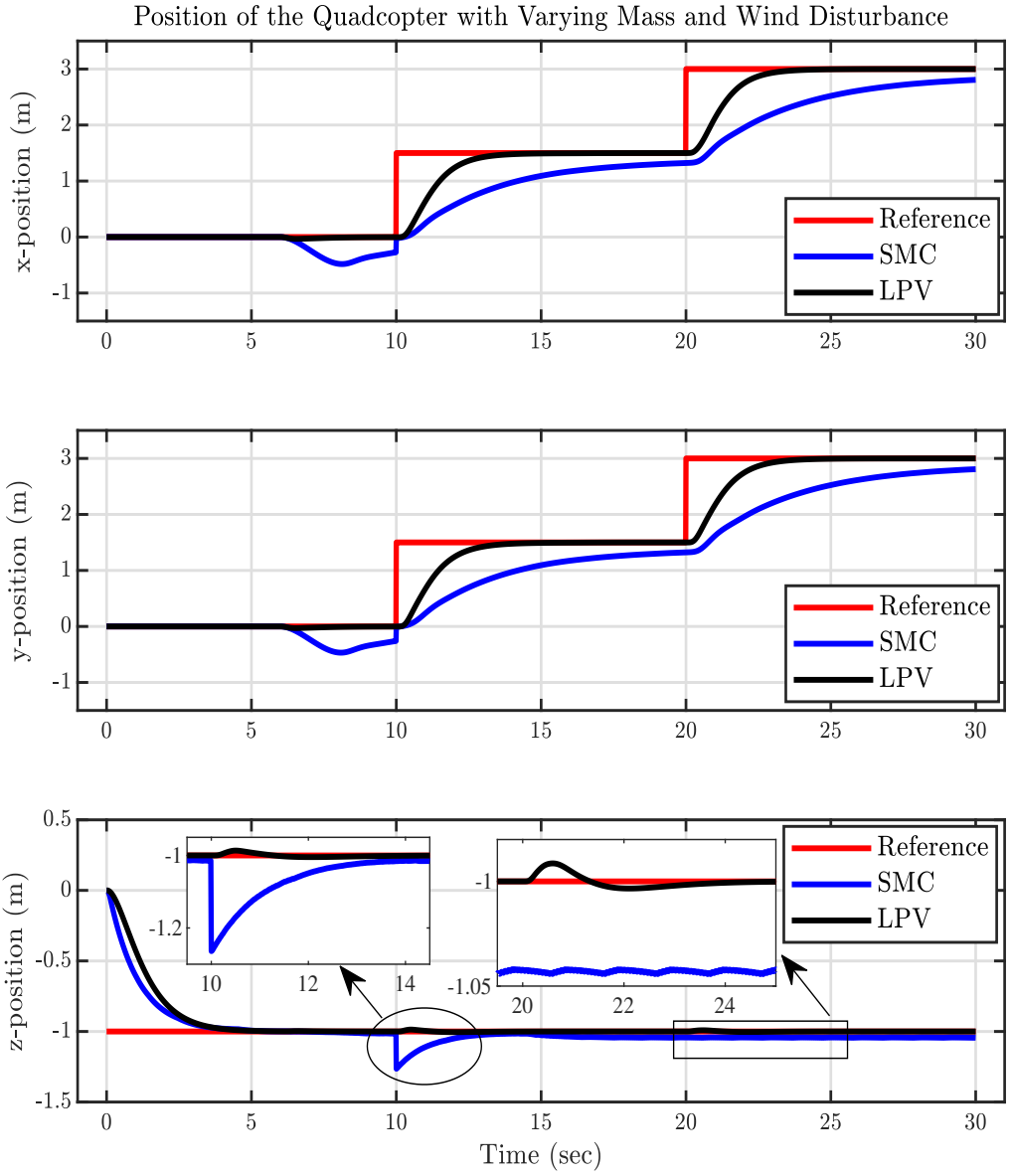

FIGURE 5.28: Positions (x, y, z) of quadcopter with varying mass and wind disturbance.

Figure 5.28 depicts the quadcopter's position in response to a square reference signal for x and y positions, and a unit step signal for z position, in the presence of varying mass and wind disturbance introduced simultaneously at $t = 6$ sec. The simulation results reveal that the SMC controller exhibits more deviations from the reference trajectory compared to the LPV controller, which efficiently follows the trajectory. The wind speed is considered to be 2.3 m/sec. Improved

performance by the LPV controller is highlighted in Table 5.10 in comparison to the SMC control scheme.

TABLE 5.9: The closed-loop performance parameters with fixed mass.

	Performance Parameters	**SMC**	**LPV**	**% Improvement**
x-position	t_r	2.159 *sec*	2.0837 *sec*	3.49
	t_s	4.4922 *sec*	3.96 *sec*	11.85
	RMSE_{TR}	0.50367 m	0.3776 m	25.03
	RMSE_{SSR}	0.05897 m	0.03754 m	39.88
y-position	t_r	2.2419 *sec*	2.0832 *sec*	7.08
	t_s	4.7675 *sec*	3.9587 *sec*	16.96
	RMSE_{TR}	0.4874 m	0.3726 m	23.55
	RMSE_{SSR}	0.06210 m	0.0347 m	44.08
z-position	t_r	2.1674 *sec*	2.2458 *sec*	−3.62
	t_s	3.9858 *sec*	3.9284 *sec*	1.44
	RMSE_{TR}	0.3489 m	0.3809 m	−9.18
	RMSE_{SSR}	0.0488 m	0.02823 m	42.16

TABLE 5.10: The RMSE with varying mass and wind disturbance.

	Performance Parameters	**SMC**	**LPV**	**% Improvement**
x-position	RMSE	0.6172 m	0.3671 m	40.52
y-position	RMSE	0.6147 m	0.3592 m	41.56
z-position	RMSE	0.2174 m	0.1702 m	21.71

TABLE 5.11: The closed-loop performance parameters with varying mass.

	Performance parameters	SMC	LPV	% Improvement
x-position	t_r	2.8266 *sec*	2.0841 *sec*	26.27
	t_s	8.9104 *sec*	3.9667 *sec*	55.48
	RMSE_{TR}	0.4653 m	0.3775 m	18.87
	RMSE_{SSR}	0.0725 m	0.0353 m	51.24
y-position	t_r	2.5155 *sec*	2.0836 *sec*	17.17
	t_s	8.8950 *sec*	3.9606 *sec*	55.47
	RMSE_{TR}	0.4619 m	0.3725 m	19.35
	RMSE_{SSR}	0.0572 m	0.0345 m	39.61
z-position	t_r	2.2825 *sec*	2.2461 *sec*	1.59
	t_s	4.2723 *sec*	3.9287 *sec*	8.04
	RMSE_{TR}	0.3471 m	0.3803 m	−9.58
	RMSE_{SSR}	0.05704 m	0.0283 m	50.41

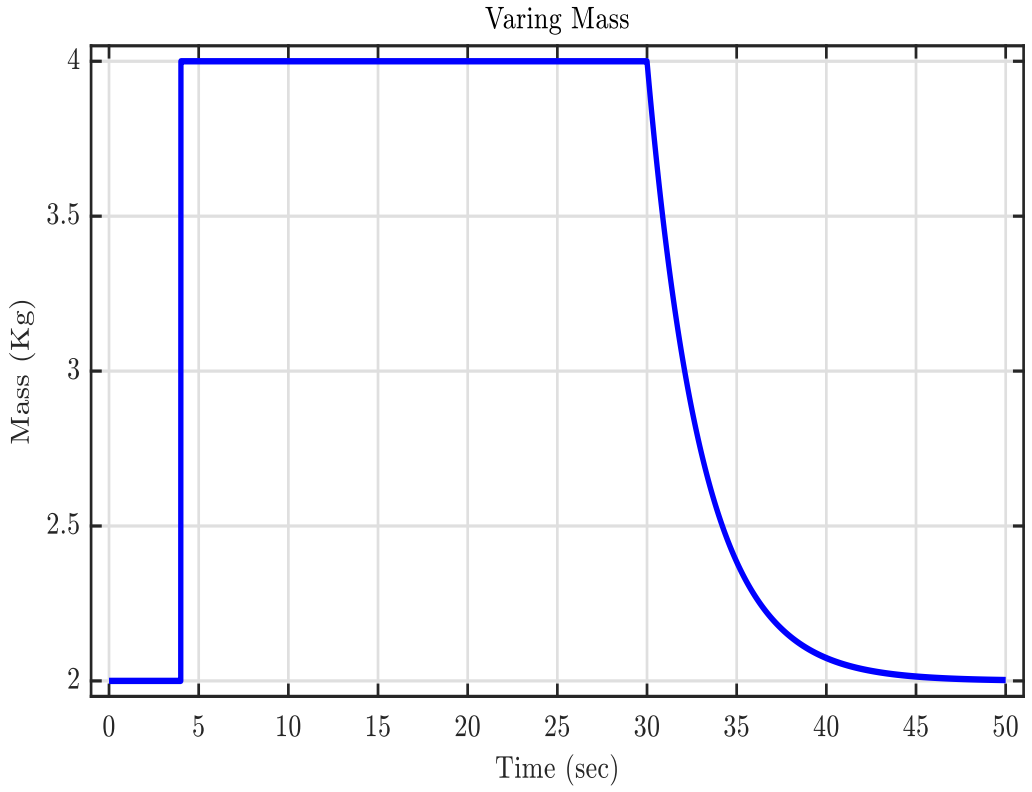

FIGURE 5.29: Mass variation with time [44].

The outcomes of the LPV control approach are compared with the ASMC control algorithm proposed in [44]. The evolution of mass over time is illustrated in Figure 5.29. The mass remains constant until $4sec$, at which point a step change of $2kg$ is introduced, followed by an exponential decay in mass starting at $t = 30sec$. Figure5.30 displays the quadcopter's altitude tracking for a ramp reference input. The findings suggest that the ASMC control scheme effectively follows the ramp reference input in the presence of varying mass, in contrast to the SMC scheme, which exhibits deviation from the reference signal.

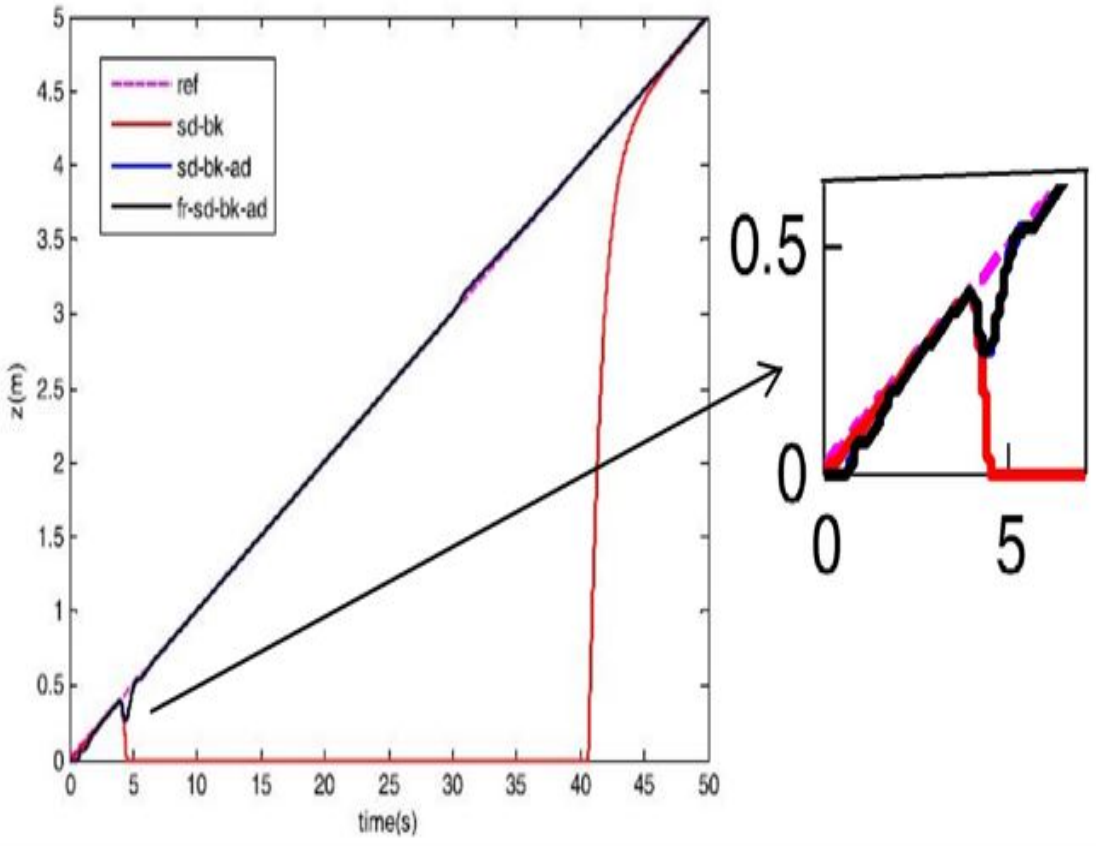

FIGURE 5.30: Altitude ramp tracking of quadcopter in the presence of varying mass using ASMC [44].

The effectiveness of the proposed LPV control scheme in achieving ramp altitude tracking for a quadcopter, despite fluctuations in mass, is depicted in Figure 5.31. The visualization highlights the LPV controller's ability to successfully track a ramp reference signal even when faced with variations in mass over time. This observation underscores the robust performance of the LPV control scheme in

addressing the challenges posed by dynamic changes in the system's mass during altitude tracking.

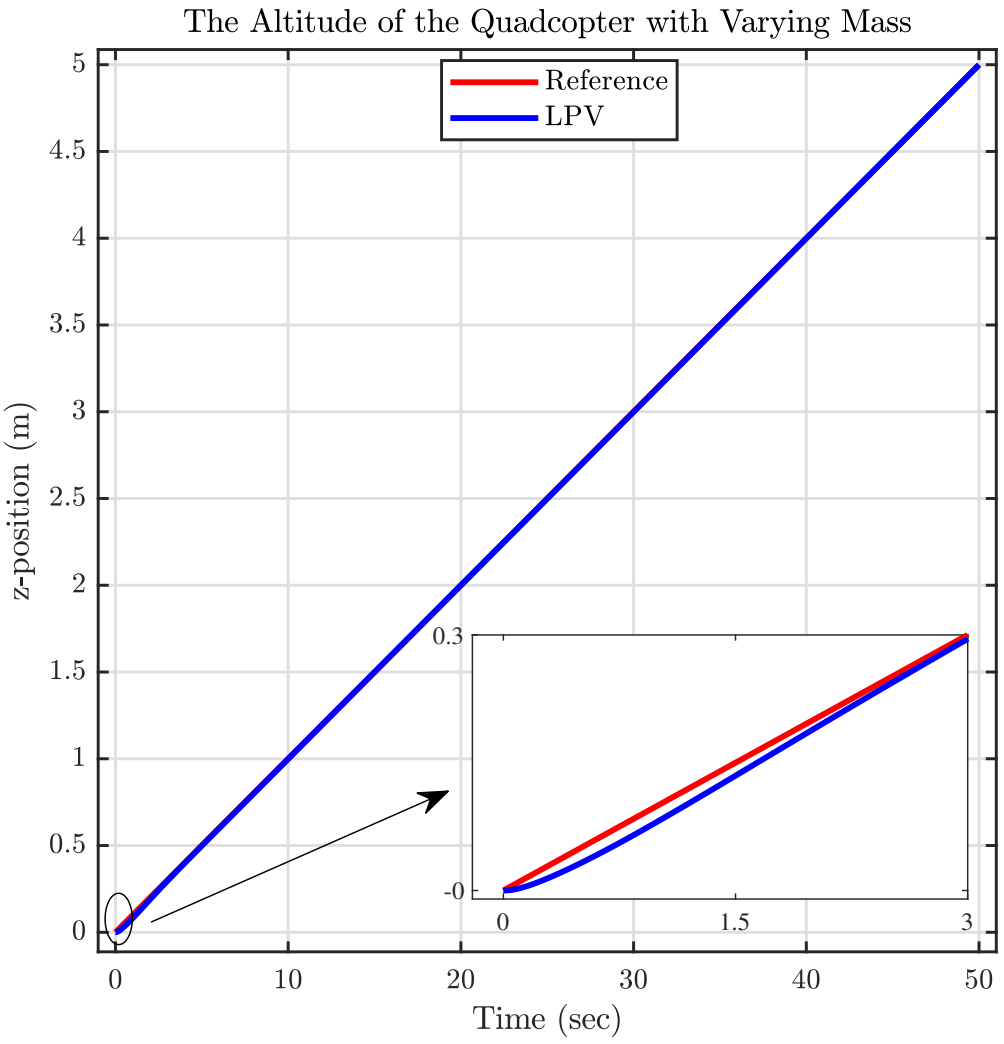

FIGURE 5.31: Altitude ramp tracking of quadcopter in the presence of varying mass using LPV.

5.4 Chapter Summary

This chapter contains the simulation findings for the three control design techniques. Main focus of this chapter revolved around the discussion on achieved results through simulation using MATLAB/SIMULINK. Different scenarios are considered to test the validity of the designed schemes. Section 5.1 provides the

simulation results of the LPV control scheme. In Section 5.2, a comparison of the LPV control strategy with the H_∞ control design with pole placement constraint is carried out to ascertain which approach is more efficient for quadcopter position control with variable payload. LPV control scheme has achieved better results as compared to the linear control approach. Finally, In Section 5.3, we compare three different ways of controlling a quadcopter: the LPV strategy, the SMC design, and the ASMC algorithm. We want to find out which one works better for keeping the quadcopter in position, especially when dealing with changes in payload weight and windy conditions. This comparison helps us understand how well each control method performs in real-world situations.

Chapter 6

Conclusion and Future Work

The control design of an under-actuated dynamical system in the presence of varying parameters, external disturbances, and actuator constraints is a challenging control problem. The effect of these variable parameters, outside disturbances, and actuator limitations on the system dynamics should be carefully considered during the control scheme design phase, as these perturbations can aggravate the system's performance and/or even cause instability in the system. For these reasons, the control design problem for under-actuated system has become a principal area of research. Quadcopter is an under-actuated dynamical system whose application with varying payload is increasing day by day. Quadcopters used for spraying chemicals have a variable payload. The mass is not fixed and varies over time. The variation in mass will alter the moment of inertia. These variations in parameters, in addition to the complex dynamics of quadcopter, such as nonlinearities, under-actuation, external disturbances, actuator constraints, sensor noise, etc., make the control system design a challenging problem.

6.1 Conclusion

Based on the research work, the thesis summary is revealed as follows:

The dynamics of the quadcopter with variable payload is presented in Chapter 3. Varying parameters of the quadcopter are found using the 3D-CAD (3-dimensional computer-aided design) model of the quadcopter with payload developed in SOLIDWORKS. Model equations are obtained for the varying mass and inertia parameters using empirical modeling. The RMSE is used for assessing the accuracy of predictive models. The RMSE of the fitted curve for mass is 5.352×10^{-7}, for inertia about x-axis is 3.366×10^{-7}, for inertia about y-axis is 3.448×10^{-7} and for inertia about z-axis is 6.196×10^{-8}. The small values of RMSE indicate the goodness of fit. The derived equation for mass illustrates how the quadcopter's mass parameter changes as the liquid level in the tank decreases. Similarly, the obtained equations for inertia parameters reveal the variations in these parameters with the changing mass. An LPV model is developed to represent the nonlinear quadcopter system with a variable payload. To ensure its accuracy, the LPV model's response is compared with that of the nonlinear model for validation purposes. Additionally, a linear model is introduced for the quadcopter's nonlinear dynamics and is presented in Section 3.3.2. The improvement in RMSE for fully actuated dynamics (altitude and yaw) of the quadcopter is 85% and 84%, respectively. In the under-actuated dynamics (roll, pitch, x-position, and y-position), the RMSE improvement is 84%, 90%, 78%, and 71%, respectively. The results presented in Section 3.4 demonstrate that the LPV model outperforms the linear model significantly, especially for quadcopters with variable payloads.

Linear matrix inequalities (LMIs)-based linear parameter varying (LPV) control algorithms are proposed for the full motion control of a 6-DOF (degrees of freedom) quadcopter model. Chapter 4 discusses the design of LMIs-based LPV and linear control schemes. The LPV control algorithm is an optimal, robust control technique whose gains vary with the scheduling parameters. The main objective of an LPV control methodology was to control the plant over a predefined operating range. LMIs-based LPV control scheme is proposed for quadcopter position control subject to varying mass, varying inertia, mass flow rate, large tilt angles, and external disturbances. LMIs of quadratic H_∞ performance and D-stability are used to design the LPV control strategy for the LPV model. The quadrtaic

stability and H_∞ performance are analyzed. The achieved values of quantity t_{min} is negative (i.e., $t_{min} < 0$) which indicates the robust stability of the closed loop system. The quadratic H_∞ performance γ is less than 4, which is required in H_∞ control design framework. Moreover, a multi-objective linear time invariant (LTI) controller based on the LMIs of H_∞ performance and pole placement in LMI regions is designed for the linear model of quadcopter.

To evaluate the efficacy of the proposed LPV scheme, simulations are performed in MATLAB/SIMULINK for the desired position tracking of the quadcopter. Chapter 5 discusses the simulation results of the LMIs-based control schemes. The simulation results of the LPV control scheme is presented in Section 5.1. The results indicate that the quadcopter is efficiently tracing the reference trajectory in the presence of varying payload and wind disturbance simultaneously. The suggested control scheme forces the error signals to zero in the steady state without actuator saturation.

The outcomes of the LPV algorithm are compared with the H_∞ control design with pole placement constraints. Several scenarios are simulated and studied. The comparison of the results is provided in Section 5.2. In Case 1, the quadcopter's position is required to track a unit step signal, while the yaw angle needs to be maintained at $\angle 0^0$. A unit step signal was applied in the presence of full payload, varying payload, and empty payload. The tracking performance was examined in terms of system rise time , settling time, overshoot, and root mean squared error. The values of the performance parameters and percentage improvements are listed in Tables 5.1, 5.2, 5.3, 5.4, 5.5, 5.6, 5.7, and 5.8, respectively. Better position tracking and yaw angle stabilization were accomplished in the presence of variable mass and moment of inertia using the LPV scheme as compared to the linear control scheme. The proposed LPV scheme improves the rise time up to 28%, the settling time up to 26%, root mean squared error up to 91%, and root mean squared of control signal up to 92%. In Case 2, 30% variation in the inertia parameters were considered and the results of the two schemes were compared. In Case 3, position tracking in the presence of dynamic payload and wind disturbance was considered. In Case 4, Gaussian noise $N(\mu, \sigma^2)$ was introduced into the quadcopter

outputs, and the performance of the control schemes were tested and compared. The numerical results indicate that the recommended LPV approach can achieve better position tracking in the presence of variable mass, variable inertia, mass flow rate, wind disturbance, and noise without actuator saturation in contrast to the LTI H_∞ control scheme.

The effectiveness of the LPV scheme is further assessed through a comparison with the SMC controller across various scenarios, including fixed mass, variable mass, and wind disturbance. The performance parameter values are detailed in Tables 5.9, 5.10, and 5.11, corresponding to each scenario. The findings highlight that the LPV control scheme demonstrates good position tracking when contrasted with the SMC control scheme. Specifically, the LPV scheme enhances the rise time, settling time, and root mean squared error by up to 26%, 55%, and 42%, respectively.

The conclusion drawn from the overall dissertation is as follows:

1. Development of LPV model of quadcopter with varying payload, large tilt angles, and wind disturbance.
2. Validation of the LPV model of the quadcopter by comparing its response with the nonlinear 6-DOF model with varying payload.
3. Design and development of LMIs-based LPV control for quadcopter position control in the presence of varying payload and wind disturbance.
4. Analysis of robust stabilty and quadratic H_∞ performance of closed loop system using LMIs.
5. The efficacy of the proposed robust multi-objective LMIs-based LPV control is established using simulations in MATLAB/SIMULINK. The simulation results indicate that the proposed framework addresses the position control problem of quadcopter with varying payload in a comprehensive way.
6. The results of the multi-objective LMIs-based H_∞ and SMC control strategies are compared with the LPV scheme. The simulation results show that

the LPV framework gives better position tracking in the presence of variable payload and wind disturbance.

7. Improvement is achieved in the performance parameters such as t_r, t_s, RMSE, and RMS of control signal. Moreover, smooth control action without actuator saturation and smooth transition in the tilt angles are achieved with the LPV scheme in contrast to the LTI control approach.

6.2 Future Directions

The study work that is presented in this thesis can be expanded in plenty of ways. Certain problems are highlighted that can be broadened for quadcopters with varying payload. Future tasks recommended for quadcopter control with variable payload are outlined as:

1. Estimation of the system states
2. Pressure pump dynamics in the quadcopter model
3. Real-time implementation of the proposed LMIs-based LPV technique

Estimation of the system states:
In many control systems designs, not every state of the system can be directly measured. State estimation techniques allow the estimation of unmeasured states based on available measurements. For the suggested LPV model of quadcopter, an LPV observer may be developed to estimate the states of the system. LMIs-based LPV controller with observer can be designed for the position tracking of quadcopter with varying payload. The stability of the closed-loop system with observer may be assessed and the effectiveness and precision of the LPV controller with observer can be evaluated.

Inclusion of the sprayer pump in the quadcopter dynamic model:
Quadcopters used for spraying chemicals have a spray system attached to it. The

components of the spray system include a liquid tank, a sprayer pump, and nozzles. A water pump is used in the sprayer drone to maintain the flow rate of liquid. When the pump is turned on, the liquid in the tank is pumped to the nozzles, where it is then released as a spray. The pressure pump dynamics have not been added to the quadcopter model developed in this thesis. The dynamics of the pressure pump can be included in the quadcopter model.

Real-time implementation of the LMIs-based LPV technique:
Real-time implementation of control design approaches is of paramount importance in control systems. Implementing a control design scheme in a physical system allows researchers to evaluate the stability and performance of the proposed methodology. It helps to validate and verify the robustness and effectiveness of the design control algorithms. It allows the researchers to compare the simulation results with the actual system results, ensuring that the control scheme design fulfil the required objectives. The proposed LPV control approach can be implemented in real-time for quadcopter with varying payload, and its stability, robustness, efficacy, and performance for position tracking can be tested.

6.3 Chapter Summary

In this chapter, final remarks were developed, followed by suggestions for the continuation of this dissertation study. Section 6.1 of this chapter provides a conclusion on the results achieved. In Section 6.2, the future work based on this research work is presented.

Bibliography

[1] P. Castillo, R. Lozano, and A. E. Dzul, *Modelling and control of mini-flying machines*, 1st ed. Springer Science & Business Media, 2005.

[2] T. Bresciani, *Modelling, identification and control of a quadrotor helicopter*. M.Sc thesis, Lund University, Sweden, 2008.

[3] U. R. Mogili and B. Deepak, "Review on application of drone systems in precision agriculture," *Procedia computer science*, vol. 133, pp. 502–509, 2018.

[4] D. Falanga, K. Kleber, and D. Scaramuzza, "Dynamic obstacle avoidance for quadrotors with event cameras," *Science Robotics*, vol. 5, no. 40, pp. 1–51, 2020.

[5] T. Krajník, V. Vonásek, D. Fišer, and J. Faigl, "AR-drone as a platform for robotic research and education," *Research and Education in Robotics-EUROBOT: International Conference, Prague, Czech Republic*, pp. 172–186, 2011.

[6] S. M. ME, R. Maguteeswaran, N. G. BE, and G. Srinivasan, "Quadcopter UAV based fertilizer and pesticide spraying system," *Int. Acad. Res. J. Eng. Sci*, vol. 1, pp. 8–12, 2016.

[7] "Agriculture Spraying Drone," https://www.hobby-wing.com/arris-yrx410-10l-capacity-agriculture-spraying-drone.html, accessed: 22-04-2023.

[8] "Camera Drone," https://unsplash.com/photos/duNHkmSkW6M, accessed: 22-04-2023.

[9] "Toy Drone," https://www.amazon.co.uk/Parrot-Drone-Elite-Quadricopter\-Sand/dp/B00FS7SSD6, accessed: 22-04-2023.

[10] Y. Li and S. Song, "A survey of control algorithms for quadrotor unmanned helicopter," *IEEE fifth international conference on advanced computational intelligence (ICACI)*, pp. 365–369, 2012.

[11] M. Maaruf, M. S. Mahmoud, and A. Ma'arif, "A survey of control methods for quadrotor uav," *International Journal of Robotics and Control Systems*, vol. 2, no. 4, pp. 652–665, 2022.

[12] K. K. Shaw and R. Vimalkumar, "Design and development of a drone for spraying pesticides, fertilizers and disinfectants," *International Journal of Engineering Research & Technology (IJERT)*, vol. 9, no. 5, pp. 1181–1185, 2020.

[13] A. S. Hanif, X. Han, and S.-H. Yu, "Independent Control Spraying System for UAV-Based Precise Variable Sprayer: A Review," *Drones*, vol. 6, no. 12, pp. 1–25, 2022.

[14] J. Li and Y. Li, "Dynamic analysis and PID control for a quadrotor," *IEEE International Conference on Mechatronics and Automation*, pp. 573–578, 2011.

[15] W. Dong, G.-Y. Gu, X. Zhu, H. Ding *et al.*, "Modeling and control of a quadrotor UAV with aerodynamic concepts," *World Academy of Science, Engineering and Technology*, vol. 7, no. 5, pp. 901–906, 2013.

[16] V. Praveen, S. Pillai *et al.*, "Modeling and simulation of quadcopter using PID controller," *International Journal of Control Theory and Applications*, vol. 9, no. 15, pp. 7151–7158, 2016.

[17] S. Abdelhay and A. Zakriti, "Modeling of a quadcopter trajectory tracking system using PID controller," *Procedia Manufacturing*, vol. 32, pp. 564–571, 2019.

[18] J. Yoon and J. Doh, "Optimal PID control for hovering stabilization of quadcopter using long short term memory," *Advanced Engineering Informatics*, vol. 53, pp. 1–12, 2022.

[19] S. Bouabdallah, A. Noth, and R. Siegwart, "PID vs LQ control techniques applied to an indoor micro quadrotor," *IEEE/RSJ International Conference on Intelligent Robots and Systems (IROS)*, vol. 3, pp. 2451–2456, 2004.

[20] L. Martins, C. Cardeira, and P. Oliveira, "Linear quadratic regulator for trajectory tracking of a quadrotor," *IFAC-PapersOnLine*, vol. 52, no. 12, pp. 176–181, 2019.

[21] F. Ahmad, P. Kumar, A. Bhandari, and P. P. Patil, "Simulation of the Quadcopter Dynamics with LQR based Control," *Materials Today: Proceedings*, vol. 24, pp. 326–332, 2020.

[22] A. Acakpovi, F.-X. Fifatin, M. Aza-Gnandji, F. Kpadevi, J. Nyarko *et al.*, "Design and Implementation of a Quadcopter Based on a Linear Quadratic Regulator (LQR)," *Journal of Digital Food, Energy & Water Systems*, vol. 1, no. 1, pp. 1–14, 2020.

[23] L. M. Argentim, W. C. Rezende, P. E. Santos, and R. A. Aguiar, "PID, LQR and LQR-PID on a quadcopter platform," *International Conference on Informatics, Electronics and Vision (ICIEV)*, pp. 1–6, 2013.

[24] A. Mokhtari, A. Benallegue, and B. Daachi, "Robust feedback linearization and GH/sub/spl infin//controller for a quadrotor unmanned aerial vehicle," *IEEE/RSJ International Conference on Intelligent Robots and Systems*, pp. 1198–1203, 2005.

[25] O. Falkenberg, J. Witt, U. Pilz, U. Weltin, and H. Werner, "Model Identification and Attitude Control for Quadrotor MAV's," *International Conference on Intelligent Robotics and Applications*, pp. 460–471, 2012.

[26] O. Araar and N. Aouf, "Full linear control of a quadrotor UAV, LQ vs H_∞," *UKACC International Conference on Control*, pp. 133–138, 2014.

[27] A. Saeed, A. I. Bhatti, and F. M. Malik, "2-DOF H_∞ Output Feedback Control of Quadrotor Subject to Parametric Uncertainties and Time Delay," *International Conference on Recent Advances in Electrical Engineering & Computer Sciences (RAEE & CS)*, pp. 1–5, 2022.

[28] S. L. Rangajeeva and J. F. Whidborne, "Linear parameter varying control of a quadrotor," *6th International Conference on Industrial and Information Systems*, pp. 483–488, 2011.

[29] P. S. Cisneros, C. Hoffmann, M. Bartels, and H. Werner, "Linear parameter-varying controller design for a nonlinear quad-rotor helicopter model for high speed trajectory tracking," *American Control Conference (ACC)*, pp. 486–491, 2016.

[30] L. Nie, B. Cai, S. Lu, H. Qin, and L. Zhang, "Finite-time switched LPV control of quadrotors with guaranteed performance," *Journal of the Franklin Institute*, vol. 358, no. 14, pp. 7032–7054, 2021.

[31] E. Altug, J. P. Ostrowski, and R. Mahony, "Control of a quadrotor helicopter using visual feedback," *IEEE international conference on robotics and automation*, vol. 1, pp. 72–77, 2002.

[32] T. Madani and A. Benallegue, "Backstepping control for a quadrotor helicopter," *IEEE/RSJ International Conference on Intelligent Robots and Systems*, pp. 3255–3260, 2006.

[33] T. Madani and A. Benallegué, "Control of a quadrotor mini-helicopter via full state backstepping technique," *Proceedings of the 45th IEEE Conference on Decision and Control*, pp. 1515–1520, 2006.

[34] S. H. Lee, S. H. Kang, and Y. Kim, "Trajectory tracking control of quadrotor UAV," *11th International Conference on Control, Automation and Systems*, pp. 281–285, 2011.

[35] I. González, S. Salazar, and R. Lozano, "Chattering-free sliding mode altitude control for a quad-rotor aircraft: Real-time application," *Journal of Intelligent & Robotic Systems*, vol. 73, no. 1-4, pp. 137–155, 2014.

[36] I. Gonzalez-Hernandez, S. Salazar, R. Lopez, and R. Lozano, "Altitude control improvement for a Quadrotor UAV using integral action in a sliding-mode controller," *International Conference on Unmanned Aircraft Systems (ICUAS)*, pp. 711–716, 2016.

[37] D. J. Almakhles, "Robust backstepping sliding mode control for a quadrotor trajectory tracking application," *IEEE Access*, vol. 8, pp. 5515–5525, 2019.

[38] K. S. Brahim, A. El Hajjaji, N. Terki, and D. L. Alabazares, "Finite Time Adaptive SMC for UAV Trajectory Tracking under Unknown Disturbances and Actuators Constraints," *IEEE Access*, vol. 11, pp. 66 177–66 193, 2023.

[39] T. H. Pham and S. Mammar, "Quadrotor LPV control using static output feedback," *IEEE 16th International Conference on Networking, Sensing and Control (ICNSC)*, pp. 74–79, 2019.

[40] T. H. Pham, D. Ichalal, and S. Mammar, "LPV and Nonlinear-based control of an Autonomous Quadcopter under variations of mass and moment of inertia," *IFAC-PapersOnLine*, vol. 52, no. 28, pp. 176–183, 2019.

[41] T.-H. Pham, D. Ichalal, and S. Mammar, "LPV state-feedback controller for Attitude/Altitude stabilization of a mass-varying quadcopter," *20th International Conference on Control, Automation and Systems (ICCAS)*, pp. 212–218, 2020.

[42] L. Nie, B. Cai, Y. Zhu, J. Yang, and L. Zhang, "Switched linear parameter-varying tracking control for quadrotors with large attitude angles and time-varying inertia," *Optimal Control Applications and Methods*, vol. 42, no. 5, pp. 1320–1336, 2021.

[43] J. E. Sierra, M. Santos *et al.*, "Wind and payload disturbance rejection control based on adaptive neural estimators: application on quadrotors," *Complexity*, vol. 2019, pp. 1–20, 2019.

[44] M. Vahdanipour and M. Khodabandeh, "Adaptive fractional order sliding mode control for a quadrotor with a varying load," *Aerospace Science and Technology*, vol. 86, pp. 737–747, 2019.

[45] J. Zhao, X. Ding, B. Jiang, G. Jiang, and F. Xie, "A novel control strategy for quadrotors with variable mass and external disturbance," *International Journal of Robust and Nonlinear Control*, vol. 31, no. 17, pp. 8605–8631, 2021.

[46] J.-W. Lee, N. Xuan-Mung, N. P. Nguyen, and S. K. Hong, "Adaptive altitude flight control of quadcopter under ground effect and time-varying load: Theory and experiments," *Journal of Vibration and Control*, vol. 29, no. 3-4, pp. 571–581, 2023.

[47] R. C. Nelson *et al.*, *Flight stability and automatic control*, 2nd ed. WCB/McGraw Hill New York, 1998.

[48] D. Lee, T. C. Burg, D. M. Dawson, D. Shu, B. Xian, and E. Tatlicioglu, "Robust tracking control of an underactuated quadrotor aerial-robot based on a parametric uncertain model," *IEEE international conference on systems, man and cybernetics*, pp. 3187–3192, 2009.

[49] F. Sabatino, *Quadrotor control: modeling, nonlinear control design, and simulation.* M.Sc thesis, KTH, Stockholm, Sweden, 2015.

[50] Z. Benić, P. Piljek, and D. Kotarski, "Mathematical modelling of unmanned aerial vehicles with four rotors," *Interdisciplinary Description of Complex Systems: INDECS*, vol. 14, no. 1, pp. 88–100, 2016.

[51] B. Etkin and L. D. Reid, *Dynamics of flight: stability and control*, 1st ed. John Wiley & Sons, 1995.

[52] S. Bouabdallah, "Design and control of quadrotors with application to autonomous flying," Ecole Polytechnique Federale de Lausanne, Tech. Rep., 2007.

[53] X. Wu, B. Xiao, and Y. Qu, "Modeling and sliding mode-based attitude tracking control of a quadrotor UAV with time-varying mass," *ISA transactions*, vol. 124, pp. 436–443, 2022.

[54] P. Yang, Z. Wang, Z. Zhang, and X. Hu, "Sliding mode fault tolerant control for a quadrotor with varying load and actuator fault," *Actuators*, vol. 10, no. 12, pp. 1–17, 2021.

[55] D. W. Kun and I. Hwang, "Linear matrix inequality-based nonlinear adaptive robust control of quadrotor," *Journal of Guidance, Control, and Dynamics*, vol. 39, no. 5, pp. 996–1008, 2016.

[56] W. Mizouri, S. Najar, L. Bouabdallah, and M. Aoun, "Dynamic modeling of a quadrotor UAV prototype," *New Trends in Robot Control*, vol. 270, pp. 281–299, 2020.

[57] M. Okasha, J. Kralev, and M. Islam, "Design and Experimental Comparison of PID, LQR and MPC Stabilizing Controllers for Parrot Mambo Mini-Drone," *Aerospace*, vol. 9, no. 6, pp. 1–20, 2022.

[58] A. Noordin, M. Basri, and Z. Mohamed, "Simulation and experimental study on PID control of a quadrotor MAV with perturbation," *Bulletin of Electrical Engineering and Informatics*, vol. 9, no. 5, pp. 1811–1818, 2020.

[59] P. Gahinet, A. Nemirovskii, A. J. Laub, and M. Chilali, "The LMI control toolbox," *Proceedings of 33rd IEEE conference on decision and control*, vol. 3, pp. 2038–2041, 1994.

[60] B. Mouaad, B. Z. Razika, R. H. Ramzi, and C. Karim, "Control design and visual autonomous navigation of quadrotor," *International Conference on Advanced Electrical Engineering (ICAEE)*, pp. 1–7, 2019.

[61] K. E. Hamidi, M. Mjahed, A. E. Kari, and H. Ayad, "Quadcopter attitude and altitude tracking by using improved PD controllers," *International Journal of Nonlinear Dynamics and Control*, vol. 1, no. 3, pp. 287–303, 2019.

[62] A. Patel, A. Banerjee, B. Lindqvist, C. Kanellakis, and G. Nikolakopoulos, "Design and model predictive control of a mars coaxial quadrotor," *IEEE Aerospace Conference (AERO)*, pp. 1–11, 2022.

[63] S. Boyd, L. El Ghaoui, E. Feron, and V. Balakrishnan, *Linear matrix inequalities in system and control theory*, 1st ed. SIAM, 1994.

[64] H. Pfifer, *LPV/LFT Modeling and its Application in Aerospace*, 1st ed. Verlag Dr. Hut, 2013.

[65] J. M. Biannic, "Linear parameter-varying control strategies for aerospace applications," *Robust Control and Linear Parameter Varying Approaches: Application to Vehicle Dynamics. Berlin, Heidelberg: Springer Berlin Heidelberg*, vol. 437, pp. 347–373, 2013.

[66] O. Sename, P. Gaspar, and J. Bokor, *Robust control and linear parameter varying approaches: application to vehicle dynamics.* Springer, 2013, vol. 437.

[67] H. Zhang, G. Zhang, and J. Wang, "$\mathcal{H}_\infty$ Observer Design for LPV Systems With Uncertain Measurements on Scheduling Variables: Application to an Electric Ground Vehicle," *IEEE/ASME Transactions on Mechatronics*, vol. 21, no. 3, pp. 1659–1670, 2016.

[68] P. Li, A.-T. Nguyen, H. Du, Y. Wang, and H. Zhang, "Polytopic LPV approaches for intelligent automotive systems: State of the art and future challenges," *Mechanical Systems and Signal Processing*, vol. 161, pp. 1–27, 2021.

[69] C. Hoffmann and H. Werner, "A survey of linear parameter-varying control applications validated by experiments or high-fidelity simulations," *IEEE Transactions on Control Systems Technology*, vol. 23, no. 2, pp. 416–433, 2014.

[70] M. M. Morato, D. J. Regner, P. R. Mendes, J. E. Normey-Rico, and C. Bordons, "Fault analysis, detection and estimation for a microgrid via H2/H_∞ LPV observers," *International Journal of Electrical Power & Energy Systems*, vol. 105, pp. 823–845, 2019.

[71] J. S. Shamma and M. Athans, "Gain scheduling: Potential hazards and possible remedies," *IEEE Control Systems Magazine*, vol. 12, no. 3, pp. 101–107, 1992.

[72] J.-S. Shamma and M. Athans, "Analysis of gain scheduled control for nonlinear plants," *IEEE Transactions on Automatic Control*, vol. 35, no. 8, pp. 898–907, 1990.

[73] J. S. Shamma and M. Athans, "Guaranteed properties of gain scheduled control for linear parameter-varying plants," *Automatica*, vol. 27, no. 3, pp. 559–564, 1991.

[74] Y. Ameho, F. Niel, F. Defaÿ, J.-M. Biannic, and C. Bérard, "Adaptive control for quadrotors," *IEEE International Conference on Robotics and Automation*, pp. 5396–5401, 2013.

[75] A. Akbari, F. Rahemi, M. J. Khosrowjerdi, and S. Ebadollahi, "Roll and Pitch Estimation From IMU Data Using an LPV H_∞ Filter," *IEEE Transactions on Instrumentation and Measurement*, vol. 72, pp. 1–10, 2023.

[76] P. Aplarian, "Lmi techniques in control engineering from theory to practice," in *Workshop Notes at the 35th IEEE Conference on Decision and Control, Kobe*, 1996.

[77] J. Han, X. Liu, X. Wei, and S. Sun, "A dynamic proportional-integral observer-based nonlinear fault-tolerant controller design for nonlinear system with partially unknown dynamic," *IEEE Transactions on Systems, Man, and Cybernetics: Systems*, vol. 52, no. 8, pp. 5092–5104, 2021.

[78] P. Apkarian, P. Gahinet, and G. Becker, "Self-scheduled H_∞ control of linear parameter-varying systems: a design example," *Automatica*, vol. 31, no. 9, pp. 1251–1261, 1995.

[79] M. D. Zollars, R. G. Cobb, and D. J. Grymin, "Optimal path planning for SUAS waypoint following in urban environments," *IEEE Aerospace Conference*, pp. 1–8, 2018.

[80] J. Theis and H. Pfifer, "Observer-based synthesis of linear parameter-varying mixed sensitivity controllers," *International Journal of Robust and Nonlinear Control*, vol. 30, no. 13, pp. 5021–5039, 2020.

[81] Y. Liu and C. Jiang, "Mixed-Sensitivity Control for Drag-Free Spacecraft Based on State Space," *Aerospace*, vol. 9, no. 11, pp. 708–723, 2022.

[82] P. A. Gbadega, Y. Sun, and H. Zhang, "Robustness and stability analysis for parametric uncertainties in a three-area AGC power system using TLBO-LMI-tuned PI controller," *Energy Reports*, vol. 9, pp. 153–164, 2023.

[83] G.-R. Duan and H.-H. Yu, *LMIs in control systems: analysis, design and applications*, 1st ed. CRC press, 2013.

[84] N. Wada, A. Takahashi, M. Saeki, and M. Nishimura, "Vehicle yaw control using an active front steering system with measurements of lateral tire forces," *The Abstracts of the international conference on advanced mechatronics: toward evolutionary fusion of IT and mechatronics*, pp. 319–324, 2010.

[85] H. Atoui, O. Sename, V. Milanes, and J. J. Martinez, "Interpolation of multi-LPV control systems based on Youla–Kucera parameterization," *Automatica*, vol. 134, pp. 1–6, 2021.

[86] K. Laib, O. Sename, and L. Dugard, "String stable H_∞ LPV cooperative adaptive cruise control with a variable time headway," *IFAC-PapersOnLine*, vol. 53, no. 2, pp. 15 140–15 145, 2020.

[87] W. Wu, W. Xie, and L. Li, "Switching linear parameter-varying controller design with H_∞ performance based on Youla parameterization," *IEEE Access*, vol. 8, pp. 184 765–184 773, 2020.

[88] H. T. Ngo, E. Kamal, and B. Marinescu, "EMT three-phase VSC grid-connected converter reactive power control using H_∞ LMI MIMO approach," *IEEE PES Innovative Smart Grid Technologies Conference Europe (ISGT-Europe)*, pp. 1–6, 2022.

[89] M. Chilali and P. Gahinet, "H/sub/spl infin//design with pole placement constraints: an lmi approach," *IEEE Transactions on automatic control*, vol. 41, no. 3, pp. 358–367, 1996.

[90] C. Trapiello, V. Puig, and B. Morcego, "Position-heading quadrotor control using LPV techniques," *IET Control Theory & Applications*, vol. 13, pp. 783–794, 2019.

[91] R. Elagib and A. Karaarslan, "Sliding mode control-based modeling and simulation of a quadcopter," *Journal of Engineering Research and Reports*, vol. 24, no. 3, pp. 32–41, 2023.